A systematic approach for modelling modern turbofan engines

Thesis

S.S.Ramdin

Delft University of Technology

TU Delft

KLM Engineering & Maintenance

A systematic approach for modelling modern turbofan engines

Thesis

by

S.S.Ramdin

to obtain the degree of Master of Science
at the Delft University of Technology,
to be defended publicly on Thursday October 13, 2022 at 09:30 AM.

Student number:	4606248	
Project duration:	November, 2021 - October, 2022	
Thesis committee:	Prof. dr. ir. P. Colonna,	TU Delft, chair
	Dr. ir. W. P. J. Visser,	TU Delft, supervisor
	Ir. P. C. Roling,	TU Delft
	Ir. J. Regueiro Cueva,	KLM Engine Services, supervisor

This thesis is confidential and cannot be made public until September 28, 2024.

Cover Image: GE9X Engine

TU Delft

Preface

This master thesis marks the end of my graduate project at KLM Engine Services and my time as an aerospace engineering student at the Delft University of Technology. I am extremely thankful for the opportunity to do my thesis project at KLM Engine Services as a graduate intern, amidst the COVID-19 pandemic. During this period, I learned a lot about the MRO industry and aero engines. I also had the opportunity to work from the office with a great atmosphere and inspiring colleagues. The coffee breaks were always enjoyable, and the walks around the hangers never ceased to amaze me.
I kindly want to thank my supervisors Wilfried Visser and Juan Regueiro for helping and guiding me through this amazing journey. Without their supervision, guidance and expertise I would not have achieved this result. Additionally, I would like to express my gratitude to the other KLM colleagues involved in my thesis project: Tim Rootliep, Albert Timmer and Antonis Paradeisanos. I would also like to thank prof. dr. ir. Colonna and ir. Roling for being a part of my graduation committee. Furthermore, I would like to thank my fellow ex-interns as well for the interesting discussions and pleasant times at the office. Finally, I would like to express my gratitude to my family, friends, and girlfriend for the support trough my studies.

S.S.Ramdin
Delft, September 2022

Summary

Modern turbofan engine technology has evolved over several decades resulting in highly efficient and reliable propulsion systems for commercial airliners. Maintenance costs have also drastically decreased, but still represent a major part of the overall aircraft operating costs. To further minimize these, engine maintenance needs to be planned timely and strategically. The maintenance concept currently applied at KLM Engine Services (ES) is based on preventive and corrective maintenance. Advanced diagnostics and health monitoring methods are being developed to assess engine component condition to improve maintenance planning, work scope decision making and also safety. This requires test cell and on-wing data. Gas path analyses (GPA) is used for health monitoring by comparing simulated data with measured data and requires an accurate engine performance model. The software used for engine performance modelling and simulation at KLM ES is the Gas Turbine Simulation Program (GSP). GSP is a 0-D object-oriented gas turbine system simulation tool developed at the National Aerospace Laboratory (NLR) and Delft University of Technology.

The increasing complexity of aero engines imposes additional modelling challenges. Adding to the latter are the reduced number of sensors in modern gas turbines and the proprietary nature of design data. Several projects have been conducted in the past at KLM ES related to turbofan modelling. The engines at focus were the CF6-80C2 engine and the state-of-the-art GEnx-1B turbofan engine. These models demonstrate acceptable performance, however, they can still be improved. Additionally, the modelling approach can not easily be applied to other engines. Therefore, this thesis focusses on developing a systematic approach for modelling modern turbofan engines. The main steps for modelling a gas turbine are twofold. Firstly, the design point modelling is conducted. At the design point the key dimensions are determined, which is subsequently used for the (second) off-design modelling part. For the design point a critical operating point of the flight envelope, that the engine was designed to meet, is chosen. Off-design modelling mainly concerns component characteristics maps generation or tuning. These maps, which are proprietary to the manufacturer, describe the behaviour of the turbomachinery components, and present the relation between the pressure ratio, corrected mass flow, spool speed and isentropic efficiency.

For the design point modelling, test cell data have been used. Test cell data includes additional parameters that are not recorded on-wing: thrust, mass flow and humidity. Physical relations have been used as constraints, to bridge the gap caused by the fewer sensors. These include efficiency relations for compressors and turbines, and the fan pressure ratio that maximises thrust by ensuring an optimum jet velocity ratio. An optimiser was required for minimising the difference between the simulated and measured data. The component performance parameters (e.g., the pressure ratios and efficiencies) were adapted in this process. From literature Genetic algorithms (GA) were found to be the most suitable optimiser. GA can deal with noise, escape local minima due to its stochastic nature, and are also suitable for underdetermined systems.

The off-design modelling approach has also been done using test cell data. The cycle reference scaling point, attained from the design point modelling process, was placed such that acceptable operating lines were achieved, which provided sufficient surge margin and realistic component performance parameters. The reference component maps were adapted by using a second order scaling polynomial for each performance parameter. For this problem Genetic algorithms were employed as well to determine the polynomial coefficients. Maps of comparable turbomachinery, with similar operating regimes, were selected from the literature as baseline maps. The optimised maps were subsequently checked for physical correctness in order to prove their validity. This was done by comparing the underlying physics with the literature. The modelling approach described above has been applied to the CF6-80C2, and the GEnx-1B engine to demonstrate its applicability to different engine types.

The approach has been validated using the developed GEnx-1B engine model and CEOD. The results were promising, with an average error of 2.4 % over the take-off, climb and cruise flight phases. This is an improvement of 1.2 % over the old GEnx-1B model, however, the accuracy can still be improved. Residual errors are due to secondary performance parameter effects, such as variable geometry and clearance control, which are highly dependent on operating settings and flight conditions. The settings

during test cell runs are different from on-wing records. Also, losses in the propelling nozzles are different in flight compared to on the test cell, causing additional error. This can be addressed by adjusting the nozzle velocity and/or thrust coefficient parameter functions. Furthermore, Reynolds effects were found to be responsible for the model deviations. These were not included in the modelling process, which is acceptable for low altitudes where high Reynolds numbers are encountered. For cruise, however, the Reynolds numbers are low and need to be corrected for. Including these corrections will make the models more accurate for on-wing conditions.
The resulting systematic approach will make engine modelling tasks at KLM ES more efficient and provides a consistent approach to deal with missing sensors and data, unlike previous modelling projects at KLM ES. Moreover, using an automated machine learning procedure for modelling, is more efficient and effective than a manual process. Additionally, the approach can straightforwardly be utilised for developing new and accurate engine models (e.g., the LEAP). This in turn will improve the gas path analysis accuracy and reliability, resulting in more effective engine maintenance in terms of more accurate diagnostics and prognostics by providing tailored work scopes.

Contents

Nomenclature

Acronyms

ACC	Active Clearance Control
BAI	Booster Anti Ice
BO	Bayesian Optimisation
BPR	Bypass Ratio ..... [-]
CAI	Cowling Anti Ice
CCC	Core Compartment Cooling
CEOD	Continuous Engine Operating Data
DP	Design Point
EA	Evolutionary Algorithms
EGT	Exhuast Gas Temperature ..... [K]
EI	Expected Improvement
EIS	Entry into Service
ESN	Engine Serial Number
FPR	Fan Pressure Ratio ..... [-]
GA	Genetic Algorithm
GE	General Electric
GPA	Gas Path Analysis
HPC	High Pressure Compressor
HPT	High Pressure Turbine
IGV	Inlet Guide Vane
IM	Installation Manual
LCB	Lower Confidence Bound
LHV	Lower Heating Value
LPC	Low Pressure Compressor
LPT	Low Pressure Turbine
MPI	Maximum Probability of Improvement
MRO	Maintenance, Repair & Overhaul
OD	Off Design
OEM	Original Equiment Manufacturer
OF	Objective Function
OPR	Overall Pressure Ratio ..... [-]
PR	Pressure Ratio ..... [-]
Re	Reynolds number ..... [-]
RHum	Relative Humidity ..... [%]
RMSE	Root Mean Squared Error
RNI	Reynolds Number Index ..... [-]
SLS	Sea Level Static
SM	Surge Margin ..... [%]
SPP	Secondary Performance Parameters
TBV	Transient Bleed Valve
TIT	Turbine Inlet Temperature ..... [K]
TO	Take Off
TOC	Top of Climb
VBV	Variable Bleed Valve
VSV	Variable Stator Vanes

Greek symbols

δ	Pressure correction factor ..... [-]
η	Efficiency ..... [-]
γ	Heat capacity ratio ..... [-]
Φ	Flow Coefficient ..... [-]
Ψ	Stage loading coefficient ..... [-]
θ	Temperature correction factor ..... [-]

Roman symbols

$\hat{F}$	Specific thrust ..... [N/kg/s]
$\hat{z}$	Simulated Performance Parameters
r^*	Degree of reaction ..... [-]
z	Target Performance Parameters
B	Bypass ratio ..... [-]
C	Coefficient ..... [-]
f	Objective function

h	Enthaly	[J]
M	Mach number	[-]
N	Shaft speed	[rpm]
P	Power	
R	Specific gas constant	[J/kg/K]
U	Tangential velocity	[m/s]
V	Velocity (absolute)	[m/s]
W	Mass flow	[kg/s]
w	Relative velocity	[m/s]

Superscripts

*	Nominal value

Subscripts

a	Ambient
ax	Axial
c	Cold
c	Compressor
cc	Cumbustion chamber
D	Discharge
ds	Design
exp	Expansion
f	fan
gen	Generation
gg	Gas Generator
h	Hot
is	isentropic
j	Jet
mech	Mechenical
N	Net
NB	Bypass nozzle
op	Optimum
p	Polytropic
prop	Propulsive
rel	Relative
s	Static
std	Standard day
T	Turbine
t	Total
t h d y	Thermodynamic
X	Thrust

List of Figures

List of Tables

1 Introduction

Gas turbines are one of the most complex and important aircraft subsystems. They play a major role in the efficiency of modern aviation [1]. The design trends for modern aircraft engines are driven by various requirements. Two of the most important ones currently are the reduction of operating costs and emissions[2, 3]. Reducing the operating costs is of utmost importance in order to remain competitive in the airline industry. Turbofans are the most widely used type of civil aircraft engines these days. This transition revolutionised the commercial aviation sector. It allows for longer flights and lower fuel consumption, due to its higher efficiency and thrust to weight ratio. This improved performance is achieved by increasing the overall pressure ratio (OPR), turbine inlet temperature (TIT), and component efficiencies, which increase the thermal efficiency. Additionally, the propulsive efficiency is also increased by lowering the fan pressure ratio (FPR) and increasing the bypass ratio (BPR). The latter also reduces jet noise, which is another important design requirement. Lower emissions are achieved by advanced combustion technologies and alternatives for jet fuel.

Another important contributor of the operating costs is the maintenance of aircraft engines. The maintenance of these can be done by the maintenance, repair, and overhaul (MRO) facilities of airliners, or the original equipment manufacturers (OEM). For large airliners it can be financially beneficial to perform maintenance in-house, rather than outsourcing. KLM together with Air France industries form Air France Industries KLM Engineering & Maintenance (E&M), one of the big names in the MRO world. Engine Services (ES) is one of the maintenance divisions of KLM E&M. Maintenance, repair and inspection are provided for engines from the KLM fleet and other airliners. The CFM-56-7B, CF6-80C2, and GEnx-1B are some of the engines for which these services are provided. The more recent LEAP engines are also gradually being introduced now.

In order to reduce the operating costs, the engine maintenance needs to be conducted efficiently. The maintenance strategies that are currently applied at KLM ES are based on preventive and corrective maintenance. They are slowly proceeding towards more efficient methods such as diagnostics to aid with predictive strategies. Preventive maintenance of engines is based on a predetermined fixed schedule, and some parts have a limited life. Corrective maintenance occurs if the engine does not meet the required performance. For diagnostics, engine health monitoring is required in order to assess the conditions of the components. For this, data from test cell and on-wing is being used.

Furthermore, a differential method, called gas path analyses (GPA), is used to estimate the component health by comparing simulated data with measured ones. The software employed by KLM ES for modelling and simulation is Gas Turbine Simulation Program (GSP). For accurate health monitoring, a high fidelity reference model is required. Creating such a model is becoming increasingly challenging due to less instrumentation and OEM proprietary design data. Several projects have been conducted in the past at KLM ES to improve the accuracy of health monitoring. A Multi-Operating Point Gas Path Analysis (MOPA-EA GPA) tool has been developed for the GEnx-1B engine in order to deal with the fewer sensors. Furthermore, a tool to include the secondary performance parameters in the health monitoring has been developed as well. These tools fulfil their intended purpose, however, there is still some uncertainty present. Not all the component conditions can be predicted accurately, and the model does not perform properly at cruise. This mainly originates from the lack of data available for modelling purposes. That is why the goal for this project is to develop a systematic model that can

handle the gap caused by the reduced amount of data available. Work has been done in the past to tackle this problem. The models generated, however, are tailored to a specific engine type and lack motivation for design choices. Additionally, the models tackled missing data in different ways, which leads to inconsistent results along engine types and flight phases. A systematic approach can also improve the engine component condition monitoring MOPA-EA GPA tool accuracy.

1.1. Research question and objective

With all the provided information above, and the research gap now identified the research question and objective can be formulated.

1.1.1. Research Question(s)

The following main research question has been formulated in order to fulfil the goal of this project:

How can a systematic modelling approach be developed for new generation turbofan engines for component health monitoring purposes by utilising test cell data, on-wing measurements and general physical relations?

In order to answer this main question systematically, sub-questions are mapped-out below.

1. How can one effectively deal with the reduced amount of measurements for modern turbofan engines?
2. How can a systematic framework be created for design point modelling?
3. How can a systematic approach be developed for off-design modelling?
4. Is it possible to check the underlying physics of the component performance maps with the available resources?
5. Which methods can be used to validate the developed approach for modelling a turbofan engine?

1.1.2. Research Objective

The main research objective of this thesis project is defined as follows:

The objective of this research project is to improve Gas Path Analysis at KLM Engine Services, by developing a systematic approach for modelling new generation turbofan engines in an MRO environment using data available in an MRO environment and general physical relations.

Similarly as for the main research question, the main objective can be divided into sub-objectives as well. The first sub-objective is related to the reduced amount of available data. It will be inspected if generic (non engine specific) data and optimum parameters form a good estimation for unknown parameters. This will be done using an existing engine model.
The next sub-objective focuses on setting a framework for developing a systematic design point modelling approach. It will be analysed if the available data and general physical relations can be used to make-up for the missing parameters. The same will be done for the off-design modelling, which mainly consists of generating or tuning component maps. The subsequent step will be to analyse if the outcome is in line with the physics. This includes checking the generated component maps for physical correctness, and if the performance changes along the operating lines are realistic. Finally, the approach needs to validated. This can be done by assessing the performance of the model using data that has not been run through the model before.

1.2. Structure of the report

This report consists of 12 chapters and is structured as follows. Firstly, some background information is provided in Chapter 2. Then the past and current aircraft engine design trends are introduced in Chapter 3, which give an indication of the current technology level. Subsequently, the available data sources are elaborated upon in Chapter 4. The modelling strategies are discussed in Chapter 5, which aid with identifying the best suited approach for developing a model to be used for component health monitoring. Chapter 6 presents the physical relations obtained from the literature. This is followed by the engine descriptions and data selection for modelling in Chapter 7. The modelling approach taken

is subsequently elaborated upon in Chapter 8, which is followed by the outcome and verification in Chapter 9. In Chapter 10 the GEnx engine model validation is presented. The main steps and key modelling decisions are then addressed in Chapter 11. Lastly, the conclusions drawn from this study, and the recommendations are presented in Chapter 12.

2

Background information

This chapter includes some background information, which will lay the foundation for the work to be conducted in this project. First a brief history regarding gas turbines is given. Originating from the 1930s, major technological advancements occurred to arrive at the modern turbofan engines. Then the maintenance strategies employed at KLM ES is elaborated upon. This is followed by a description of the various projects done in the past at KLM ES related to gas turbine modelling and component health analyses.

2.1. Background on Gas Turbines

The history of gas turbines to propel aircraft originates from 1930 when Frank Whittle was given a patent for a gas turbine [4]. The compression for this machine was done using a double-sided centrifugal compressor. This was followed by a reverse-flow combustor and driven by a single stage axial turbine. Axial compressors were not developed yet due to aerodynamic instabilities. Flame instabilities prohibited the use of straight flow combustors.

Starting from this jet engine design a lot of major technological advancements occurred that led to the modern high bypass ratio turbofan jet engines we know today. The first turbofan engine to enter service was the Rolls-Royce Conway in the 1940s [5]. This was a two spool gas turbine with a bypass ratio of 0.3 and a maximum thrust of around 78 kN.

Turbofan engines are the most dominant type of jet engines today for large commercial transport aircraft. The latter due to the high efficiency and power to weight ratio. This improved performance is achieved by increasing the overall pressure ratio (OPR), turbine inlet temperature (TIT), and component efficiencies, which increases the thermal efficiency. Furthermore, the propulsive efficiency is increased as well by lowering the fan pressure ratio (FPR) and increasing the bypass ratio (BPR). This increases the thrust and also has as an additional benefit: jet noise reduction. A more efficient engine has a lower fuel consumption, which also reduces the emissions. The latter being another important driver for engine designs.

The thermodynamic working principle of a turbofan relies on a Joule-Brayton cycle. In a continuous process air is first drawn into the engine. This air is then compressed by the compressors, after which fuel is injected in the combustor and heat is added by igniting the mixture. The hot gas is subsequently expanded in the turbines and discharged through the exhaust nozzle into the atmosphere. For the bypass section, the air goes through the fan and is thereafter ejected into the atmosphere by the bypass nozzle.

The first generation jet engines only had one spool (shaft). Modern day turbofan engines, however, have two or even three spools. An example for a two spool engine is the GEnx-1B depicted in Figure 2.1. The main modules are: the fan, the low pressure compressor (LPC), the high pressure compressor (HPC), the combustor, the high pressure turbine (HPT), and the low pressure turbine (LPT). The fan, LPC and LPT operate on the low pressure spool, and the HPC and HPT operate on the high pressure spool. One of the most recent three spool turbofan engines is the Rolls Royce Trent XWB. This engine entered service in 2014 and propels the Airbus A350 XWB [6]. When a gas turbine runs at speeds lower the design speed the density of the aft stages will be lower compared to design condi-

tions. This will result in increased axial velocity hence reduced incidence for the back stages, causing blade stalling at the front stages and choking at the aft stages. For high spool speeds the opposite will be true, and the aft stages will stall. To maintain an incidence close to the design value, the speed of the first stages need to be decreased, and the one of the aft stages needs to be increased. This is achieved by splitting up the compressor into two or more parts, driven by multiple turbines operating on separate shafts [7].

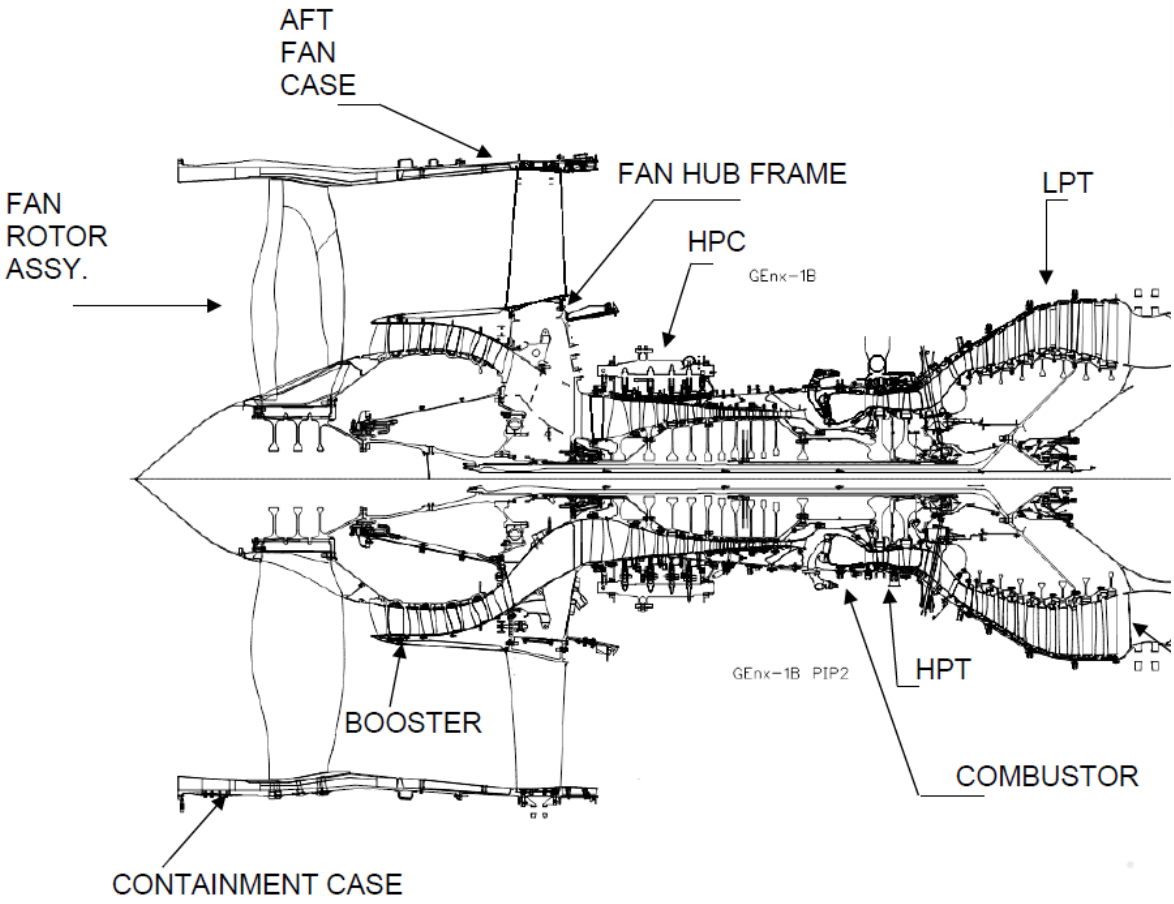

Figure 2.1: Turbofan modules[8]

2.2. Gas path analyses at KLM Engine Services

This section describes the work done previously, and the strategies being used for jet engine maintenance at KLM ES.

2.2.1. Maintenance strategies

As mentioned before, engine health assessment is an important factor when it comes to reducing operating costs of an airliner. Currently KLM Engine Services (ES) applies preventive and corrective maintenance. The first strategy is maintenance on a fixed schedule. The second method is employed when hardware deterioration is observed. This is the case when the exhaust gas temperature (EGT) or high pressure spool speed margin has decreased below a predefined limit. KLM ES also employs an in-house tool developed in collaboration with General Electric (GE) for engine monitoring, called Prognos for Engine. This tool creates alerts if performance deviation is identified, by utilising similarity-based modelling. The above mentioned strategies, however, can result in too early or too late maintenance, as the part health is not actually monitored. The latter triggered the need for a different strategy. This strategy is based on diagnostics, and will be applied at KLM ES in the near future. Engine components

deterioration and impending failure will be determined by utilising engine sensor data. In such a way components can be replaced and/or repaired prior to failure. New engine maintenance advancements are towards, more efficient, prognostic techniques. Using a prognostic method the future condition of engine components can be determined by trending sensor data, and thereby predicting when the maintenance should be scheduled.

2.2.2. Gas path analyses at KLM Engine Services

The diagnostic maintenance approach mentioned above utilises engine sensor data. The health of the engine and its components is then determined using a model based approach, called gas path analyses (GPA) [8–10]. The software used for modelling and simulation at KLM ES is the Gas Turbine Simulation Program (GSP) [11, 12]. GSP is a 0-D non-linear object-oriented gas turbine simulation tool developed at the National Aerospace Laboratory (NLR) in association with Delft University of Technology. GSP is created using the object-oriented Borland Delphi environment. One can not only perform steady-state calculations with this tool, but also off-design and transient calculations.

GPA is a differential method, where the reference model output is compared with measured data. The first GPA method employed at KLM ES was adaptive modelling (AM), developed by Verbist [13]. This approach adapts the turbomachinery performance maps of the engine model in order to match the measured sensor data. Two map modifiers, also called health parameters, are used for each turbomachine to describe the differences in component health between the reference model data and sensor measurements. A limitation of adaptive modelling is its deterministic nature—compromising the accuracy and stability due to noise—and its inability to solve matrix systems that are not square [14]. The latter reduces the amount of health parameters that can be determined, and their accuracy for modern turbofan engines. Modern turbofan engines have fewer sensors available, hence more unknown parameters [15, 16]. This challenge sparked the need for a different method for estimating component health. Rootliep [8] developed an evolutionary algorithm based multi operating point gas path analysis (MOPA-EA GPA) method to deal with the under-determined problem. A Genetic algorithm employing a 'survival of the fittest' process is used to determine the components condition. The component maps are adapted until the reference model and measurement data match. This is done for the take-off and cruise operating condition in order to improve the accuracy of the results. The results of the MOPA-EA GPA tool are promising, however, there are some inconsistencies present for the GEnx-1B engine. These are expected to originate from an incorrect GEnx-1B design point model and component characteristics maps. GPA requires an accurate reference engine model in order to predict the component condition correctly. In an endeavour to improve the accuracy of the MOPA-EA GPA tool. Otten [17] modelled the effect of the secondary performance parameters. Otten utilises an evolutionary algorithm to find a correlation between secondary performance parameters and map modifiers. These correlations can be applied on top of the reference model. Thus the reference model itself does not feature any secondary performance parameters effects. The results indicate improved accuracy for the MOPA-EA GPA tool. Still there are points for improvement. Amongst these are the improvement of the baseline on-design and off-design model.

A brief description of some other projects, focussed on design and off-design modelling, at KLM ES is presented next. Van Moorselaar [10] created the design point and off-design GEnx-1B model starting from the CF6-80C2 model. For the design point model the simulated cycle parameters were matched with the measurement data by performing iterations manually. For off-design conditions the component maps were generated by tuning the CF6-80C2 maps. The latter was done by relocating and relabelling the constant speed lines. To prove the validity of the model adaptive modelling was applied using GSP, for engine health prediction. The results were satisfactory, but there was quite some room for improvement. den Haan [9] created a model for CF6-80 engine component health monitoring purposes. The design point model was also created using an iterative procedure. The component characteristics were generated by relabelling speed lines and shifting the design point on the map using a trial and error procedure. Standard GSP maps are used as the starting maps. Satisfactory results are obtained using the developed model. This can mainly be attributed to sufficient amount of data available for modelling purposes. The model for off-design conditions is further improved by Beishuizen [18]. The operating range where the model can be applied is increased by including on-wing data in the analyses. The AM module of GSP is used for the latter. A similar modelling project as den Haan [9] was conducted by Bouazzaoui [19] for the CFM56-7B engine. At the design point the simulated results match the measured data. The off-design model is not very accurate and reliable, since generic component

maps were used that are only scaled to the design point. Finally, the project done by Röell [20] focuses on determining the discrepancies between on-wing and test cell corrected performance indicators.
It should be pointed out that only Beishuizen [18], Rootliep [8] and Otten [17] utilised on-wing data. The other projects only based their work on test cell data. Snapshots were also not used. The main reason for this is that test cell measurements included more measurements. One of which is the thrust measurement.

3

Gas turbine design trends

With some background information provided, one can dive deeper into the design trends of aircraft propulsion. This chapter presents an overview of the past and current aircraft engine design trends. These trends aim to improve the performance of the engine, whilst considering other factors such as noise, environmental impact, dimensions and weight. In order to make good approximations for unknown parameters and cross-check the obtained results with reference data, the trends for turbofan engine design and modelling are also suitable.

3.1. Current engine design Trends

Engine design trends give a good indication if the obtained engine design parameters agree with the technology level in the entry into service (EIS) or certification year of the engine. In Figure 3.1[2] the trend of the overall pressure ratio (OPR) is given. It can be observed that the OPR has been increasing. A similar trend can be observed for the turbine inlet temperature (TIT) in Figure 3.2[2]. This figure also shows the trend of maximum allowable temperature for metals over the years, which is substantially lower than the TIT. That is why turbine cooling is applied to lower the temperatures. Increasing these cycle parameters leads to higher thermal efficiencies. The trend for the bypass ratio (BPR) is depicted in Figure 3.3[21], which goes paired with a reduction in fan pressure ratio [2]. These two changes lead to a higher propulsive efficiency. The improvement of the two efficiencies mentioned above is illustrated in Figure 3.4 for different aircraft at cruise conditions. An increasing trend is clearly visible. Consequently, the overall efficiency—a product of the thermal, propulsive and transmission efficiency—increases as well. The main reason why manufacturers are pushing towards better performance and higher efficiencies is to reduce the specific fuel consumption (SFC) [2]. Reducing the SFC will also reduce the emissions, which is becoming an increasingly important factor due to the expeditious environmental awareness growth [3, 22].

The performance improvements mentioned above, are all allowed due the improved manufacturing technologies which allow for materials and parts with better properties [22]. These can for example withstand higher loads and temperatures, and are lighter. Additionally, improved simulation and optimisation techniques (e.g., , , for blade design of the fan, compressor or turbine) also give an additional performance improvement. This is possible due to the increased computational power and more advanced simulation software. Other technologies such as cooling and variable geometry also aid to the improved performance [2].

3.2. Trends for turbomachinery

The developments for turbomachinery design are also dictated by the aim to reduce the SFC. Head *et al.* [24] describe several engine parameter trends. Although these are obtained using a GSP model, the trends are still representative. The trends are given for a span of 50 years, ranging from 1960 to 2010. For all the components an increase in polytropic efficiency with certification year can be observed. The latter also contributes to the increase in the overall efficiency. It can be observed as well that the average stage pressure ratio has increased. This allows for lower spool speeds, and thereby reducing

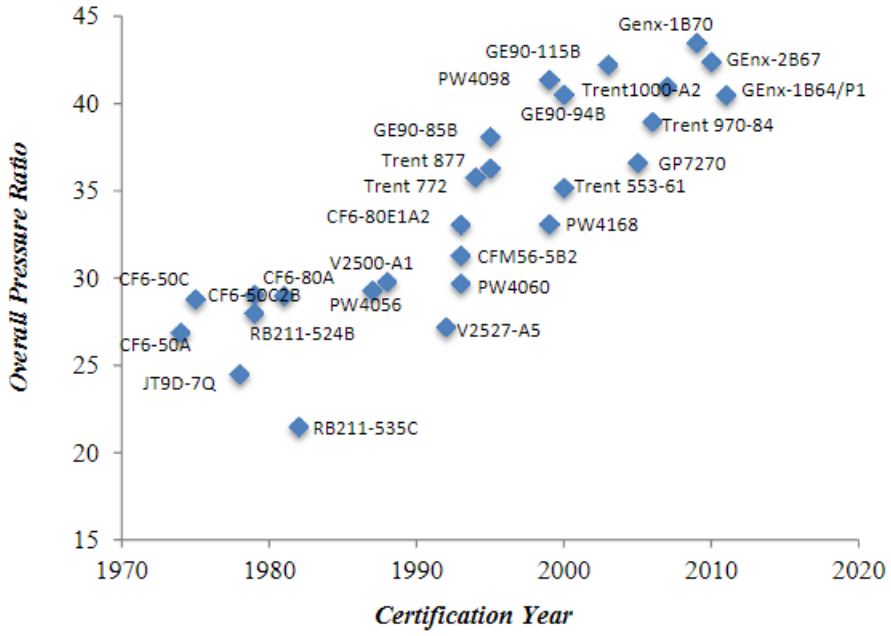

Figure 3.1: Gas turbine overall pressure ratio (OPR) change over the last 50 years [2]

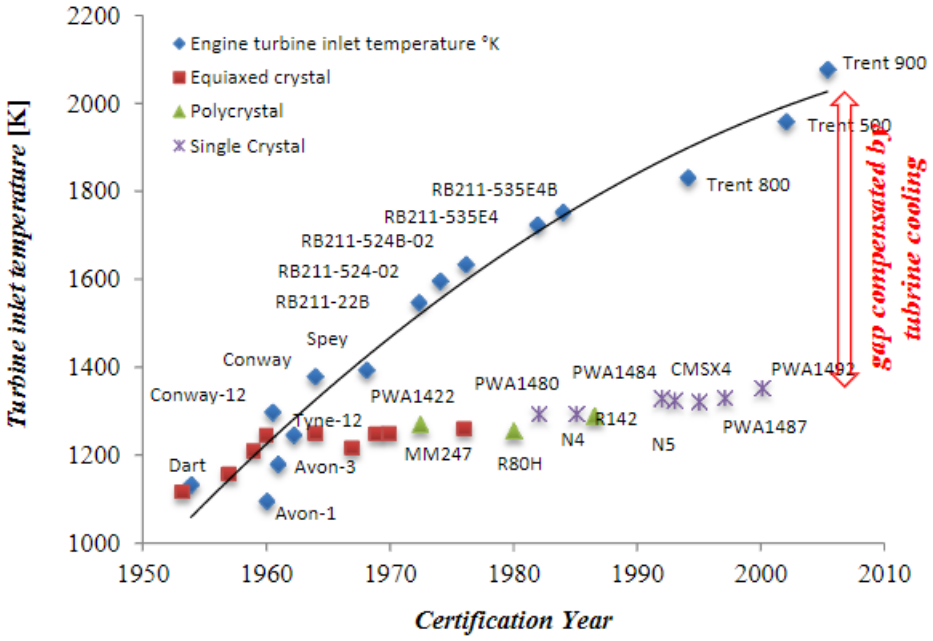

Figure 3.2: Turbine inlet temperature (TIT) trend over the last 50 years [2]

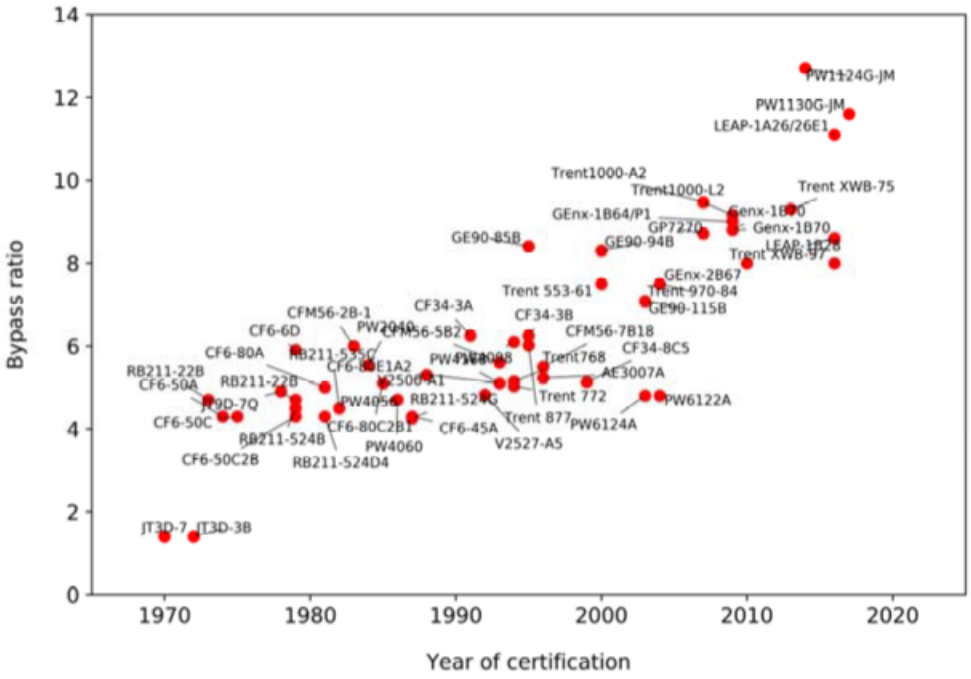

Figure 3.3: Bypass ratio (BPR) variation over the last 50 years [21]

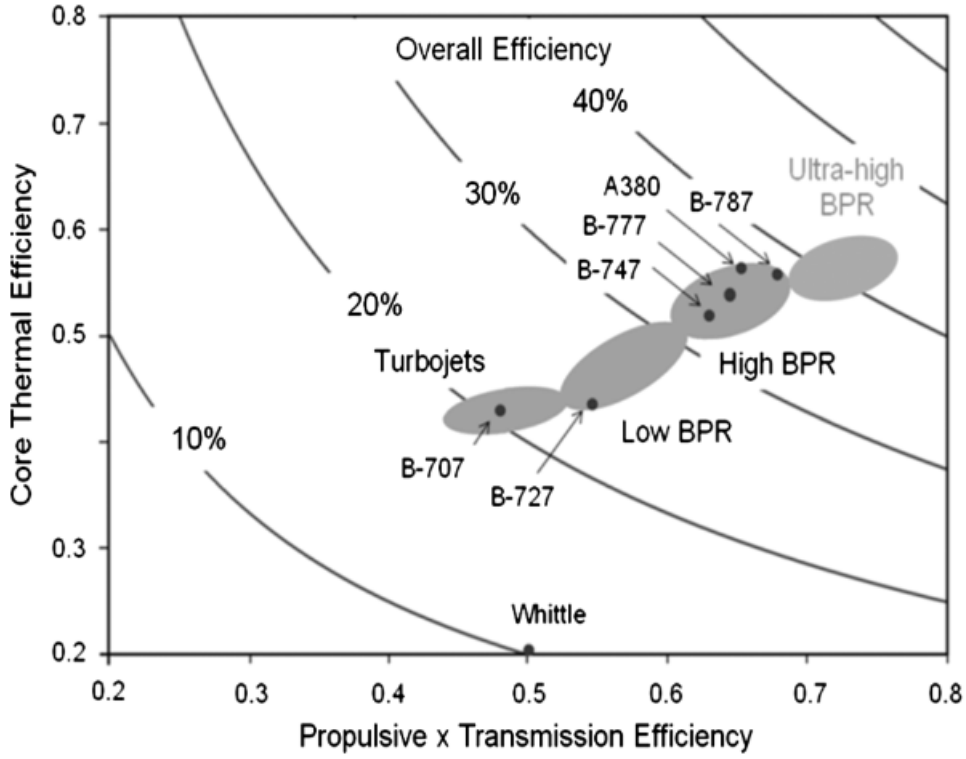

Figure 3.4: Core thermal and propulsive efficiencies for various commercial aircraft engines at cruise[23]

the stresses and weights of the disks. The increase in blade loading can also allow for a reduction of the number of stages, which decreases the weight of the compressor as well [25]. A higher stage loading, however, can lead to increased tip losses which can hurt the efficiency of the module. Furthermore, the aspects ratio of the blades is also being lowered. This increases the Reynolds number, and as a result the profile losses are reduced [21]. Variable pitch blades are used to increase the efficiency of the compressors at off-design conditions. The blades are rotated such that the flow incidence angle is optimum, given the flow axial velocity and spool speed. Furthermore, active clearance control is utilised for the turbines to ensure the optimum tip clearance that maximises the component efficiency and/or prevents blade abrasion.
The higher performance demands for turbomachines also requires different materials that can withstand the higher pressures and temperatures. Additionally, these also should possess a high fatigue strength and erosion/corrosion [26]. More advanced materials are also required to increase the durability and reliability of gas turbines. Another method that is used to deal with the high temperatures is turbine cooling. Here bleed air is used from one of the compressors. This air does not contribute to the cycle performance, thereby penalising the efficiency.

4

Data sources

In this chapter the data sources available and the challenges involved for modelling gas turbines are discussed. The limited amount of data available complicate the development of accurate engine models and have an impact on the health assessment of turbofan engines. Moreover, it forms an obstacle for MRO facilities to move towards more efficient and cost effective maintenance strategies. Having an overview of all the available data will aid with deciding on the modelling approach.

4.1. Challenges

Creating a reference model is challenging for modern turbofan engines due to the reduced number of sensors. Fewer sensors decrease the weight, cost and complexity of the engine [15]. Besides this obstacle, a lot of data is also proprietary to the original equipment manufacturer (OEM), and not available to the MRO (maintenance, repair and overhaul) provider [27, 28]. OEMs want to pursue other sources of income and are therefore showing more interest in the aftermarket. This is an interesting market as at least four times the engine purchase value is spent during its life-cycle [27]. By limiting the amount of available data and ways for interpreting data to the MRO, only the OEM can provide accurate prediction of the engine health and tailored workscopes. This way the OEMs can retain their competitive edge.

Kurzke [29] states that there is no amount of data that will allow to model every detail occurring inside an engine. However, the extend of the detail to be modelled depends on the application of the model. In some cases it is sufficient to have an agreement with the fuel flow and thermal efficiency of the measured data. Over- or underestimating some parameters in such a case does not matter. Kurzke also mentions that it does not make much sense to create a high fidelity model, if the amount of information available is scarce.

In an MRO environment various sources can be consulted to obtain data for modelling purposes. These will be discussed next.

4.2. Brochures and Official engine data

Not everything in advertising can be trusted. Additionally, the operating conditions for the given data are unknown, and probably inconsistent. Thus it will be difficult to create a thermodynamic model based on this information. Nonetheless, the information available in these brochures is fairly limited and often only consist of some overall performance parameters.

Official engine data should also be looked at more critically. Official engine data can be influenced by commercial aspects. Often data is only presented for a good or average performance engine and does not account for engine-to-engine differences or a worse performing engine. Official engine data is mostly proprietary to the OEM. The OEM provides a limited amount of data to the MRO provider, that describes the overall performance of the engine. This can be for example the exhaust gas temperature (EGT), the fuel and mass flow. It can be challenging to create an accurate model using this data only.

As an MRO provider KLM has access to MyGE and MyCFM portals. These contain flight data, engine manuals, and other technical documents useful for maintenance practices. The Prognos tool, used

for performance monitoring, also provides engine data from the manufacturer. The models used in this tool, however, are a black-box. It is not known how the data is processed and how computations are done. The reference engine model is for an average performing engine. The measured data is compared to the reference model in order to identify deterioration. Moreover, this tool also does not account for engine-to-engine differences.

4.3. Measured data

In flight and test cell measurements are available to the MRO. However, the measured parameters are limited for modern gas turbines due to the reduced amount of instrumentation.

4.3.1. Test Cell data

In bound and out bound test cell runs can be distinguished. The former is mainly done to confirm on-wing issues before the engine is repaired, and the latter is done to quantify the performance restoration and to demonstrate that the performance requirements for entering service again are met. Besides the performance, leak checks, acceleration tests and vibration tests are also conducted. The engine test cell of KLM at Schiphol Oost can facilitate the CFM56 and the CF6-80 engines. The GEnx and GE90 engines are tested at the test facility of AFI, Zephyr, at Charles de Gaulle Airport Paris. Test cell data is only available for ground, flight idle, maximum continuous and static take-off operating points. Calibrating a full engine model based on these operating points only is quite challenging, since these points do not cover the full operating range of the engine. As a result, only some small performance regions can be modelled with reasonable accuracy. The test cell data available for the CF6-80 and GEnx engines can be seen in Table 4.1. Notably, there are not sufficient measurements to determine the pressure ratios of the different turbomachines. Using this data only, creates an underdetermined system with a non-unique solution.

There are corrections applied to the test cell measurements to eliminate the test cell effects and make the data representative for free stream conditions. This is done using facility modifiers included in a correlation report provided by the OEM. They remain valid unless the test cell, testing equipment or data acquisition system is adapted. The calibration report also includes a range of measurement data for different N1 (low pressure) spool speeds. These can be useful for off-design modelling, more specifically component map tuning.

After maintenance or modifications of the test cell, back-to-back testing needs to be conducted. This is done to determine the possible impact on the test cell facility modifiers. During back-to-back testing, runs for multiple ratings of the same engine type are conducted. The operating points are mostly similar as for the in bound and out bound test cell runs. This data can also be used for off-design modelling purposes.

Factors that account for the installation effect are provided by the OEM. These are constant and have no dependency on flight conditions. The latter introduces some uncertainties when using this data. Additionally, the test cell measurements do not incorporate the effects for atmospheric distortion [20]. This can lead to slightly different inlet thermodynamic conditions as compared to the on-wing case. Moreover, during the test cell runs no bleed or power off-take is included. Another drawback of the test cell is, that the runs are only for sea level static atmospheric conditions. The atmospheric conditions cannot be addapted to represent other altitudes. A dedicated bell-mouth inlet is used for the engines during the test cell run. This inlet ensures steady non-distorted flow, as opposed to the on-wing inlet cowling.

Table 4.1: Available test cell measurements for the GEnx and CF6-80 engine

Parameter	Description	GEnx-1B	CF6-80
T_{t12}	Total fan inlet temperature	x	x
T_{t25}	Total HPC inlet temperature	x	x
T_{t3}	Total HPC outlet temperature	x	x
T_{t49}	Exhaust Gas Temperature (EGT)	x	x
T_{t5}	Total LPT outlet temperature	-	x
P_{t2}	Total fan inlet pressure	x	x
P_{t14}	Static pressure duct	-	x
P_{t25}	Static booster outlet pressure	-	x
P_{t3}	Static HPC outlet pressure	x	x
P_{t49}	Static HPT outlet pressure	-	x
N1	Fan speed	x	x
N2	Core speed	x	x
W_F	Fuel flow	x	x
$\dot{M}_{total}$	Total Mass flow	x	x
$\dot{M}_{Core}$	Core Mass flow	-	-
F_N	Net thrust	x	x
RHUM	Relative humidity	x	x

4.3.2. On-wing data

In flight data can be obtained from snapshots, and also from Continuous Engine Operating Data (CEOD) for modern turbofan engines. This data is recorded by the Full Authority Digital Engine Control (FADEC).

Snapshot data

The snapshot data is one of the data types recorded on-wing, and consists of one measurement for take-off and cruise phase. Prior to the introduction of CEOD, the snapshots were used for on-wing engine monitoring. These measurements are averaged over 10s in order to minimise measurement noise. It is not known if the data is taken during steady state conditions, and how it is decided at which moment during the flight phase the snapshot should be taken [13]. Additionally, GE did not provide any information on how the pre-processing of this data is done.

Continuous measurements

CEOD includes data from the complete mission, hence the user has the freedom of selecting the operating points as desired. For the GEnx-1B engine over 300 parameters are recorded during each flight. Unlike snapshots CEOD also contains secondary performance parameters. These are parameters related to variable geometry, bleed and power off-takes. Including this information in the model increases the accuracy [30] and is done by Otten [17].

Using CEOD data also has some drawbacks. The complex aerodynamic phenomenon occurring at the engine inlet, and installation effects introduce some modelling uncertainty. The thrust measurement is lacking [10], and the sensor data has more noise. The accuracy of the sensors of the GEnx engine is given in Table 4.2. Similar values are also expected for the CF6-80C2 engine. Furthermore, choosing incorrect operating points can lead to inaccurate results [20]. To calibrate the GSP engine model the operating point has to be chosen such that there is a thermal equilibrium (steady-state). Test cell data is most of the time recorded after a certain settling time, thus it can be assumed to be steady-state data. For the CEOD, steady state points have to be selected manually. Especially during take-off and climb the engine operates under highly transient conditions and the operating points need be selected carefully. Rootliep [8] uses the core speed rate of change to determine if the engine is operating at or near steady state. This is also one of the parameters included in the CEOD. An important parameter not included in the CEOD is the humidity. The humidity affects the gas properties and has a notable effect on the performance of the turbofan engines. Vuuren [31] researched the effects of humidity on the performance of turbofans and concluded that incorporating humidity effects increases the reliability

Table 4.2: Accuracy of the GEnx engine sensors [10]

Sensor	parameters	Range	Accuracy
Thermocouple	$T_{t,2}, T_{t,25}, T_{t,3}, T_{t,49}$	$-54 - 1137°C$	$\pm 1.1°C / \pm 0.4\%$
Frequency interface	N1, N2	$0 - 13,750 rpm$	± 0.12
Total pressure sensor	$P_{t,2}$	$1.6 - 20 psi$	± 0.01
Static pressure sensor	$P_{s,3}$	$5 - 750 psi$	± 0.36
Flow meter	W_f	$400 - 30,000 pph$	$\pm 3.5\%$

of the on-wing measured performance indicators. Note that for higher altitudes the humidity is lower, and consequently the performance will be less affected.
The gas path measurements available in the CEOD recordings can be found in Table 4.3. Besides these measurements, secondary performance parameters are also recorded and are given in Appendix D. The atmospheric conditions can be determined from typical data such as the flight altitude and Mach number. It should be kept in mind that CEOD is only available after the first 400 engine cycles. This means that the data is not representative for a new engine and cannot be used to create an engine model. The data recorded after a complete performance restoration can be used for modelling purposes. Eventhough there still will be some permanent degradation present, the data can be assumed to originate from a healthy engine.

Table 4.3: Available CEOD for the GEnx and CF6-80 engine

Parameter	Description	GEnx-1B	CF6-80
T_{t12}	Total fan inlet temperature	x	x
T_{t25}	Total HPC inlet temperature	x	x
T_{t3}	Total HPC outlet temperature	x	x
T_{t49}	Exhaust Gas Temperature (EGT)	x	x
T_{t5}	Total LPT outlet temperature	-	x
P_{t2}	Total fan inlet pressure	x	x
P_{t14}	Static pressure duct	-	x
P_{t25}	Static booster outlet pressure		x
P_{t3}	Static HPC outlet pressure	x	x
P_{t49}	Static HPT outlet pressure	-	x
N1	Fan speed	x	x
N2	Core speed	x	x
W_F	Fuel flow	x	x
$\dot{M}_{total}$	Total Mass flow	-	-
$\dot{M}_{Core}$	Core Mass flow	x	x
F_N	Net thrust	-	-
RHUM	Relative humidity	-	-

4.4. Geometric engine data

When engines are in for a shop visit, advantage can be taken from the availability of the engines to take geometric measurements. Different parameters such as cross-sectional areas, and cone angles can be acquired this way. Furthermore, some technical drawings are also available to the MRO operator, which can be used to complete the geometric measurements. This information will be useful for setting the design point, where the engine is sized.
When using measured data for modelling purposes one should be aware that the model will not generalise well to all engines of the same type. This is caused due to manufacturing differences, sensor variances, and geometry variations due to deterioration [32]. In previous work at KLM ES calibration factors (CFs) are applied for aligning the model with the engine of interest. These are also used to account for installation effects when using on-wing data [8–10].

5

Design and off-design modelling

Gas turbine modelling tasks are generally split into two parts. Firstly, on-design (design point) modelling is done to size the engine, which is subsequently used for off-design modelling. More recent work also discuss combined modelling in case data is available for multiple operating points. For the design point a critical operating point of the flight envelope, that the engine was designed to meet, is chosen. The top of climb, where the maximum corrected airflow is obtained, is the most commonly used condition. Off-design modelling mainly focusses on generating component characteristic maps, or tuning existing ones. These maps, which proprietary, describe the behaviour of the turbomachinery, and present the relation between the pressure ratio, corrected mass flow, spool speed and isentropic efficiency. This chapter describes gas turbine modelling in more depth. Additionally, common modelling practises in literature are also elaborated upon. Finally, the most promising optimisers found in the literature are presented.

5.1. Design point modelling

At the design point or cycle reference point the engine is sized, i.e., its geometry is defined. Consequently, a design point model is fixed and required prior to any other performance analyses. The design point of components in the detailed design phase can be different from the engine design point, depending on the sizing condition. For the concept phase, however, the same point can be used [33]. For the design point, turbo-machinery performance characteristics are not needed since all the required data for this operating point are considered to be known prior to using the characteristics. The design point data is also used as input for the characteristic component maps. The available data for the design point can directly be used as input for the design point computations. The component efficiencies can then be obtained iteratively by matching the known properties. The typical steps for turbofan cycle computations can be found in Appendix B.

For the cycle reference point, a critical operating point of the flight envelope that the engine was designed to meet is chosen [34]. This point is typically hot day take-off or top of climb for transport aircraft. The top off climb condition is used because it sets the maximum corrected airflow and maximum corrected engine speed [35]. For a high bypass ratio, separate flow turbofan designed for subsonic flight, the take-off condition, on the other hand, determines the maximum combustor exit temperature (T_4) for the engine [35, 36]. Furthermore, cruise is also taken sometimes as the design operating point [37]. Although cruise is not a critical operating condition, it is the longest flight regime for civil aircraft and the most fuel is burned during this phase. Thus, having optimal cycle performance conditions at cruise is also crucial. Avellan [38] classifies these points as follows:

- **The thermal design point:** The hot-day take off point where the highest temperatures can be found in the gas path.
- **The aero design point:** The TOC operating point with the highest corrected mass flow.
- **The energy design point:** This is the cruise operating condition, where energy efficiency is of high importance.

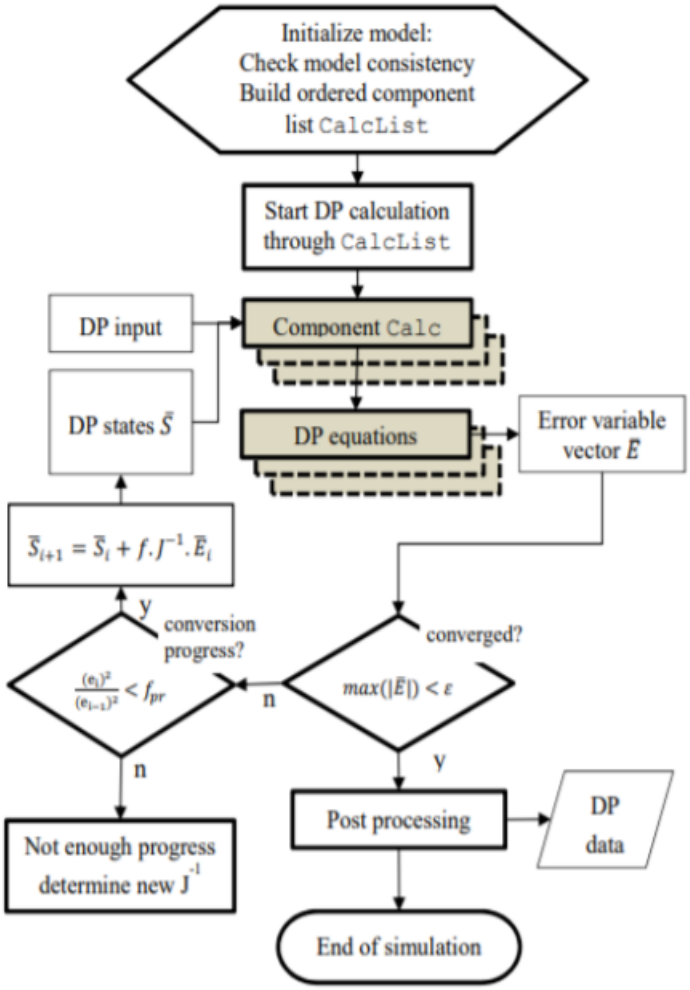

Figure 5.1: GSP design point modelling scheme [39]

There are some additional factors that should be considered when choosing a design point. Firstly, choosing operating points with variable geometry and off-takes should be avoided if possible. Often their exact settings are unknown and will cause uncertainty in the model. Secondly, the occurrence of condensation shocks at the engine inlet, at a certain relative humidity, should be considered as well. These can affect the engine inlet conditions by an uncertain amount [32]. Additionally, in order to neglect Reynolds number effects low power operating points should be avoided [32]. Viscous losses is one of these effects, which is higher at low Reynolds numbers. These also increase the modelling uncertainty.

The design point calculation procedure implemented in GSP is given in Figure 5.1[39]. An iterative procedure is used to minimise the errors of the design point equations by varying the cycle parameters and utilising the user specified design parameters as input. The iterations are halted once the specified tolerances are met.

Multiple approaches for design point modelling are available in the literature. These are briefly discussed next. Kurzke [29] uses an iterative procedure to match the measurement data. The open literature is used to check if the obtained parameters are in line with expectations and the technology level. Kurzke also mentions that it is practical to combine the fan core and booster in case sensors between these two components are lacking. It will not be possible to separate the performance of those two components in such a case. This has been done in the past, and proved to increase the accuracy of GPA [9, 10].

Sjögren *et al.* [40] uses data available in open literature, generic engine data and optimum relations for

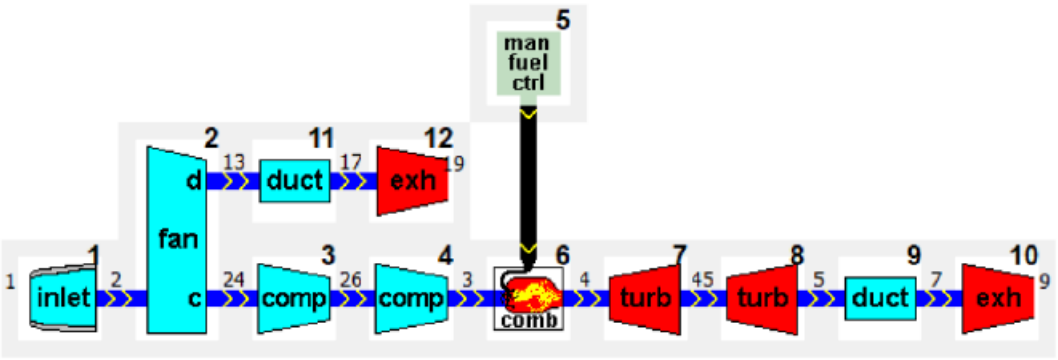

Figure 5.2: Turbofan model as implemented in GSP

design parameters to increase the model accuracy for a GEnx-1B engine. Contrary to this project he does not have access to measurement data. A method to tackle an under-determined problem is also discussed by Li *et al.* [41], however the focus is more on the cycle optimisation problem rather than estimating the unknowns using non-engine specific data. Similar work is also done by Li *et al.* [42], but using a non-gradient based approach for the optimisation. Stevenson [37] analyses which operating condition the most suitable is for the design point. He selects multiple operating conditions and creates a design point model for each of those points. Subsequently, he selects the point for which the exhaust nozzle areas are the closest to the actual measured areas of the engine. This turned out to be the top of climb (TOC) operating condition.

5.2. Off-design modelling

Once the engine has been sized using the design point data, the off-design modelling can be done. The design point is used as a cycle reference point, and its location should be specified on the component map. The map will then be scaled to this reference point such that the values of the corrected parameters at the design operating point are matched. This way, a generic map can used for an engine of interest. When for a fixed design point the operating condition of a gas turbine changes, the gas turbine will move to a different steady state condition in order to satisfy the laws of conservation between the different components along the gas path. These are the conservation of mass, momentum and energy. For these off-design conditions component characteristic maps are required that describe the performance of the components over the complete operating range. Depending on the change in operating conditions, each component will move to a unique point on its map for that specific setting. Thus the operating point of each component relies on the module they are linked or matched to. This is an iterative procedure where a scheme similar to the one for the design point calculations is executed repeatedly until the errors between the computed values and the ones read from the maps are sufficiently small.

Component maps are often proprietary to the OEM and not available in open literature. Consequently, modellers often attempt to generate these maps by themselves. Generic component maps are tuned in order to match off-design performance data. In order to get as close as possible to the actual maps, reference maps of components that are similar to the ones being modelled should be selected. The number of stages, pressure ratio, type of machinery (e.g., axial or centrifugal) and design mass flow should be the same to have the best accuracy [32]. In Figure 5.3 and Figure 5.4 a typical compressor and turbine map is illustrated respectively. The corrected parameter groups used in these maps can be seen in Table 5.1. They are corrected to the ISA values using Equation 5.1 and 5.2. This allows to compare the performance of different components of the same type.

Table 5.1: Corrected parameter groups used in performance maps

Parameter	Quasi-Dimensionless Group	Unit
Mass flow	$\dot{m}' = \frac{\dot{m}\sqrt{\theta}}{\delta}$	$\left[\frac{\text{kg}}{\text{s}}\right]$
Engine shaft speed	$N' = \frac{N}{\sqrt{\theta}}$	[rpm]

$$\boldsymbol{\delta} = \frac{\boldsymbol{p_{t,a}}}{\boldsymbol{p_{ref}}} = \frac{\boldsymbol{p_{t,a}}}{101325Pa} \tag{5.1}$$

$$\boldsymbol{\theta} = \frac{\boldsymbol{T_{t,a}}}{\boldsymbol{T_{ref}}} = \frac{\boldsymbol{T_{t,a}}}{288.15K} \tag{5.2}$$

The following curves can be seen in these graphs:

- **Constant efficiency lines:** These are the contours for a constant isentropic efficiency.
- **Constant speed line:** These are lines for constant (corrected) engine shaft speeds.
- **Surge line:** The surge line indicates where compressor stalling occurs. The latter occurs when the flow cannot withstand the adverse pressure gradient ($\frac{dp}{dx} > 0$), and causes flow separation and reversal consequently. Surging does not occur for the turbine due to the favourable pressure gradient ($\frac{dp}{dx} < 0$).
- **Choking area:** Here the maximum mass flow is obtained for a certain shaft speed and cross-sectional area. As mentioned before in Section 2.1, this can either occur for the front or the aft stages of the compressor depending on the shaft speed.

In off-design cycle evaluations, the compressor maps need to be evaluated numerically, which is not as straight forward as one would expect. The corrected speed and flow cannot always be used, since the speed lines are vertical in the high speed region. In the low speed region, in contrast, the speed lines are horizontal. The latter creates difficulties when reading the maps using the corrected speed and pressure ratio. This problem is tackled by introducing the so-called β-lines. An example of such a map is given in Figure 5.5[43]. By using these lines, which have unique intersections with the speed lines, the aforementioned problem is remedied. One of the map parameters together with a β-line value can be used to read the map. These β-lines can have a parabolic or linear shape, and often run parallel to the line going through the peak efficiency points on each speed line also depicted in Figure 5.5 and Figure 5.3, called the back-bone of the map. If the latter is the case the loading coefficient (Ψ) is constant along the β-lines. Furthermore, the β-line values vary from 0 for the lowest line to 1 for the highest line.

5.2.1. Underlying physics component maps

It is of foremost importance to check if the reference and produced component maps are in line with the underlying physics. This can be done using the Smooth C and Smooth T software [44, 45]by Kurzke. These computer programs can be used to check the quality, smoothen and generate component maps. Kurzke proposes several ways to check performance maps and the underlying physics. These will be discussed below.

Compressor map

The loss characteristics listed below can be used to check if the compressor maps are in line with the physics.

- $(\Psi - \Psi_{\text{is}}) - (\Psi - \Psi_{\text{is}})_{\text{min loss}}$ versus $(\Psi - \Psi_{\text{min loss}}) * |\Psi - \Psi_{\text{min loss}}|$: On the x-axis the squared distance from the peak efficiency point is expressed in terms of the difference in Ψ . On the y-axis a comparison in losses is made with the point of the maximum efficiency also using Ψ. In the lower speed range these become sensitive to small changes, thus it is best suited for the high iso speed lines.
- $1 - \frac{P_2}{P_{2,is}}$ versus β: On the x-axis one can find the β line values. The total pressure loss is given on the y-axis. $P_{2,\text{is}}$ is the pressure that would be obtained using the actual work in an isentropic process. This loss characteristic is suited for the full speed range.
- $|\Psi - \Psi_{\text{min loss}}|$ versus $\Phi - \Phi_{\text{min loss}}$: Here Ψ is the loading coefficient, and Φ is the flow coefficient. On the x-axis the distance from the minimum loss point is given in terms of the flow coefficient and the on the y-axis the same, however, now in terms of the absolute loading coefficient. This characteristic is suited for maps with non-vertical speed lines.

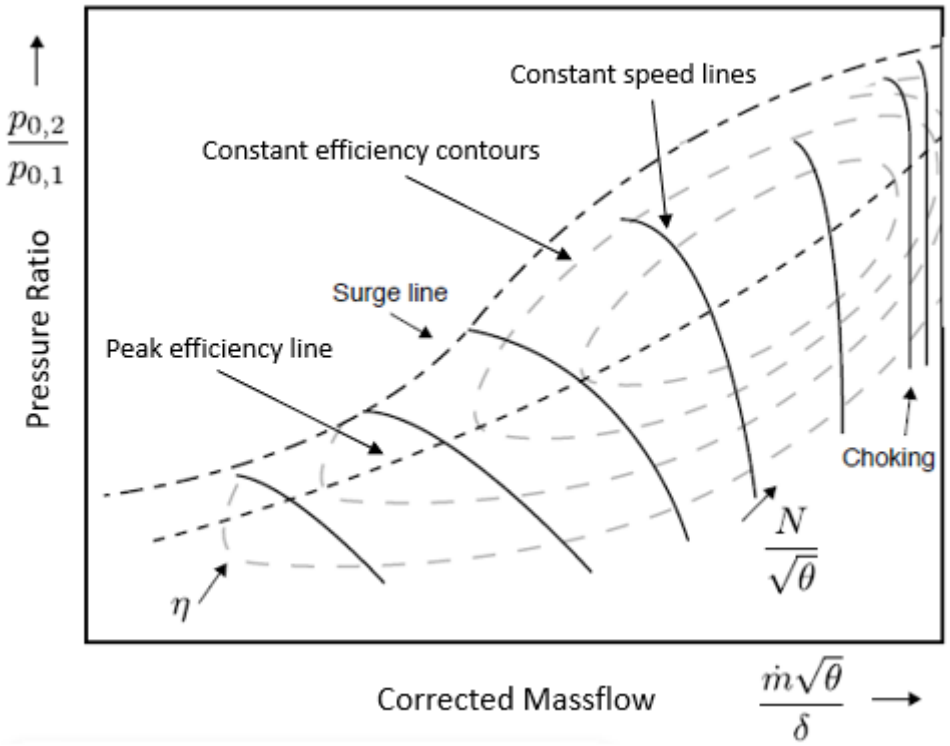

Figure 5.3: Typical map of an axial compressor

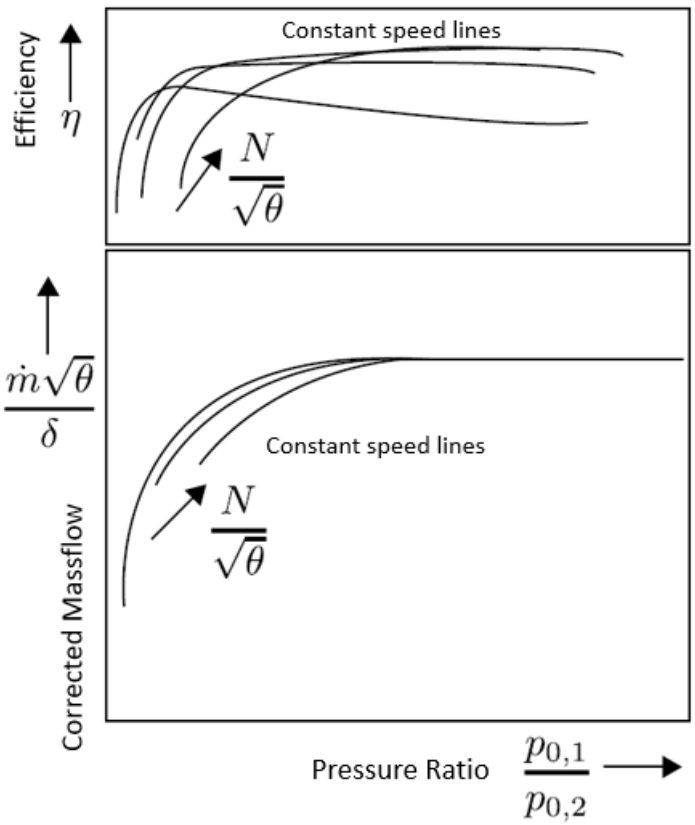

Figure 5.4: Typical map of an axial turbine

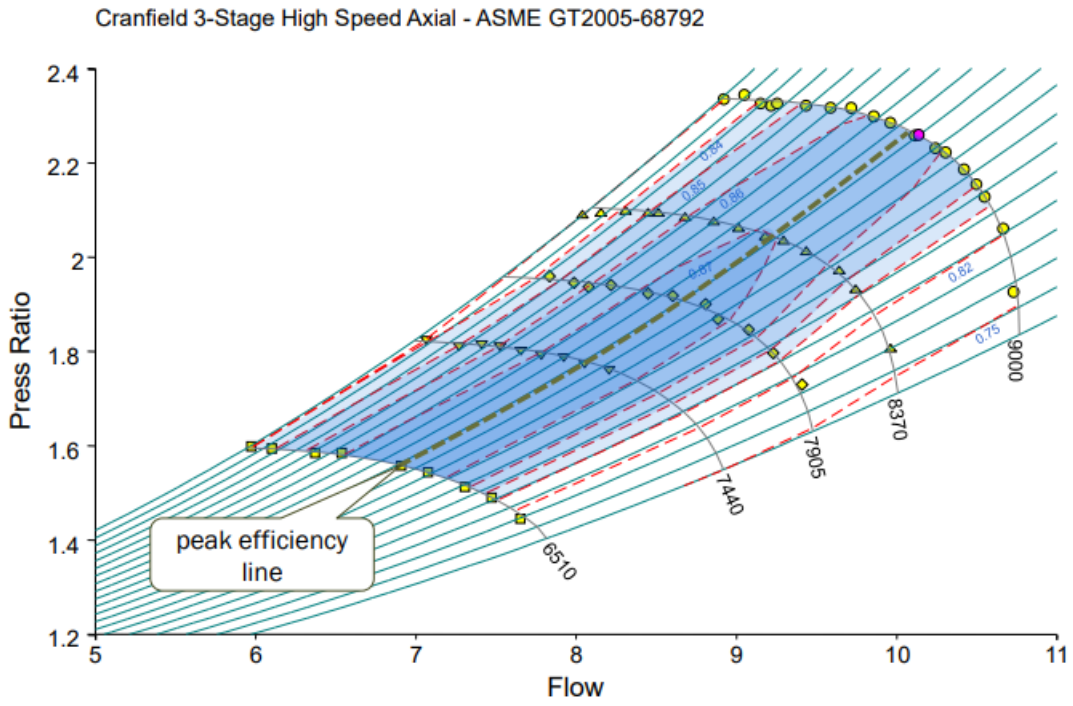

Figure 5.5: Typical map of an axial compressor with β-lines [43]

These loss characteristics should have a bucket, independent of speed, where the losses are minimal. Furthermore, the speed-flow and speed-work relations can be visualised as well in order to check for inconsistencies. Following incompressible compressor theory the specific work is proportional to velocity squared. Hence, at zero velocity the work will be zero as well. Additionally, the specific work can become negative as well, before passing through the origin. This occurs at windmilling conditions for very low speeds. If there is variable geometry present there will be kinks in the beta lines at certain speed values. The latter is expected to be minimal, since the effects of variable geometry are not explicitly modelled during this study.

Kurzke [43] also discusses hidden correlations in compressor maps, and how these are influenced. Some of the main findings are presented subsequently. For subsonic compressors there generally should be a noticeable difference (decreasing with speed) between the surge and choke mass flow. For maps with vertical iso speed lines the maximum efficiency on a line is attained at the point where the maximum corrected mass flow starts decreasing.
Furthermore, the vertical speed lines in compressor maps are elaborated upon as well. The vertical speed lines can be the result of supersonic flow conditions at the compressor inlet (rotor) or choking of the compressor outlet (stator). This can be identified by analysing the specific work over pressure ratio graphs. If the constant speed lines in this graph are horizontal, then the outlet is choked. Decreasing the pressure ratio in this case does not effect the flow field of the rotors. As the rotors do all the work, the specific work remains constant. If the contours are not horizontal, i.e., the specific work is not constant, then the first rotor experiences supersonic flow. Reducing the pressure ratio effects the flow field in the rotor, thereby changing the specific work. Finally, it is mentioned that a map intended for a compressor with variable geometry should not be used for simulating a module of which the geometry is invariant. The other way around, on the contrary, is allowed by using a schedule for the variable geometry

Turbine map
For a turbine map it is difficult to visualise the efficiency contours. For this reason the following loss characteristics can be used to check if the efficiency islands are smooth and coherent with physics:

- $(\Psi - \Psi_{is}) - (\Psi - \Psi_{is})_{min\ loss}$ versus $(\Psi - \Psi_{min\ loss}) * |\Psi - \Psi_{min\ loss}|$: This is identical to the first loss characteristic for compressor maps.

- $1-\frac{P_2}{P_{2,is}}$ versus $W^*\sqrt{T_2}/P_2-\left(W^*\sqrt{T_2}/P_2\right)_{\text{min loss}}$: Here W is the mass flow, and P is the pressure. On the x-axis one can find the distance from the peak efficiency point expressed in terms of the corrected mass flow. The total pressure loss is given on the y-axis.
- $|\Psi-\Psi_{\text{min loss}}|$ versus $\Phi-\Phi_{\text{min loss}}$: This is similar to the third loss characteristic of the compressor.

Similarly to the compressor map loss characteristics, there should be a bucket as well where the minimum losses occur that is consistent with speed.
The turbine velocity ratio (blade over jet speed) - static efficiency is another relation that can be inspected to validate the underlying physics. For a single idealised turbine stage the static efficiency change with turbine velocity ratio is parabolic. The maximum efficiency occurs at the optimum incidence angle (zero) and is only dependent on the turbine stator exit angle. At turbine velocity ratios lower or higher than the peak efficiency, the incidence angle is suboptimal and the efficiency is penalised as a result. In a real case this behaviour is similar, and the maximum efficiency should be attained for a velocity ratio between 0.4 and 0.5 [46].
Moreover, the trends in a mass flow over speed plot with constant beta lines should be consistent for both, the high and low flow area. Furthermore, the first stator of highly loaded turbines is usually choked. In this case the maximum mass flow is constant for a large part of the map and independent of speed. If the latter is not the case, the maximum (corrected) mass flow will slightly decrease with the (corrected) spool speed.

5.2.2. Combined modelling

Several attempts have been made in order to combine on-design and of-design modelling [35, 47, 48] . The latter can be useful if the on-design data is very limited, and data for multiple operating points is available. For this approach the design point parameters and performance maps are adapted each iteration. The objective for such a modelling approach is to match performance and cycle parameters defined for multiple operating points. These are called the target parameters. They can be used as equality or inequality targets. There are also synthesis variables. These can either be fixed or varied during the multipoint procedure [47]. Typical operating points that are used for the multi-point approach are the take-off, top of climb and cruise.

5.2.3. Performance maps generation

Various methods for component map tuning can be found in the literature. Most of these studies, such as the study by Yan *et al.* [49], consist of developing analytical solutions for the component performance maps. Tuning factors are then used to modify these analytical maps in order to fit experimental data. These methods have proven to be effective and reliable. There is, however, much more data required in order to produce accurate results. The data need to be sufficient in order to generate the iso speed lines. Additionally, using analytical solutions can easily lead to unphysical maps. Due to the reasons mentioned above it has been decided not to use analytical map solutions.
One of the most promising methods found in the literature for component map generation/tuning, that did not include parametrisation of the maps, was the work conducted by Li *et al.* [50]. Li *et al* proposes a scaling method for reference characteristics maps using a second order polynomial function defined in Equation 5.3. Here ***a***, ***b***, and ***c*** are the polynomial coefficients. The subscript ***x*** denotes the characteristic parameters, which are the pressure ratio (PR), efficiency (η), and corrected mass flow (W_c). L_{DP} and L_{OD} represent the relative non-dimensional rotational spool speed for the design and off design point, respectively. It should be noted that ***a*** is set to unity in order to keep the scaling factor to 1 at the design point. This means that at the design point the model is assumed to be calibrated, and this point will remain unmodified during the adaption process. A minor drawback of this choice is that the modifications close to the reference point will be small. The effect of scaling polynomial coefficients on the scaling factors can be seen in Figure 5.6. Additionally, it can also be noticed that the scaling factor at the design point (DP) is equal to unity.
The coefficients for the scaling functions are in this reference determined using Genetic Algorithms. Multiple component maps were adapted simultaneously, and the results postulate that the approach was effective. It has been decided to continue with this method.

$$SF_X = a + b\left(\left|\frac{L_{\text{OD}} - L_{\text{DP}}}{L_{\text{DP}}}\right|\right) + c\left(\left|\frac{L_{\text{OD}} - L_{\text{DP}}}{L_{\text{DP}}}\right|\right)^2 \tag{5.3}$$

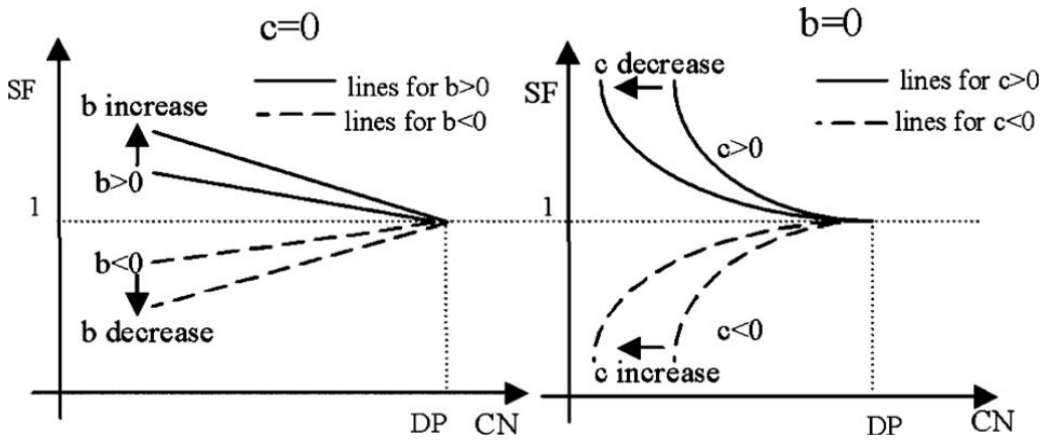

Figure 5.6: Variations of the scaling equations [50]

5.3. Optimisers

As mentioned above the unknown parameters need to be adapted such that the known cycle parameters(measurement data) are obtained. To make this matching process efficient an optimiser, which minimises the difference between computed and measured cycle parameters, needs to be included in the design procedure. The optimisers that can be used are limited to non-gradient based methods, since the Jacobian of the system of equations is not available to the user in GSP. Discrete gradients can be computed, however, are computationally expensive. Furthermore, deterministic methods are avoided due to their difficulties to handle noise. Different non-gradient based optimisers were found in literature and are described in the literature study conducted by the author [51]. From the conducted literature study two of the most promising optimisers were Genetic Algorithm (GA) and Bayesian Optimisation (BO). These are able to deal with noise, local minima and there are readily available Python implementations. The two above mentioned optimisers will be discussed next.

5.3.1. Genetic Algorithm

Genetic algorithms (GA) is a nature inspired algorithm [48]. Nature inspired algorithms are based on processes in the nature. They incorporate the intelligence found in biological evolution, swarm behaviour and physical processes. GA have been applied in the past at KLM ES. Rootliep [8] employed GA to account for the fewer instrumentation in modern turbofan engines. Otten [17] used GA to find correlations between the secondary performance parameters and the component health parameters. Genetic algorithms, a part of evolutionary algorithms, are based on the principles of evolution. They mimic a survival of the fittest process, and consists of the following main steps:

- **Selection:** Individuals are chosen for the next generation based on their fitness value.
- **Crossover:** Swapping entries of the parameter vector in order to create new individuals.
- **Mutation:** Introduces random changes into the parameter vector.

These steps are executed for each population until the predefined number of generations or termination criteria is reached. GA in its standard form cannot deal with constraints. A workaround method for this is to add a penalty to the objective function if the constraint is not met. This method is not deterministic of nature and can deal with noise and handle underdetermined systems. The Pseudocode for GA can be seen below.

Pseudocode Genetic Algorithm

1: **Initialization**
2: Population size N
3: Define objective function f(X)
4: Define set of functions and terminals

Initialize the population of programs
Compute the fitness of the initial population
Choose the genetic operators
Define termination criteria, if any
Maximum number of iterations MaxIter
iter = 1
while (iter $\leq$ MaxIter) **do**
    Select parents for mating and reproduction
    Apply crossover and mutation (optional) to produce offspring
    Strategically choose the next generation population (N)
    Compute the fitness values of the entire population
    if Termination criteria **then**
        Exit
    end if
    iter = iter + 1
end while
Program with highest fitness value is the global optimum solution

5.3.2. Bayesian optimisation

Bayesian optimisation[52] (BO) is a derivative free optimisation strategy for functions whose internal structure is unknown, also known as black-box functions. Such functions are difficult and take a lot time to evaluate. Furthermore, it is suited for continuous functions consisting of fewer than 20 dimensions. It has a stochastic nature and withstands noise. A Bayesian optimisation builds a surrogate of the objective function using Gaussian process regression. The latter is a statistical function building method for modelling functions. Bayesian optimisation aims to find the optimal solutions with the least amount of objective function evaluations. On a different note, the goal of Bayesian optimisation is not to find the best solution. For this approach the constraints are incorporated by adding penalties to the objective function. The Pseudocode and the common terms used for BO can be seen below.

Pseudocode Bayesian Optimisation

Initialization
Place a Gaussian process prior on *f*
Observe *f* at n_0 points according to an initial space-filling experimental design.
Define termination criteria, if any
Set maximum number of function evaluations, *N*
Set $n = n_0$.
while $n \leq N$ **do**
    Update the posterior probability distribution on *f* using all available data
    Let x_n be a maximizer of the acquisition function over *x*, where the acquisition function is computed using the current posterior distribution.
    Observe $y_n = f(x_n)$.
    if Termination criteria **then**
        Exit
    end if
    n = n + 1
end while
Return a solution: either the point evaluated with the largest *f(x)*, or the point with the largest posterior mean.

- **Gaussian process prior:** Assumes that the objective function can be modelled using a Gaussian/Normal probability distribution.
- **Posterior probability distribution:** This a combination of the prior distribution and the information extracted from new data points, originating from the likelihood function. The posterior

distribution describes the 'fitness' of new coordinates.

- **Termination criteria:** The termination criteria for Bayesian optimisation can be the maximum change between two subsequent objective values.
- **Acquisition function:** This function utilises the information provided by the posterior distribution to evaluate the objective value for some candidate point $\boldsymbol{x}$.

6

Physical relations

As can be concluded from Chapter 4 and 5 the modelling problem is underdetermined and will not have a unique solution. Additionally, there are no robust strategies found in the related work that deal with the fewer measurements, and design data. For these reasons, additional relations need to be introduced that reduce the difference between the number of unknown parameters and available equations. Relations that can be used, obtained from open literature, can be found in this chapter. These include semi-empirical and optimum parameter relations. Prior to implementing the obtained relations, they will be verified using an existing engine model.

6.1. Estimating efficiencies

This section presents methods found in literature for estimating the polytropic efficiency of the turbomachinery. These are based on historical turbomachinery experimental data and can be used during the preliminary design or modelling.

6.1.1. Polytropic efficiency as a function of stage loading

Walsh *et al.* [33] provides some correlations for the polytropic efficiency of the fan and compressor. These are depicted in Figure 6.1 and Figure 6.2. The polytropic efficiency for the components is correlated against the (average) stage loading. These charts are applicable for large civil turbofan engines. The correlation for the fan can separately be applied to the pitch line of the fan root and tip. Note that the fan efficiencies should be reduced by 1.5% if snubbers or clappers[1] are installed to provide acceptable vibrational properties for the fan blades. These graphs can be incorporated as constraints. The obtained polytropic efficiency and loading should be in line with the trends depicted in these graphs.

[1] These are ring-like structures going through the middle of the fan

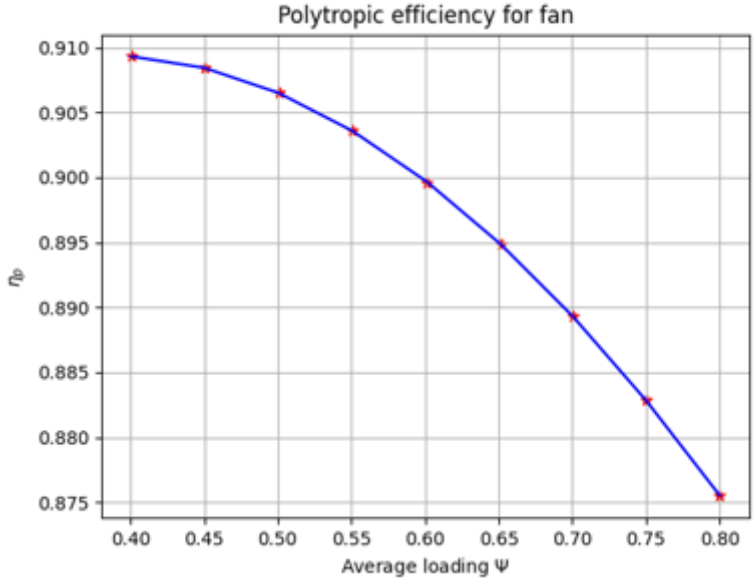

Figure 6.1: Stage loading against polytropic efficiency for the fan [33]

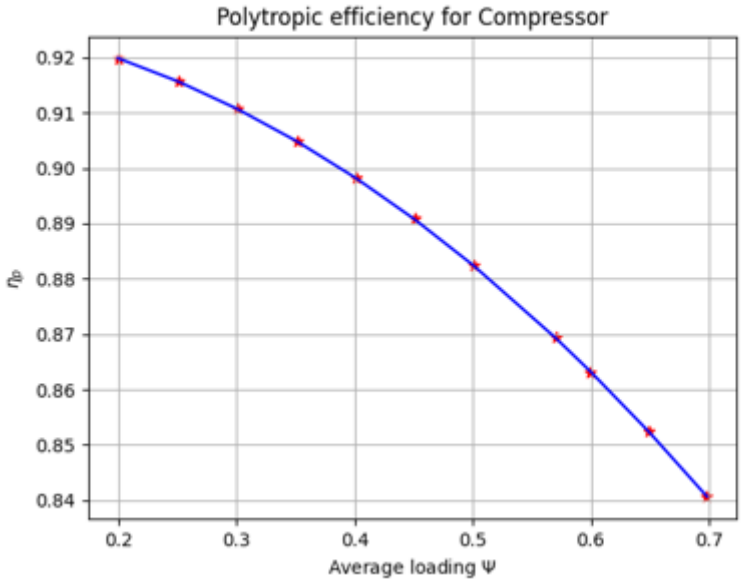

Figure 6.2: Average stage loading against polytropic efficiency for the compressor [33]

6.1.2. The Smith Chart

Originally developed by Smith [53], the Smith chart consists of constant isentropic efficiency lines as a function of the loading and flow coefficient. Smith created this chart based on experimental data from 70 different turbines. The contours are empirical, however, within one percent of the experimental data. The initial chart is for a 50 % reaction stage with zero tip leakage, and can be seen in Figure 6.3. The effects of the blade aspect ratio, and the space to chord ratio are also not incorporated in this correlation.

A more recent version of of the Smith chart is published in the book by Walsh *et al.* [33], and is for a higher technological level. The latter can also be concluded by comparing the initial and the updated chart depicted in Figure 6.4. It can be observed that the revised chart has higher efficiencies and the

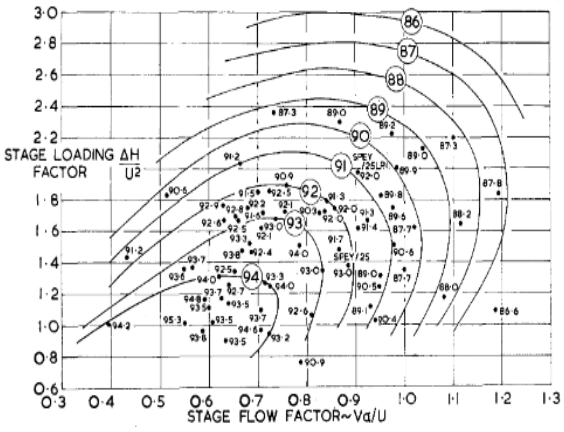

Figure 6.3: Original Smith Chart[53]

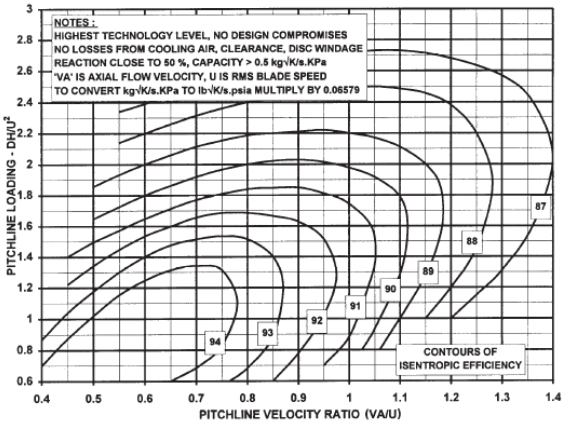

Figure 6.4: Modified Smith chart[33]

iso lines are shifted to the right. This chart is also produced for a stage reaction of 50 % and excludes the effects of the various factors mentioned above for the initial chart.

6.2. Turbomachinery Loading, flow coefficient and degree of reaction

The performance of turbomachines can be described by three dimensionless parameters. These are defined in Table 6.1. The coefficients are local and can uniquely be defined for each stage. Notably, there are two definitions for the load coefficient, which are commonly used. The load or work coefficient (Ψ or λ) gives an indication of the work capacity and aerodynamic blade loading of the stage. The flow coefficient (ϕ) is a measure of the flow capacity of the stage. The degree of reaction (r^*) is a measure of the static expansion or compression in the rotor. With these three parameters the velocity triangles of the stage can be determined, which are useful for the performance analyses of turbomachinery — especially in the conceptual design phase. Typical velocity triangles for a compressor and turbine stage can be seen in Figure 6.5. Here *U* is the tangential velocity, *V* is the absolute velocity and *W* is the relative velocity.

Table 6.1: Duty coefficients

Coefficient	Description	Equation
Ψ	Load coefficient	$\frac{w}{U^2}$
λ	Load coefficient	$2\frac{w}{U^2}$
ϕ	Flow coefficient	$\frac{V_m}{U}$
r^*	Degree of reaction	$\frac{\Delta h_{rotor}}{w}$

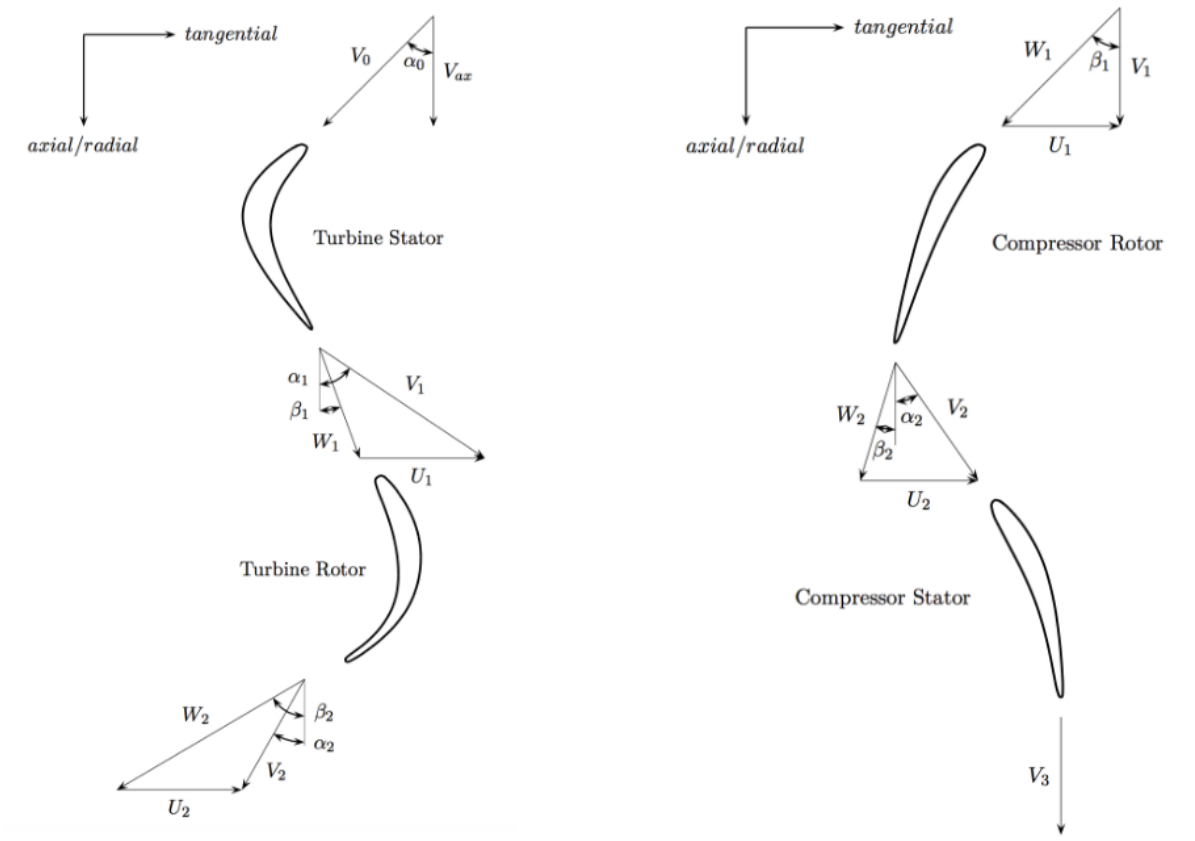

Figure 6.5: Typical velocity triangles for a compressor and turbine stage

How the velocity triangles can be determined from the above mentioned coefficients are given by Equation 6.1 and Equation 6.2, for the compressor and turbine respectively.

$$\begin{aligned}
\lambda &= 2\left(-\phi \tan\alpha_1 + \phi \tan\beta_2 + 1\right) \\
r^* &= -\frac{\lambda}{4} - \phi \tan\alpha_1 + 1 \\
\tan\beta_1 &= \tan\alpha_1 - \frac{1}{\phi} \\
\tan\alpha_2 &= \tan\beta_2 + \frac{1}{\phi}
\end{aligned} \tag{6.1}$$

$$\begin{aligned}
\lambda &= 2\left(\phi \tan\alpha_1 - \phi \tan\beta_2 - 1\right) \\
r^* &= \frac{\lambda}{4} - \phi \tan\alpha_1 + 1 \\
\tan\beta_1 &= \tan\alpha_1 - \frac{1}{\phi} \\
\tan\alpha_2 &= \tan\beta_2 + \frac{1}{\phi}
\end{aligned} \tag{6.2}$$

In the literature various values can be found for turbomachinery loading, flow coefficients, and degree of reaction. Some typical values from different sources are given in Table 6.2. For the degree of reaction, a value of 0.5 is often recommended [7, 54]. This indicates that 50 % of the enthalpy change of a stage occurs in the rotor and 50 % in the stator. This averts large pressure losses, hence increases the efficiency of the process [7]. Furthermore, the loading for high pressure turbomachines is generally higher than for the low pressure ones.

Table 6.2: Typical loading flow and loading coefficients

Source	Module	Loading coefficient	Flow coefficient
Lewis [54]	Compressor	0.4-0.45	0.5-0.9
	Turbine	-	0.6
Walsh *et al.* [33]	Compressor	0.25-0.5	-
Saravanamuttoo *et al.* [7]	Fan	-	0.4 -1
	Turbine	3-5	0.8-1.0
Dixon *et al.* [55]	Compressor	0.4	0.4-0.8

6.3. Nozzle coefficients

For gas turbines the exhaust nozzles are of high importance. Typically, a turbofan engine has two nozzles, namely a core and a bypass nozzle. Even though they are the final component the flow has to move through, they can still affect the operating line of the engine. The latter is explained by means of Figure 6.6. Here a constant corrected mass flow indicates that the module is choked. It can clearly be observed how a choked nozzle fixes the operating point of the turbines. The turbines are connected to the compressors through the shafts, and consequently also determine the operating points of these modules on the cold side of the engine.

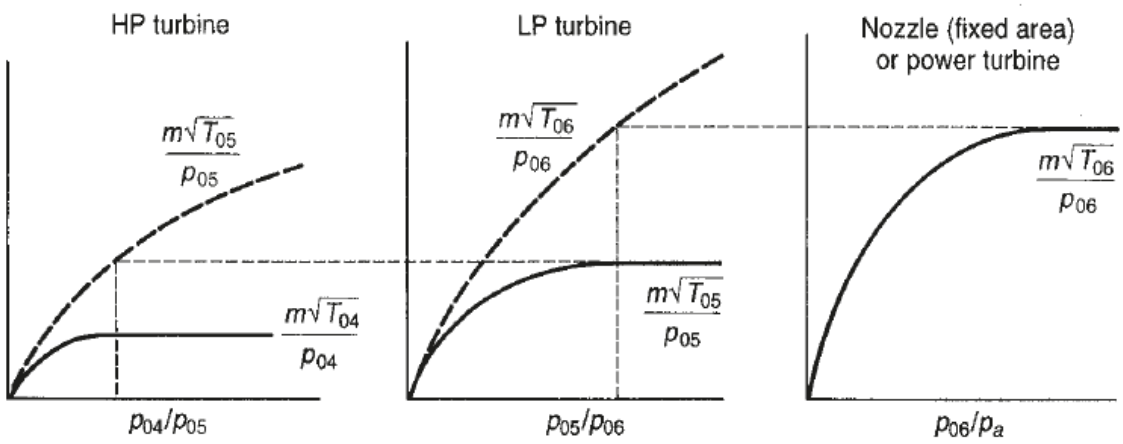

Figure 6.6: Component matching for the hot side (after combustor) of the engine [7]

To describe the performance of nozzles, three coefficients are typically used. These are the velocity coefficients (C_V), the discharge coefficient (C_D) and the thrust coefficient (C_X) [4, 33]. They describe the ratio of the real over the ideal property. C_V accounts for the pressure losses at the exhaust plane caused by viscous flows. C_D is used to incorporate the effects of the boundary layer formation inside the nozzle. This reduces the effective nozzle area and can be seen as blockage. An imperfect expansion can also introduce losses at the nozzle exit. For such a case the flow in the nozzle is not expanded to the free stream ambient pressure, and the thrust has a pressure term. Ideally, the thrust would only consist of a momentum term. The ratio of the actual thrust over the ideal thrust due to the underexpansion is C_X.

6.4. Optimum parameter relations

Next optimum parameter relations are discussed that can be utilised to extend the system of equations and thereby reducing the numbers of unknowns. It should be noted that an assumption has to be made first, stating that a specific parameter has been optimised during the design of the gas turbine. In reality, it is never known which parameter(s) are optimised during the design of an engine.
Guha [56] derived a model for the optimum fan pressure ratio. The obtained relation can be found in

Equation 6.3, where *B* is the bypass ratio and *M* is the flight Mach number. This equation is obtained by first determining the velocity ratio V_{jc}/V_{jh} that maximises the net thrust F_N for a constant fuel consumption. The outcome was found to be $V_{jc}/V_{jh} = \eta_{KE}$, with η_{KE} being the efficiency of energy transfer between the core and bypass, and is given by Equation 6.4. η_{NB} is used for the bypass nozzle -, and η_f for the fan isentropic efficiency. Next, this velocity ratio relation is utilised to obtain the equation for the optimum fan pressure ratio. For this derivation it is assumed that the fan and bypass nozzle are isentropic.

$$(\mathrm{FPR})_{\mathrm{op}}^{(\gamma-1)/\gamma} = 1 + \frac{(\gamma-1)}{2+(\gamma-1)M^2} \times \left[\frac{(1+B)^2}{(B+1/\eta_{\mathrm{KE}})^2} \left\{ \frac{\hat{F}_N}{\sqrt{\gamma R T_a}} + M \right\}^2 - M^2 \right] \tag{6.3}$$

$$\eta_{\mathrm{KE}} \approx \eta_{\mathrm{LPT}} \eta_f \eta_{\mathrm{NB}} \eta_{\mathrm{mech}} \tag{6.4}$$

7

Engine description and Data availability

This chapter describes the selected engines and data sources used for developing the systematic modelling approach. To prove the validity of a systematic approach two engines will be used as test cases, namely the CF6-80C2 and the GEnx-1B. It is also important to consider the health of the engine when selecting test cell or on-wing data. The engine should be representative for all the other engines of the same type. The data used as input is also presented.

7.1. Engine description

In this section the selected engines used for analyses during this project are briefly discussed. These are the CF6-80C2 and the GEnx-1B engine as mentioned before. For both these engines KLM ES provides its MRO services. The engines are either from the KLM fleet or external clients.

The CF6-80C2 engine

The CF6-80C2 is a twin spool turbofan engine that is propelling multiple widebody aircraft models, amongst which the Boeing B747-400, the Airbus A300, and the Lockheed C-5M. This engine entered service in the 1980s, and it forms the largest installed group of widebody engines up to date. With a bypass and overall pressure ratio of around 5.1 and 30.4 respectively, the CF6-80C2 is able to deliver a static thrust of 263kN. Moreover, the fan has a diameter of 2.36m. The LPC and HPC consist of 4 and 14 stages, respectively. The turbines contain 2 and 5 stages for the high and low pressure system, respectively.

The CF6-80C2 engine has variable geometry integrated for performance control. These are the Inlet Guide Vanes (IGV) and Variable Stator Vanes (VSV). They are rotated to an optimal angle (relative to the airflow) by the electronic engine control (EEC) to prevent surging of the compressor. This way stable operation is ensured over a larger operating range and the efficiency is improved. By adapting the geometry of the compressor, its map is modified as well, since closing the VSVs and IGVs reduce the pressure ratio and mass flow for the same corrected iso-speed line [4]. Variable bleed valves are also present to control the engine's performance, especially at unstable low speed operating regions. Excess booster air is directed from the core to the bypass in order to improve the surge margin of the HPC. The latter causes the compressor operating line to shift away from the surge line.

Moreover, power and parasitic bleed off-takes are also present in the engine. The power off-takes are used to fulfil power demands for electrical systems. Parasitic bleed air is used for turbine or internal cooling, anti-icing, active clearance control (ACC), core compartment cooling (CCC) or for some aircraft requirements such as cabin pressurisation. ACC is employed for the turbines or their casing in order to prevent abrasion of the blade tip, and ensure an optimal tip clearance that improves the turbine efficiency. ACC is required due to the centrifugal forces originating from the high spool speeds, and the thermal expansion caused by the elevated temperatures. Additionally, the clearance between the HPT blades and casing are also controlled for the same reasons as mentioned before. Air for ACC and CCC is extracted from the bypass flow.

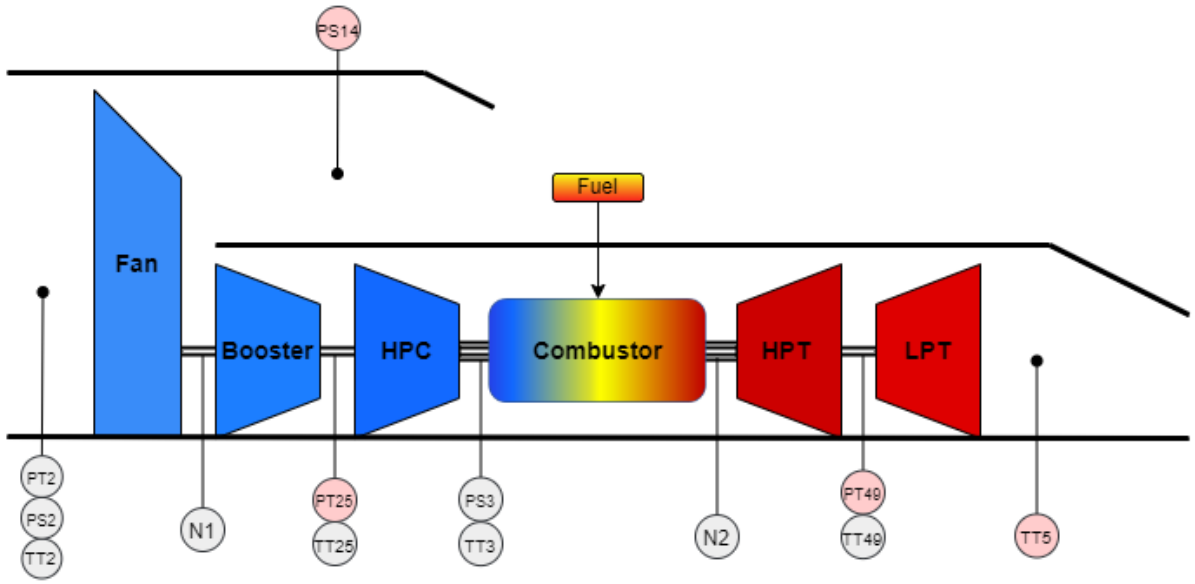

Figure 7.1: Drawing illustrating sensor positions for the CF6-80C2 and GEnx-1B engine. All the indicated sensors are installed on the CF6, while the GEnx only contains the grey ones.

A model for the CF6-80C2 has been created in the past by den Haan [9]. The model is acceptable, however, choices for performance parameters are not substantiated and the modelling approach is not clear. Furthermore, not all the available data within the MRO environment is leveraged. This includes the exhaust nozzle areas. Verbist [13] has also done some extensive analysis for gas path analysis using the CF6-80 engine for his PHD project.
The available sensors for this engine can be seen in Figure 7.1. Note that all the indicated sensors in this figure are installed on the CF6-80C2. Their positions are also described in Table 7.1. It can be observed that no measurements are available between the fan core and booster. Therefore it is a good choice to merge the fan core and booster as mentioned before in Section 5.1.

The GEnx-1B engine

The GEnx-1B (General Electric Next-generation), entering service in 2008, is one of the latest turbofan engines and a successor of the CF6 engine. It propels the Boeing 787 Dreamliner and is also a twin spool engine with a fan diameter of 2.82m, consisting of state of the art composite fan blades. With a bypass and overall pressure ratio of around 9 and 46 respectively, the GEnx-1B is able to deliver a static thrust of 330kN. The GEnx-1B has relative to the CF6-80C2 not only a better fuel efficiency, but also lower emissions and noise. The compressors consist of 4 and 10 stages for the low and high pressure modules, respectively. While the HPT and LPT have 2 and 6 stages in the respective order.
The vast majority of the control and cooling devices from the CF6-80C2 turbofan engine are also installed on the GEnx-1B. Bleed air for some additional purposes is extracted, namely: transient bleed valve (TBV), booster-anti ice bleed (BAI) and the cowling anti-ice bleeds (CAI). The TBV is used to unload the compressor during starting, acceleration, and in icing conditions [7]. It functions in a similar way as the VBV and the extracted air is discharged into the bypass.
Moreover, the GEnx-1B engine does not have to deliver any customer bleed air. This owing to the full electric pressure system of the Boeing 787 cabin which does not require pressurised bleed air from the engine.
This engine has been modelled in the past by Van Moorselaar [10], however clear argumentation and description of the design choices are lacking. Rootliep [8] developed a Multi-Operating Point Gas Path Analysis (MOPA-EA GPA) tool for the GEnx-1B engine in order to deal with the fewer sensors. While Otten [17] developed a tool to include the secondary performance parameters in the health monitoring process.

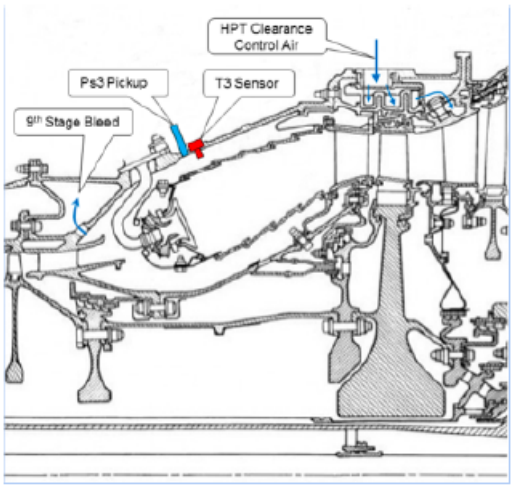

Figure 7.2: T3 and PS3 location for the CFM56-3 engine [57]

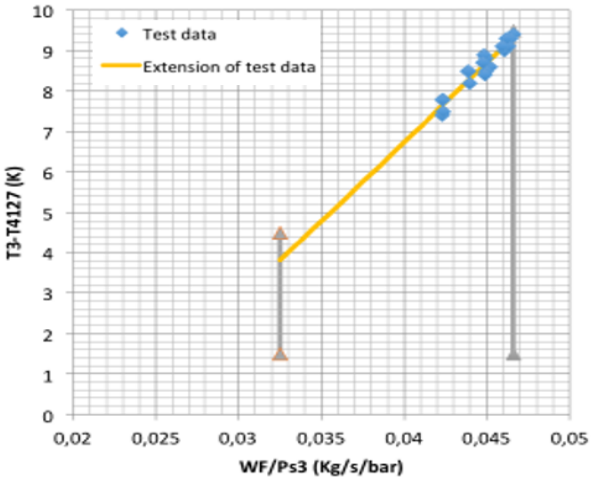

Figure 7.3: Difference between T3 and T41 test cell data [57]

Table 7.1: Sensor locations for the GEnx and CF6-80C2 engine

Sensor	GEnx-1B	CF6-80
T_{t12}	The nacelle inlet cowl, protrudes the flow	The nacelle inlet cowl
T_{t25}	HPC inlet, heated with stage 4 air	HPC inlet
T_{t3}	Behind fuel nozzle, on the combustor diffuser nozzle case	In front of the fuel nozzle
T_{t49}	The inlet to the first stage of the LPT	The inlet to the first stage of the LPT
T_{t5}	—	LPC outlet
P_{t2}	Fan Hub inlet	Fan hub inlet
P_{s14}	—	Bypass duct, behind fan
P_{t25}	—	HPC inlet[1]
P_{s3}	Same as TT3 sensor	Same as TT3 sensor
P_{t49}	—	Same as T49

The available sensors for the GEnx-1B are limited to the grey ones depicted in Figure 7.1. Notably, compared to the CF6-80C2 engine, there are even fewer sensors installed. Again the sensors between the fan core and booster are lacking. The sensor positions are also described in Table 7.1. The position of the station 3 sensors is noteworthy from this table. They are not placed in front of the combustor, as one would expect, but on the combustor diffuser nozzle case. This is the same as for the CFM56-3 engine station 3 sensors depicted in Figure 7.2[57]. In such a case the temperature sensor measurements can be affected by the radiation from the combustor. From Figure 7.3[57] it can be noted that there is a difference between T_3 and T_{4127}, with the latter being the temperature of the HPT clearance control air extracted from the last HPC stage. This difference increases with the fuel flow (W_f), hence indicating the effect of the combustor heat radiation. For the static pressure measurements some uncertainties are introduced as well. In order to convert this static pressure to the total pressure, the local velocity needs to be known. The latter is computed using the area and mass flow. The area of this side channel can be obtained graphically, however, the mass flow is unknown. Additionally, there will be some pressure losses. Due to the difficulties to eliminate these uncertainties it will be assumed for the remainder of this project that the measurements are recorded in front of the combustor.

[1] In some documents P_{t25} is wrongly indicated as P_{s25}.

7.2. Data source selection

The engine model should be a virtual representation of an average performing engine that can function as a benchmark for health monitoring of other engines. Selecting the best performing engine will always overestimate the health of other engines. For a poor performing reference engine the opposite is true. The specific fuel consumption and the hot day (HD) EGT-margin are good indicators for the performance quality of an engine. Moreover, the type and level of workscope can be used to quantify the health of the engine. High level workscopes, especially to the most vulnerable modules (i.e., the core), ensure an acceptable condition of the reference engine as its performance has been restored.
The various data sources have already been discussed in Chapter 4. From the mentioned sources test cell data was the most promising source due to the availability of the thrust measurement, humidity and the total mass flow. Additionally, steady state data is recorded during test cell runs, which is not the case for CEOD. On the contrary, the test cell not including the on-wing installation effects will penalise the accuracy. All these factors are important and will affect the model accuracy.
As mentioned in Section 4.3, multiple operating points are available for the correlation runs and back-to-back tests. This is convenient, since the off-design modelling can be performed using the same data set that was used for developing the design point model. This eliminates any accuracy degradation caused by manufacturing tolerances and engine health differences.
For the CF6-80C2 both the correlation and back-to-back testing data were available. The correlation data, however, originated from the 90s and lacked a clear description of the measured parameters. Furthermore, the measurements for station 5 were not correct. The T_{t5} and P_{t54} were almost equal to the EGT position measurements. There was, however, a big advantage. That was the presence of the total pressure in the fan bypass duct. This allowed to straightforwardly compute the fan bypass pressure ratio. Nevertheless, due to the missing measurements at station 5 it was decided to opt for the back-to-back testing data. The dataset includes the total temperature at station 5 and the static pressure (instead of total) in the fan bypass duct. The available operating points are illustrated in Figure 7.4. It can be noticed that only the high speed region data are available.
The correlation data was selected for the GEnx-1B engine. In Figure 7.5 the available operating points can be found. It can be observed that some more data points are available in the lower operating range compared to the CF6-80C2 engine. The measurements of all the installed sensors are included in this dataset for the illustrated operating points.
Points at the idle power setting were also available for both engines but are not depicted in this figure. This operating point is not required for developing the engine model. Although data for the full operating range is lacking, it is deemed sufficient for demonstrating the applicability of an off-design modelling framework.

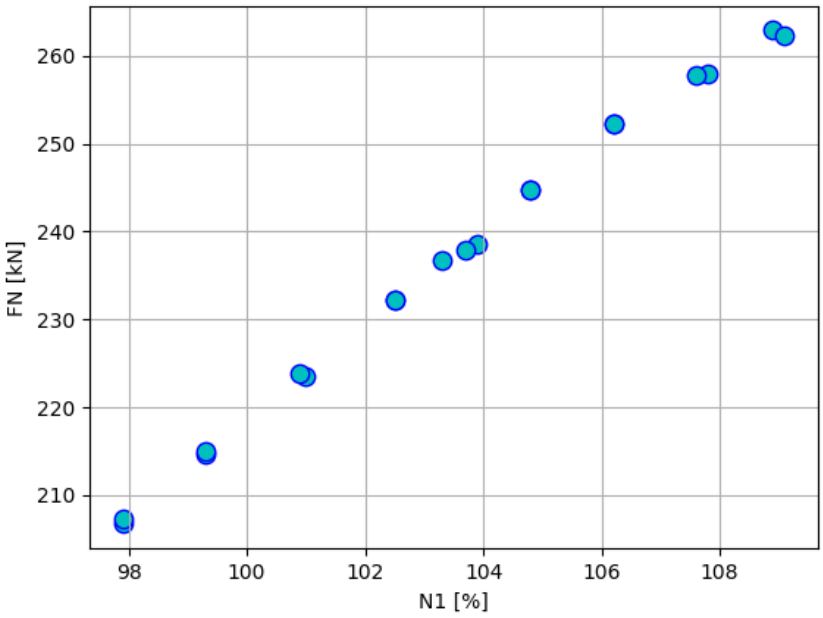

Figure 7.4: Back to back testing operating points for the CF6-80C2 engine

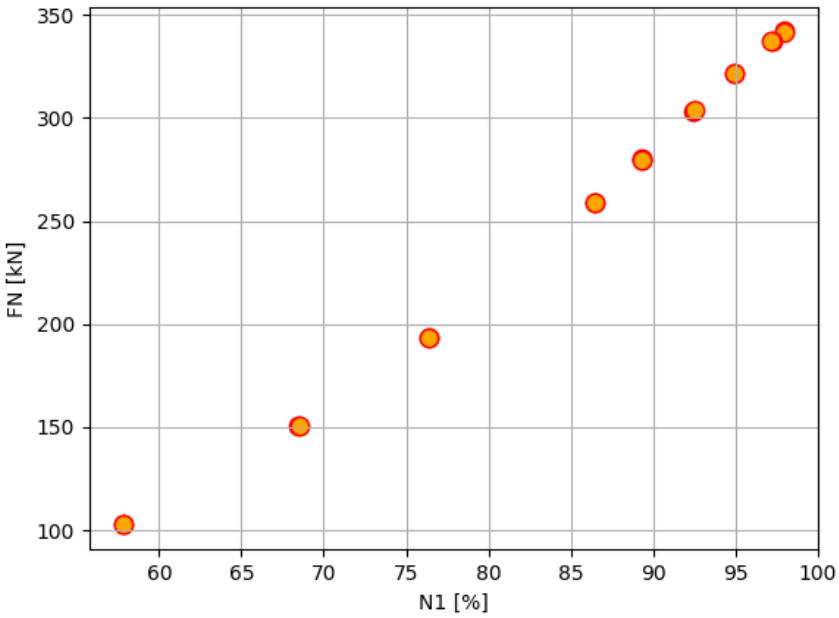

Figure 7.5: Correlation report operating points for the GEnx-1B engine

7.3. Design point input data

The data determined from the sources mentioned in the previous section are presented in Table 7.2. These are tests-cell data unless indicated otherwise. The rating used for the GEnx is the GEnx-1B74/75P2, powering the Boeing 787-9 Dreamliner. For the CF6 engine, the CF6-80C2B5F rating, designated to the Boeing 747-400 freighter, was selected. Note that the P_{t25} for the CF6-80C2 turbofan is not used as a target. Since this measurement is known, the low pressure system core pressure ratio can directly be attained using the P_{t2}, which can be specified in GSP.

Table 7.2: Design point problem inputs and targets

Parameter	GEnx-1B	CF6-80C2	Units
Target parameters			
T_{t25}	353.01	389.36	[K]
T_{t3}	886.67	847.15	[K]
T_{t49}	1193.66	1139.15	[K]
T_5	-	830.15	[K]
P_{s14}	-	1.45	[bar]
P_{s3}	45.35	32.29	[bar]
P_{t49}	-	7.64	[bar]
F_N	321.67	257.75	[kN]
Input parameters			
W_F	2.6615	2.7542	[kg/s]
$\dot{M}_{total}$	1176.94	813.16	[kg/s]
RHUM	56.71	74.35	[%]
N1	2431	3531	[rpm]
N2	12251	10648	[rpm]
P_{t10} [1]	0.996	-	[bar]
P_{t2}	-	1.014	[bar]
P_{t25}	-	2.52	[bar]
T_{t2}	275.55	292.23	[K]
Ma	0	0	[-]
Core Nozzle area	0.6698	0.615	$[m^2]$
Bypass Nozlle area	3.0968	1.77	$[m^2]$
Fan bypass exit area	4.57	2.89	$[m^2]$
Fan core exit area	0.61	0.635	$[m^2]$
HPC inlet area	0.358	0.34	$[m^2]$
HPC exit area	0.082	0.0677	$[m^2]$
Assumed Inputs			
Mechanical efficiency	0.99	0.99	[-]
Combustion efficiency	0.995	0.995	[-]
Combustor pressure losses	0.04	0.04	[-]
Reference Values			
OPR	46.3[2]	31.1 [3]	[-]
BPR	8.8[2]	4.97 - 5.31[3]	[-]

7.4. Off-design modelling input data

For the off-design modelling the same sources are used as for the design point. An overview of the parameters for both test cases is given in Table 7.3. These parameters, for the operating points depicted in Figure 7.4 and 7.5, will be utilised to tune the component maps with the goal to minimise the difference between the measured and simulated data. It should be mentioned that only one operating point will be selected in case some of them lie close to each other (i.e., are clustered). Furthermore, the design point is excluded as well.

Table 7.3: Off-design input and target parameters

Parameter	GEnx-1B	CF6-80C2	Units
Target parameters			
TT_{25}	X	X	[K]
T$_{t3}$	X	X	[K]
T$_{t49}$	X	X	[K]
T$_{t5}$	—	X	[K]
P$_{s14}$	—	X	[bar]
P$_{t25}$	—	X	[bar]
P$_{s3}$	X	X	[bar]
P$_{t49}$	—	X	[bar]
F_N	X	X	[kN]
W_F	X	X	[kg/s]
$\dot{M}_{total}$	X	X	[kg/s]
N2	X	X	[%]
Control parameters			
RHUM	X	X	[%]
N1	X	X	[rpm]
PT10	X	—	[bar]
PT2	—	X	[bar]
TT2	X	X	[K]

[1]The P$_{t10}$ is measured close to the fan tip, and the P$_{t2}$ is recorded near the fan spinner (core).
[2]From https://www.geaviation.com/propulsion/commercial/genx
[3]From https://customer.janes.com/Janes/Display/JAE_0731-JAE_

8

Modelling approach development

This chapter presents the problem description for the design and off-design modelling. This includes the main assumptions, objective, parametrisation and constraints. Finally, the chapter is concluded with a comparison between the most promising optimisation methods found during the literature study. These are Genetic algorithms (GA) and Bayesian optimisation (BO).

8.1. Design point problem description

Developing a design point model is the first step when modelling a gas turbine engine, as told before in Chapter 5. Here the key dimensions of the engine are determined. This point is subsequently used as an anchor for off design modelling. In this section the problem set-up is given, which is used for creating the design point model.

8.1.1. Problem parametrisation

In Table 8.1 the design variables are presented for the design point optimisation problem. These dictate the performance of the various gas turbine modules, and the engine as a whole. Other parameters are either known (e.g., the mass flow), or a function of the ones given below (e.g., OPR). The velocity coefficient was also not chosen, since the implementation for it in the available modelling software (GSP) is not very robust and some difficulties were encountered in the past [17]. Changing the discharge coefficient only influences the geometric area. The effective area is calculated based on the bypass ratio and mass flow. For this reason the latter is also not included in the design vector.
The bounds for the design parameters are also given in Table 8.1, and selected based on typical values found in literature and data from the OEM [1] [2].

[1] https://www.geaviation.com/propulsion/commercial/genx
[2] https://www.geaviation.com/propulsion/commercial/cf6

Table 8.1: Overview of the design variables, including its description and bounds

Parameter		Description	Lower Bound	Upper Bound	Units
		Overall performance parameters			
x(1)	BPR	Bypass ratio	95%	105%	[–]
		Turbomachinery pressure ratios			
x(2)	$FPRc$	Fan core pressure ratio	80%	120%	[–]
x(3)	$FPRbp$	Fan bypass pressure ratio	80%	120%	[–]
x(4)	$HPCpr$	High pressure compressor pressure ratio	80%	120%	[–]
		Turbomachinery efficiencies			
x(5)	*HPC_ef*	High pressure compressor polytropic efficiency	85%	95%	[–]
x(6)	*Fan_efC*	Fan core polytropic efficiency	85%	95%	[–]
x(7)	*Fan_efD*	Fan bypass polytropic efficiency	85%	95%	[–]
x(8)	*HPT_ef*	High pressure turbine isentropic efficiency	85%	95%	[–]
x(9)	*LPT_ef*	Low pressure turbine isentropic efficiency	85%	95%	[–]
		Nozzle coefficients			
x(10)	*Cx_core*	Core nozzle thrust coefficient	90%	97%	[–]
x(11)	*Cx_bypass*	Core nozzle thrust coefficient	90%	97%	[–]

8.1.2. Problem objective

The objective function for this problem is given in Equation 8.1 and is the root mean square (RMS) error. Here $\hat{z}_i$ are the simulated performance, and z_i are the target performance parameters. Weighting factors, a_i are used as well in order to account for the importance of the different parameters, and can be determined using a sensitivity analyses. ***M*** denotes the number of parameters that are to be matched.

$$OF = \sqrt{\sum_{i=1}^{M} \frac{a_i}{M} \left[\frac{\hat{z}_i - z_i}{z_i}\right]^2} \tag{8.1}$$

8.1.3. Constraints description

Next, the constraints employed for the design problem are described. These are required to reduce the number of possible solutions for the design problem. This is done by specifying general engine relations and OEM data, that can not directly be used as the model inputs, as constraints.

- **Fan core polytropic efficiency constraint:** The relation in figure Figure 6.2 is utilised to find the polytropic efficiency of the fan core using the average pitch loading. Figure 6.1 is not used, since it was decided to merge the fan core and booster. Consequently, the work of the fan core is not only delivered by a single stage fan.
- **Fan bypass polytropic efficiency constraint:** For this constraint the graph depicted in Figure 6.1 is implemented. The loading at the pitch line of the fan bypass section is used as the input.
- **HPC polytropic ratio constraint:** The same relation as used for the fan core section is employed for the HPC. In this case the HPC average stage mean line loading is used.
- **Core nozzle area constraint:** This area is obtained from the engine installation manual (IM), and is the geometric area obtained at hot operating conditions by the OEM.
- **Bypass nozzle area constraint:** This area is also specified in the IM, and determined at the same operating conditions.
- **Fan pressure ratio (FPR) constraint:** Equation 6.3 is used for this constraint. This relation is obtained using the exhaust velocity ratio of the core and the bypass nozzle that maximises the thrust. A more detailed explanation is given in Section 6.4.

- **Overall pressure ratio constraint:** The OPR specified by the OEM is used as an constraint as well. This will not be a hard constraint, since the presented data by the OEM can be affected by commercial aspects as mentioned in Section 4.2.
- **HPT isentropic efficiency constraint:** In order to select the efficiency based on the performance of the turbines a Smith chart is used. The HPT average pitch line loading, and flow coefficient are used as inputs for this chart.
- **LPT isentropic efficiency constraint:** Again a Smith chart is used for the turbine efficiency. The LPT average mean line loading, and flow coefficient are used as input this time.

For all of the constraints mentioned above, the implementation is done as given by Equation 8.2. It can be noted that the constraints are bounded.

$$\text{Lower bound} \leq \text{GSP output - General relation output} \leq \text{Upper bound} \tag{8.2}$$

The bounds are set based on the extend of applicability of the general relations to the engine type. For example the polytropic relations for the compressors are conservative, and are given larger bounds for the GEnx due to the higher technological level. The same also holds for the constraints involving the Smith chart. For the nozzle areas 3 % of the OEM specified value is used. This is done to account for engine to engine, and operating condition (thermal expansion) differences. The Fan pressure ratio constraint is also not used as a tight constraint. Some data regarding the FPR was available for the CF6 engine (from the correlation report, as mentioned in the previous chapter), and it was used as a guide to set the FPR bounds.

8.1.4. Assumptions made for design point modelling

This section describes the assumptions made for the design procedure. Assumptions are required to model the complex phenomena occurring in a gas turbine. Some additional ones are needed to bridge the gap caused by the scarcity of the modelling data. These assumptions will allow to determine the performance parameters of the different components along the gas path. The majority of these assumptions would not be required if performance data was not of propriety nature.
It is expected that the effects of these assumptions will be minimal for engine health monitoring, due to the differential method being used.

- First of all it is expected that merging the fan core and booster into one module will increase the accuracy of the model due to the missing sensors between these two modules. This was proven to be true in the past for health monitoring [9].
- The effects of variable geometry can be neglected at the design point. These are the Inlet Guide Vanes (IGV) and Variable Stator Vanes (VSV), and have already been described in Section 7.1. At the design point it is assumed that these are at their nominal position.
- The effects of VBV and TBV can be excluded from the analysis. Little is known about the their schedule for the CF6-80C2 engine. For the GEnx-1B turbofan engine their position is known. It is , however, expected that that they are close at high power settings [17].
- The active clearance control (ACC) effects can be left out from the model. AAC is done for the HPT and LPT. For CF6-80C2 turbofan engine no data is available regarding the ACC. For GEnx HPT ACC is not active at take-off, but the LPT ACC is. However, only the LPT ACC valve position in percentages is known and nothing is known about the actual clearance. Moreover, since the air for ACC is taken from the bypass flow its effects can be neglected. The same can also be said about the core compartment cooling (CCC) air.
- Other parasitic bleed air can also be excluded during on-design modelling. No data is available for core cooling and anti-ice bleed air for the CF6-80C2 engine. The latter is inactive during test cell runs. For the GEnx-1B engine the booster-anti ice (BAI) and the cowling anti-ice bleed (CAI) settings are unknown, but they are again expected to be inactive during test cell runs [10]. The same is also true for the amount of customer bleed air extracted in the CF6-80C2 engine. The GEnx engine on the other hand does not have customer bleed air as told in Section 7.1. Bleed air for CCC is however extracted in the GEnx, but the amount or its schedule is unknown.
- Power off-takes do not need to be modelled. Although the power extracted is known for take-off, it can be neglected because no power is extracted during test cell runs.

- The model generated using the data of one reference engine is representative for the entire pool of engines. For this to be true a careful selection of the reference engine has to be made, which already has been described in Section 7.2.
- The optimum FPR, using the jet velocity ratio that maximises thrust, is applicable to the design problem. It is possible that this optimum value is only used at cruise conditions by the OEM, however, the FPR at other flight phases is not expected to deviate a lot from the optimum value.
- The take-off operating condition can be used as the design point. This is the thermal design point where the highest temperatures occur along the gas path, and the highest thrust is delivered. Note that this point can differ per module and is not necessarily the design point used by the OEM. The take-off data is obtained from the test cell at sea level static conditions. More details can be found in Section 5.1.
- The Bellmouth inlet in the test cell can assumed to be perfect. On-wing, however, this is not the case due to various aerodynamic phenomena that can occur due to side wind or high angles of attack. That is why the inlet is removed from the problem. The measurements at the fan face are used as input.
- For computing the static properties the areas can reliably be measured from scaled drawings provided by the OEM.
- The velocity coefficient can be set to one, and the thrust coefficient can be used instead.

8.2. Off-design problem description

Once the design point model has been obtained, one can proceed with generating the off-design model. This involves creating/tuning component maps, which are generally proprietary to the OEM. This section gives an overview of the set-up used for obtaining these maps.

8.2.1. Problem parametrisation and objective

As told in Section 5.2.3, the map scaling method by Li *et al.* [50] was found to be the most suitable off-design modelling method. By employing a second order polynomial as a scaling function, unphysical solutions can be avoided. Furthermore, data along a single operating line are sufficient for this method to work.

The design vector of the off-design problem consists of the parameters of the scaling polynomials defined by Equation 5.3. Such a polynomial is created for each compressor map variable, namely: the pressure ratio, efficiency and mass flow. For the turbines, however, only the efficiency is adapted. The pressure ratio is not scaled since the turbines mostly operate in the choked region of the map [7, 32]. In this region the iso speed lines are almost horizontal, thus the mass flow is near to constant. As a result scaling the pressure ratio will not be fruitful. The mass flow is also not scaled for similar reasons. Scaling the mass flow can result in a map where the iso speed lines are not concentrated in the high pressure ratio region. This occurs when the rotor of the turbine is choked, since the mass flow is dependent on the rotor speed [58]. Generally the stator of the turbine is choked due to the smaller area, and causes the mass flow to be (almost) independent of the spool speed.

All the component maps will be addapted simultaneously, hence 11 parameters need to be scaled. Since the scaling function has two variables, the design vector will consist of 22 parameters. The bounds for these parameters will be set by trail and error during testing in order to obtain smooth and realistic characteristic maps that are inline with physics.

Again the RMS error, defined in Equation 8.1, is utilised as the objective function. For the off-design case the available range of data points, described in Chapter 7, is used to evaluate this function. Furthermore, no weighting factors are used for this problem, i.e., a_i is set to 1.

8.2.2. Constraints and Assumptions

There are no constraints used for the off-design problem. There are bounds used for the design parameters to avoid unrealistic maps. Moreover, GSP also assures feasible solutions, since the operating points that do not converge are avoided.

The same assumptions defined for the on-design problem are again valid for this problem. The ACC and variable geometry effects are not accounted for during this modelling task. These will be corrected for by using the tool developed by Otten [17]. Some additional assumptions are given below:

- At OD conditions the variable geometry will differ from their nominal position. However, since these are dependent on operating settings it is expected that the effects will be captured by the performance maps.
- The nozzle coefficients are assumed to be equal to the design point values. These are also not constant and are highly dependent on the flight conditions and phase [4, 33].
- The combustor pressure loss, and combustion and mechanical efficiency are assumed to be constant. The combustion efficiency can be assumed to be constant at high power settings as very little deviation is expected in this region [59]. The same is also true for the combustor pressure losses and mechanical efficiency [7, 33].
- Analysing the underlying physics of the component maps using the information given in Section 5.2.1 will be sufficient to prove their correctness.
- The DP will be positioned on the starting reference map such that there is a sufficient stall margin, which is in line with the literature [33]. It is assumed that this will also hold after the scaling procedure.

8.2.3. Reference map selection

This is a crucial step in the off-design modelling process. Good reference maps will also lead to good results, thus the *"garbage in garbage out"* phrase should be kept in mind. Kurzke [59] suggest that maps with similar design should be chosen. This can be done by looking at the number of stages, design mass flow and pressure ratio. Ideally, one should also strive for the same technological level. For compressors it is also important to consider their operating speed regime. For a booster that runs on the low speed shaft, a subsonic compressor map is expected to be more suitable than a transonic map. A transonic map has vertical high iso speed lines, and the peak efficiency region moves closer to the surge line as the mass flow (or spool speed) increases. Note that a subsonic map can also include vertical speed lines in case sonic velocity is reached at the outlet of the module as told in Section 5.2.1. Moreover, high Mach number compressor maps also have relatively narrower efficiency islands [43]. Finally, it needs to be checked if the maps are in line with the physics. This can be done by using the Smooth C and Smooth T software, as explained in Section 5.2.1.

8.2.4. Component map reference point location

GSP only allows to set the design point location in an on-design model case. Hence, the position can not be used in an automated off-design modelling process. The design point can be placed on the component map by defining the design point β value and the non dimensional design spool speed. The component map will then be scaled using these two values and other design point data. The positioning of the scaling point can be done by considering the following aspects:

- **The surge margin (SM):** The surge margin for the compressors need to be sufficient, and in line with the expectations in literature. Walsh *et al.* [33] proposes a SM at (the design point) of 10-15 for the fan, 15-20 for the booster, and 20-25 for the HPC. The SM should be sufficiently large for all the operating points used during the adaption process.
- **Operating line:** The attained operating lines should be realistic, and in accordance with the literature. The placement of the reference point effects the relation between the different component performance parameters, hence also the operating line. Smooth operating lines should be aimed for, in order to prevent jumps in component and overall performance parameters.
- **Peak efficiency during cruise:** Since cruise is the longest flight phase for civil aviation, it is quintessential to have the highest efficiencies for this phase. This can be set using trial and error by analysing the module efficiencies at the cruise operating phase.

Some additional hints given in the Smooth C and Smooth T manuals to aid with selecting the reference point location are given next. The corrected flow for the reference speed line should not be lower than 95 % of the highest corrected flow found on the map, in order to prevent unrealistic low pressure ratios. Furthermore, the peak efficiency on the selected speed line should not be lower than 90 % of the maximum map efficiency. The latter prevents attaining untypical low efficiency values.

8.3. Optimiser Selection

For solving the problems mentioned in the previous sections one needs an optimiser. Two of the most promising applicable optimisers have already been described in Section 5.3. Here the procedure to determine the best optimiser settings, and a comparison between GA and BO is done. The best optimiser will be used for solving both, the design point and off-design problems.

8.3.1. Genetic Algorithm

GA has already been described in Section 5.3. In this section the different inputs for GA are elaborated upon and a selection of the most optimal settings is done based on the computational time, constraint and objective value.

Differential evolution strategies

In this section the most common mutation and crossover strategies for GA are briefly discussed [60, 61] and a selection is made.

- **rand1bin:** Here the mutation is done by utilising a randomly chosen population member, which is subsequently perturbed using a one weighted difference vector also from random individuals. This weight is also known as the mutation constant (F). One can also use two weighted difference vectors. In the latter case it is called the 'rand2bin' strategy.
- **best1bin:** This strategy works in a similar way as the 'rand1bin', however, now the best vector of the current generation is perturbed. Again two weighted vectors can be used, which is called the 'best2bin' strategy.
- **randtobest1bin:** For this strategy both the best and a random member are utilised during the mutation step.
- **currenttobest1bin:** Here the best and the current member are used for mutation.

The above mentioned strategies employ a binomial ('bin') crossover method to determine which elements from the trial vector (created by mutation) should be selected in order to generate a new (trial) individual. In this case elements from the mutant vector are taken using a probability equal to the crossover rate (CR), and elements of the current population member are take using a probability of 1 - CR.
Besides the binomial crossover method, there is also an exponential method. The first element from the mutant vector is randomly selected. Subsequently, ***L*** other elements from the mutant vector are selected in a circular approach such that probability Pr(L = h) = CR^h [62].

Generations and Population size

The generations, also known as iterations, need to be selected such that the solution is converged and satisfactory. A lot of generations can be used to ensure convergence and accuracy. The less favourable side of a high number of iterations is the significant computational time. The run time for a single iteration is already high because GSP needs to be run to evaluate the objective function. During this project the generations are selected by running the algorithm on a dummy, and the actual problem. If the solution is satisfactory and converged, the number of generations is deemed sufficient.
The population size specifies the number of function evaluations for each generation. Large population numbers are beneficial for high dimensional problems with complex search spaces. Small population sizes mean less function evaluations thus less computational time. For simple low dimensional problems small population sizes can be used, however for complex problems the algorithm can have difficulties when exploring the search space. Storn *et al.* [63] suggest that the population size should be between 5 to 10 times the problem dimension. The population size will again be determined based on tests.
Given a certain amount of computational time, one can either opt for a high population size with greater generations or a low population size with less generations. Both cases have advantages and disadvantages as mentioned above. The algorithm will be run for both cases and the most optimal solution will be selected.

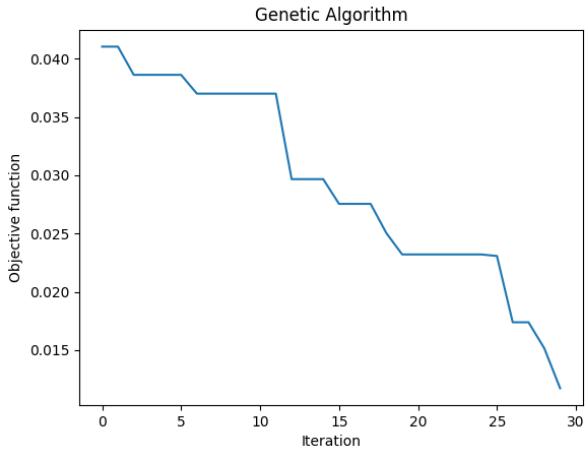

Figure 8.1: Genetic Algorithm results for a population of 5 and 30 generations

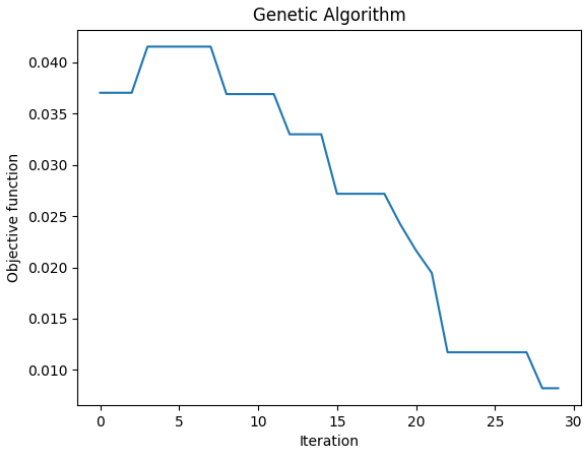

Figure 8.2: Genetic Algorithm results for a population of 10 and 30 generations

Mutation and Crossover constant

The mutation and the crossover steps of the GA have already been explained in Section 5.3. The mutation constant (F) has been defined above. A large mutation factor can increases the influence of the difference vector on the mutant, and thereby introducing more randomness. This can aid with escaping local minima and enhances the search in a large solution space. Large mutation factors can, however, sometimes lead to slower convergence. The opposite is true for a low F. Either bounds or a single value can be specified for F, which is determined in a similar way as for the population size and the generations.

The crossover rate (CR) has been defined before as well. This constant affects how many parameters from the mutant vector are used to create a trial vector. A higher CR leads to faster convergence, however results in less variety within the populations and the algorithm can get stuck in a local minimum. On the contrary a low CR increases the search radius and lowers the chance of getting stuck in a local minimum, at the cost of slower convergence. As for all the other algorithm parameters, tests are also conducted to determine this constant.

Results

The best readily available genetic algorithm implementation was found to be the Scipy [64] Python package. This package allowed to specify all the above mentioned settings, including constraints and parallel computing.

The strategy for creating the design point model is chosen by running tests for all these settings, and selecting the one that results in the best objective value. First of all the standard *'best1bin'* strategy was analysed. The results for this approach were promising. The optimiser was able to converge to a satisfactory solution that met all the constraints. The *'rand1bin'* strategy had difficulties finding solutions that met the constraints, thus it did not improve the initial objective value. This was also expected, since the members for mutation are chosen randomly. For the *'randtobest1bin'* similar behaviour is expected. The two vector difference variants of these methods were also tested, and did not improve the results. It was observed that the algorithm took more generations to converge. For the exponential methods a similar behaviour was observed. Finally, the *'currenttobest1bin'* method was employed. For this method it was observed that the algorithm converged faster, but to a local minimum. From all the tested strategies the *'best1bin'* was chosen. This outperformed all the other strategies. The latter was also expected, because the best member from the population is selected for mutation.

Next, the population size and number of generations were selected. It was observed that for larger populations fewer iterations were needed in order to converge to a certain solution. This can be concluded from the graphs in Figure 8.1, and 8.2. The computational time was approximately the same for both these cases. Additionally, it was observed that larger populations were better at finding solutions that met the constraints. It was decided to do the optimisation for 30 iterations using a population size of 15.

Subsequently, the CR was selected. By running the algorithm for multiple CRs it was noted that for higher CRs the algorithm got stuck sometimes, however, it took fewer iterations to obtain satisfactory results. As mentioned before a too high value for F can get stuck sometimes, which was also noticed during testing. 0.7 was selected for the CR and led to acceptable results.
F was also chosen based on testing results. It was observed that low values (<0.8) were favourable if a local search was to be conducted. As mentioned before low F values reduced the effect of the randomly selected vectors. Furthermore, the choice of F differed from engine to engine. Therefore, it was decided to choose a range of 0.5 to 1.5 in order to avoid getting stuck in a local minima. Once GA obtained the optimal solution, gradient descend was done using the build in *polish* function of the Scipy package. Once GA determines the minimum location, polishing improves the result by using gradient descend locally. This can be useful if high (> 0.8) F values are used, which introduce more randomness.
The selected settings are summarised in Table 8.2.

Table 8.2: GA optimum settings

Settting	Description	Value
Strategy	The mutation and crossover strategy employed by GA	*'best1bin'*
Generations	Also known as iterations	30
Population size	—	15
Probability of crossover (CR)	—	0.7
Probability of mutation (F)	—	[0.5, 1.5]

8.3.2. Bayesian Optimisation

Bayesian optimisation can be used for computational intensive objective functions. The computational time is reduced by building a surrogate model of the objective function and keeping the number of function evaluations to a minimum. The different algorithm settings are discussed next.

Acquisition function type and optimiser

The acquisition function has already been explained in Section 5.3. The following options could be selected as acquisition function: Expected Improvement (EI), Maximum Probability of Improvement (MPI) and the Lower Confidence Bound (LCB). EI determines the $\boldsymbol{x}$ value that maximises the expected improvement based on the posterior distribution. MPI selects the point with the highest probability of improvement. LCB maximises the curve that is two standard deviations below the posterior mean. Furthermore, LCB has a parameter to tune the exploitation and exploration capabilities of the optimiser. According to Snoek *et al.* [65], MPI can be aggressive if the target is unknown. Additional it is mentioned that EI behaves better than MPI and contrary to LCB it does not require a tuning parameter. This will reduce the computational time.
For the optimiser type the standard Limited memory Broyden Fletcher Goldfarb Shanno (L-BFGS) algorithm is used. This method can be used for solving non-linear optimisation problems. The Hessian matrix obtained from approximate gradient evaluations is utilised to determine the descend direction. L-BFGS is the best method according to Kumar *et al.* [66]. The two other available alternatives, Dividing Rectangles (DIRECT) and covariance matrix adaptation (CMA) do not outperform L-BFGS.

Evaluator type

One can also choose a method to evaluate the objective for batch sizes larger than one. The available methods are random, sequential, local penalisation and Thompson sampling. Local penalisation[67] is used in order to avoid less optimal points based on the previous point at its objective value. Thompson sampling (TS) selects points by exploring new regions in the search for an optimal solution, whilst exploiting the already explored points. TS is faster than local penalisation since samples are drawn from a Gaussian distribution, while the latter requires multiple function evaluations especially to avoid local minima [68].
From the literature local penalisation looked the most promising method. This will be verified by running the algorithm for the different evaluator types.

Number of initial points and batch size
The number of initial points are used to map out the search space. A lot of points are beneficial for exploring complex and high dimensional problems.
The batch size is the number of function evaluations for each iteration. Similarly, as for the initial points, larger batch sizes are favourable for complex problems. The choice for these settings are problem specific and are determined by conducting tests.

Results
The GPyOpt[68] Python package is used for BO. This was found to be the most up to date and well documented Python implementation of BO in Python. There was no implementation found that could deal with constraints, hence it was decided to include these as penalties to the objective.
From the literature is was already observed that the EI acquisition function type was the most promising one. The same was also concluded for the tests. Lower objectives could be obtained at less computational time compared to the other methods. Furthermore, unlike LCB it does not require a tuning parameter. For the acquisition function optimiser type the standard option, L-BFGS, is selected. This is according to the literature the best choice amongst the available options.
For the evaluator type local penalisation and TS were analysed. It was observed that TS converged faster than local penalisation, however, better objective values were attained for the latter.
The number of initial points is selected to be 100 in order to allow the optimiser to explore the complex design space. This can be beneficial especially since BO creates a surrogate model. The batch size is chosen to be 50 and for the number of iterations 15 was used. Beyond these values little improvement was noticed at the cost of substantial computational time.
The selected settings for BO are summarised in Table 8.3.

Table 8.3: BO optimum settings

Settting	Description	Value
Acquisition function type	—	*EI*
Acquisition function optimiser	—	*L-BFGS*
Evaluator type	—	*Local Penalisation*
Initial points	Used for exploration of the design space	100
Batch size	Similar to population size for GA	50
Iterations	—	15

8.3.3. Comparison GA and BO
For an unconstrained optimisation problem it was observed that BO converged to satisfactory objective values within less computational time relative to GA. For a constrained optimisation problem BO struggled to converge to satisfactory solutions. An example is given in Figure 8.3. The objective value in the convergence plot on the right is the sum of the constraints penalties and the RMS. The obtained RMS was 0.097. GA on the other hand converged to objective values less than 0.025 within the same computational time. This expected to be due to the way the constraints are implemented. Adding the constraints as penalties to the objective function can cause the optimiser to either focus on the objective if the penalties are small, or in the case of large penalties the optimiser will only focus on reducing the penalties. This was also observed during testing. It was not possible to create a balance between good objective values and constraint values. Furthermore, in the left plot of Figure 8.3 the distance between two subsequent design vectors is given. It can also concluded from this graph that no optimum solution has been found. For these reasons it was decided to continue with GA as the optimiser for the design point problem. For the off-design problem GA was also selected due to its advantages. Additionally, B0 is only suited for problems with a dimension lower than 20. For the OD problem there are 22 design parameters. The GA settings for the OD problem have been determined using a similar approach as for the DP.

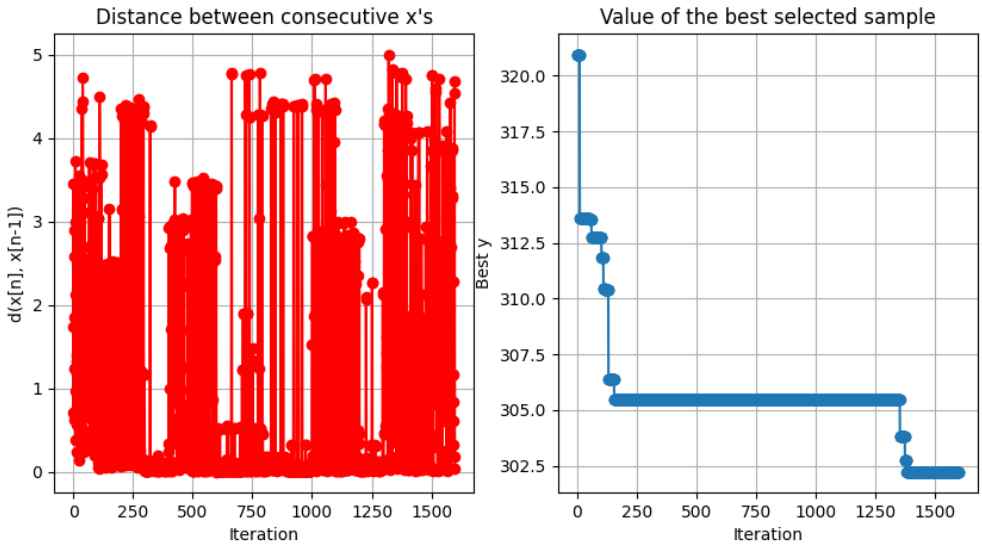

Figure 8.3: Bayesian Optimisation for a batch size of 100 and 15 iterations

9

Modelling outcome & Verification

With the defined problem set-up and the selected data the results can be generated. As mentioned before two engine models will be created to demonstrate the applicability of the systematic approach. Comparing the optimised performance parameters of the two engines, and associating them to the design inputs given in Table 7.2 will allow to verify the results. First, in this chapter, a design point sensitivity analyses is presented to aid with understanding the results. This is followed by the design point results. The off-design modelling result are presented as last.

9.1. Sensitivity analyses

The design point sensitivity analyses is presented for the performance parameters of the CF6-80C2 engine and the GEnx-1B engine. This gives an indication of how the various design variables influence the target parameters, and if they are affected or not. Additionally, a sensitivity analysis will aid with understanding the optimisation results.

9.1.1. CF6-80C2 Design point sensitivity analysis

In this section the sensitivity analyses results of the CF6-80C2 engine are presented. The effects of the design variables on the target parameters are analysed, by incrementing the former with one precent. The results are depicted in Figure 9.1, 9.2 and 9.3. The influence of each parameter is discussed below.

Fan core isentropic efficiency

By increasing the fan core isentropic efficiency, T_{t25} is reduced. This can be explained by looking at Equation B.5. A higher efficiency results in a lower fan core exhaust temperature in a real compression. This is also the cause for the decrease in T_{t3} and T_{t49}. The decrease of T_{t49} would be more substantial if the turbine exit temperature was not increased due to the lower work demand. P_{s3} increases slightly due the decreased velocity. At a constant mass flow a higher density (due to the lower temperature) reduces the velocity. From the total to static pressure relations one can conclude that for a constant total pressure the static pressure will increase if the velocity reduces. The increase in P_{t49} is also a result of the lower fan core work requirement. Finally, more thrust is generated due to increased power availability for thrust generation.

Fan bypass isentropic efficiency

The effects of the higher fan bypass efficiency are similar as for the fan core. They are, however, more pronounced (especially for the thrust) due to the higher mass flow.

High pressure compressor isentropic efficiency

Changing the HPC efficiency has similar effects as for the above mentioned efficiencies. There is an exception, however. It can be observed that T_{t49} increases slightly. The increase is caused by the lower work requirement from the compressor, and it would be higher if the increase was not counteracted by the T_{t3} reduction.

Fan core pressure ratio
An increment in the fan core pressure ratio causes the P_{t25} to increase by the same amount as expected. T_{t25} increases as well due to this pressure increase. As a result one can observe an increase in P_{s3}, T_{t3}, T_{t49}, and P_{t49}. Furthermore, one can also note a slight decrease in the T_{t5}. This is the net change caused by an increased temperatures on the cold side of the engine core, and a higher work demand from the fan core. Finally, the thrust increases as well due to the higher exhaust pressure.

Fan bypass pressure ratio
The effects are the same as for the fan core pressure ratio, except for the T_{t5} change. Evidently, a larger decrease is present due to the higher work demand from the fan bypass section. This is not counteracted since the core section temperatures are not affected by the fan bypass pressure ratio change.

High pressure compressor pressure ratio
Increasing the HPC pressure ratio has similar effects as for the above mentioned pressure ratio changes. For this change, however, T_{t49} is slightly reduced. The reason for this is the same as for the T_{t5} decrease in case of the fan core pressure ratio change.

High pressure and low pressure turbine efficiency
For the turbine performance changes only the downstream components are effected (for the design point). T_{t49} does not change since the work demand from the HPC is still the same. From Equation B.11 it can be concluded that a higher efficiency results in a higher P_{t49}, which is also seen here. This leads to an increase in thrust.
The effects are similar for the LPT efficiency change as anticipated.

Nozzle coefficients
The effects of the nozzle coefficients are illustrated as well. These are the thrust (C_x) and discharge (C_D) coefficients. The C_x leads to an increase in thrust which is self explanatory. The bypass effects are more substantial due to the larger mass flow. There are no changes visible for the discharge coefficients since GSP does not allow to modify the effective area. The C_D only changes the geometric area as told before, whilst keeping the effective area constant. The latter is set using the specified bypass ratio and mass flow. These will be discussed below.

Bypass ratio and mass flow
Both of these effect the static measurements and thrust. Increasing the bypass ratio for the same mass flow causes a part of the core flow to go through the bypass. Consequently, the bypass velocity increases. which in turn causes P_{s14} to decrease. The opposite occurs for P_{s3}. It can also be observed that the measurements at station 49 and 5 increase. This is due to the same fuel flow at a lower mass flow, which increases the T_{t4}. Since the work requirement from the compressors is lower now, the station 49 and 5 increase. That means that more power is available for thrust generation, which is also depicted. The increase is small since the core thrust increases less due to the lower mass flow.
An increase in total mass flow has a similar effect for the bypass stream. For the core, however, the changes are the opposite. The thrust also increases due to the increase in mass flow. This increase is however partially cancelled out due to the higher work demand from the compressors.

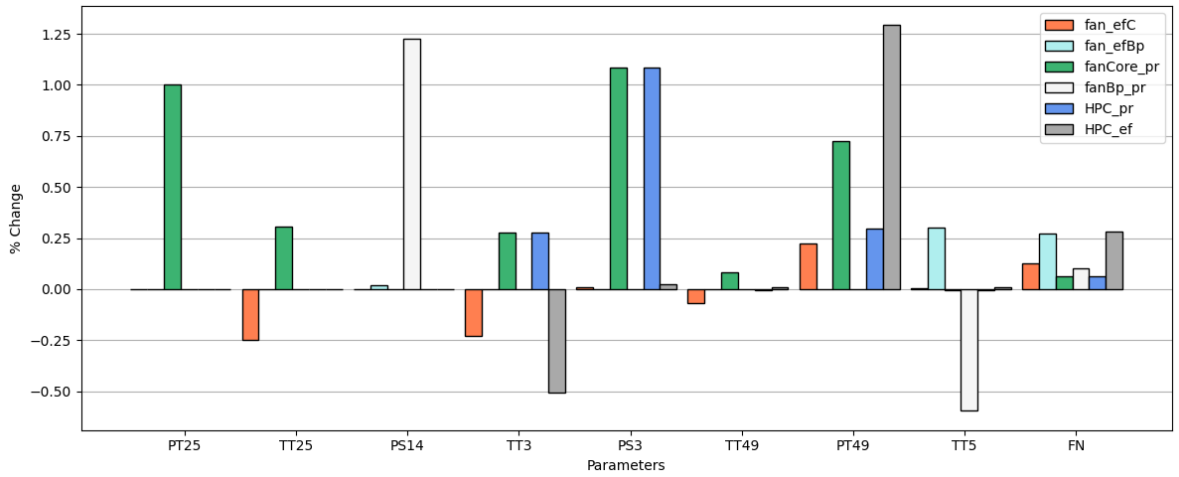

Figure 9.1: Sensitivity analyses CF6-80C2 part 1

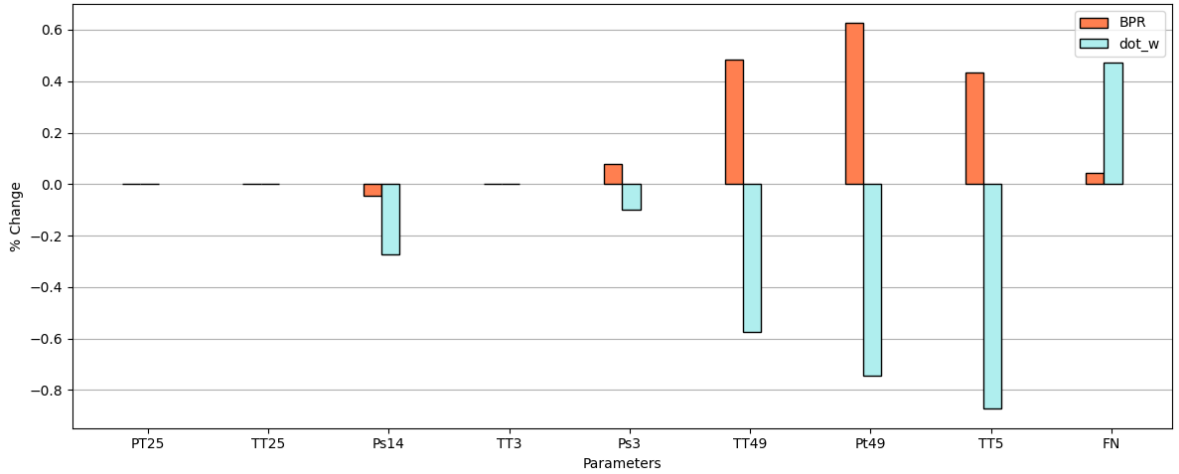

Figure 9.3: Sensitivity analyses remaining parameters CF6-80C2 part 3

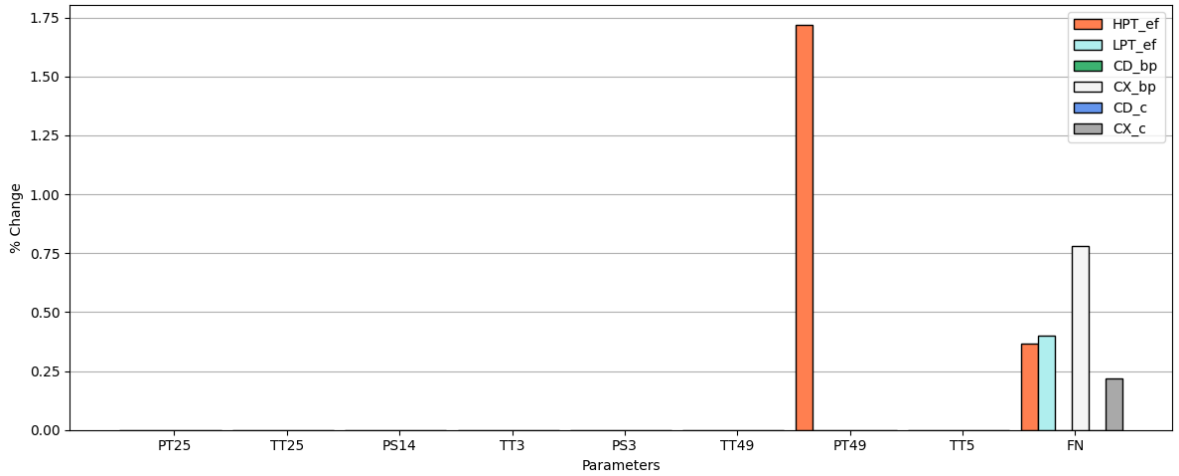

Figure 9.2: Sensitivity analyses remaining parameters CF6-80C2 part 2

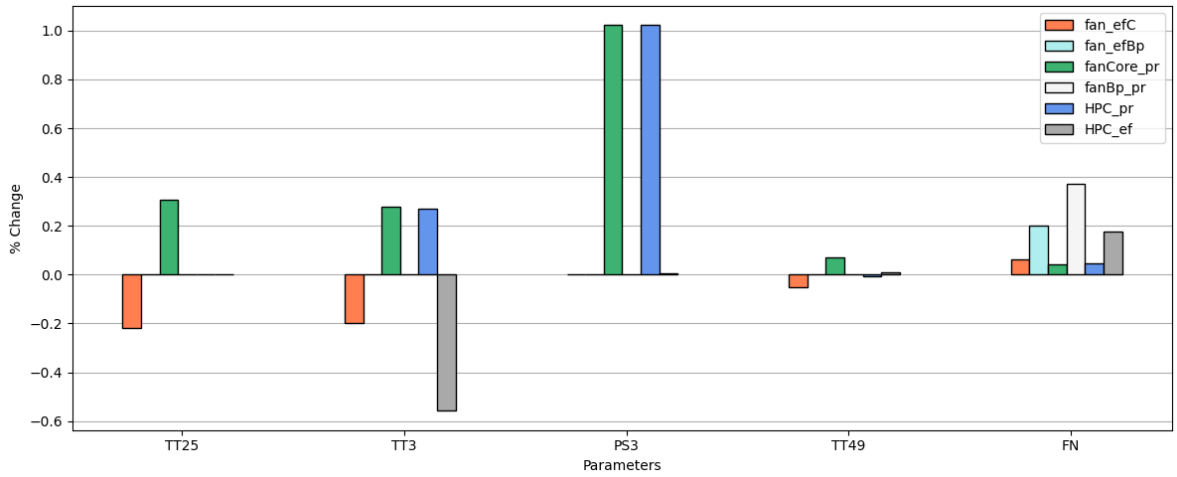

Figure 9.4: Sensitivity analyses GEnx-1B part 1

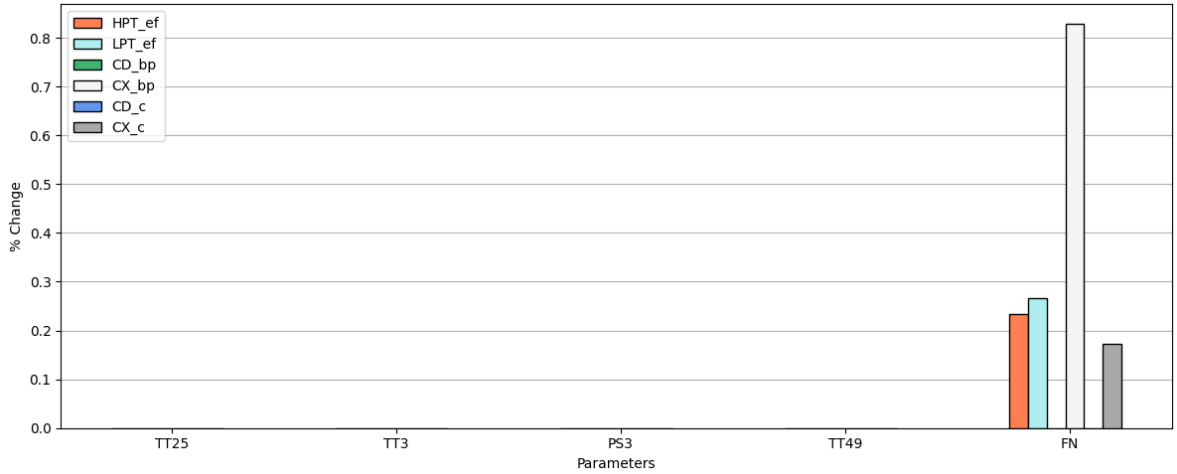

Figure 9.5: Sensitivity analyses remaining parameters GEnx-1B part2

9.1.2. GEnx-1B Design point sensitivity analysis

The effects of varying the various component performance parameters are the same as for the CF6-80C2 engine. Nonetheless, there are some magnitude differences. This can be due to the following factors, or a combination of these:

- The difference in magnitude of the reference values that are adapted: This wil result in different absolute changes, since a percentage change is used for the analyses. An example of this is the HPC pressure ratio for the GEnx-1B engine that much larger than of the CF6-80C2.
- The difference in mass flow: The GEnx-1B engine has a lower core mass flow, and higher bypass mass flow compared to the CF6-80C2 engine.
- The bypass and core size: The bypass section of the GEnx-1B is larger, contrary to its cold side of the core section. The HPT areas are smaller for the GEnx-1B, while the LPT areas are larger.
- The diverging isobars in a Temperature-Entropy (T-S) diagram: This results in more pronounced temperature changes at higher pressures. The fan of the GEnx-1B has a lower pressure ratio due to the lower spool speed. The latter is required to prevent fan tip losses.

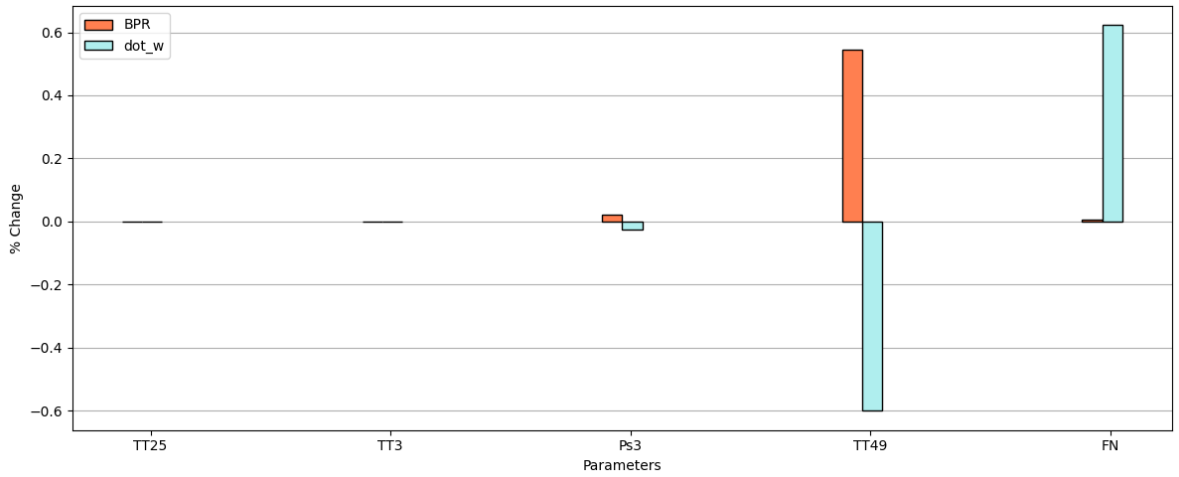

Figure 9.6: Sensitivity analyses remaining parameters GEnx-1B part 3

9.2. Design point modelling results

The results obtained using the data and problem described in Chapter 7 and 8, respectively, are presented in this section for both engines. The sensitivity analyses results will be used to explain the modelling outcome. A comparison is done between the two engines as well. This will illustrate the improvement of the engine performance over the years between the development of the CF6-80C2 and GEnx-1B engine. Additionally, the approach can also be verified this way.

9.2.1. Overview design parameters

In Table 9.1 the outcome of the design point model is presented for the CF6-80C2 and GEnx-1B engine. These are obtained using the set-up and data described in Chapter 8 and Section 7.3, respectively.
It was noticed that for the GEnx optimisation problem some of the constraints had to be relaxed. This was expected since the GEnx is more advanced compared to the CF6, and the constraints relations are conservative. Furthermore, it was observed that the optimiser had difficulties matching OPR constraint for the CF6 model. The same discrepancy was also noticed in the work done by den Haan [9]. For the best CF6 engine OPR match that could be obtained, the outcome was 3.5 % higher than the value given by the OEM. The resulting P_{s3} to P_{t2} ratio was compared with other test cell data, and a box plot is depicted in Figure 9.7. It can be observed that the simulation result is close to the average value, thus the results are deemed valid.
Related to this were also the difficulties to match the P_{s3} measurement. The test cell measurement was 4 % higher than the simulated output. This problem for the P_{s3} measurement was in the end resolved by increasing the area at station 3. The area just in front of the fuel nozzle was now used instead of the HPC exit area. This P_{s3} deviation could originate from the position of the station 3 measurements, which already has been mentioned in Section 7.1. Here the mass flow is lower, and can consequently result in a higher static pressure. Other design values are elaborated upon in Section 9.2.3.
The errors between the test cell measurements and simulated results are given in Figure 9.8 and 9.9. These gas path measurements errors are all within the limits specified in Table 4.2. Note that the sensors for the CF6-80C2 engine also have a similar accuracy. The convergence plot for both test cases can be seen in Figure 9.10, and 9.11. For the GEnx engine it can be observed that the objective value increases at some point. This occurs because the optimiser is searching for a solution that best meets the constraints. It is expected that the latter occurs since the GEnx has a higher technological level, and has more difficulties to meet the conservative constraints. It is evident from both figures that the optimiser has converged. The objectives achieved after polishing (gradient descent) are $1.5 \cdot 10^{-3}$ and $2 \cdot 10^{-3}$ for the CF6 and GEnx, respectively.

Table 9.1: Optimisation results for the design point

Parameter	GEnx-1B	CF6-80C2	Units
Overall performance parameters			
Bypass ratio	9.1	5.08	—
Overall pressure ratio	45.99	32.19	—
Turbomachinery pressure ratios			
Fan Bypass pressure ratio	1.58	1.73	—
Fan core + booster pressure ratio	2.15	2.48	—
HPC pressure ratio	21.39	12.98	—
Turbomachinery efficiencies			
η_{is} Fan bypass	0.8920	0.9117	—
η_{is} Fan core	0.8667	0.8906	—
η_{is} HPC	0.8688	0.8586	—
η_{is} HPT	0.8971	0.9083	—
η_{is} LPT	0.8969	0.872	—
Nozzle coefficients			
Cx Core nozzle	0.93	0.92	—
Cx bypass nozzle	0.95	0.93	—

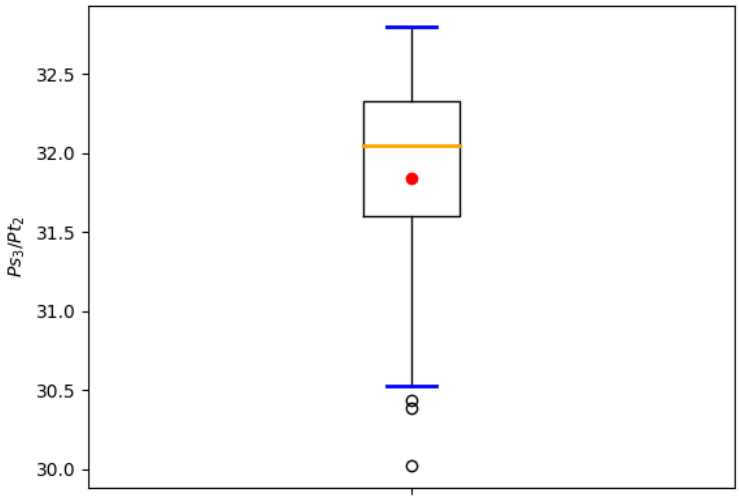

Figure 9.7: Ps3 to Pt2 ratio for test cell runs and the output for the Cf6-80C2 engine

9.2.2. Comparison with old models

In this section the differences are presented between the new and old design parameters for the CF6-80C2 and GEnx-1B engine. In Figure 9.12 the percentage differences are given for the CF6-80C2 engine, and in Figure 9.13 the differences for the GEnx-1B engine.
For the CF6-80C2 the A5 rating was used by den Haan [9], rather then the B5F rating used in this project. On the contrary, for the GEnx-1B model, the same rating was used by Van Moorselaar [10] as used in this case, namely the 74/75P2 rating. It should be noted that although the same rating is used for the

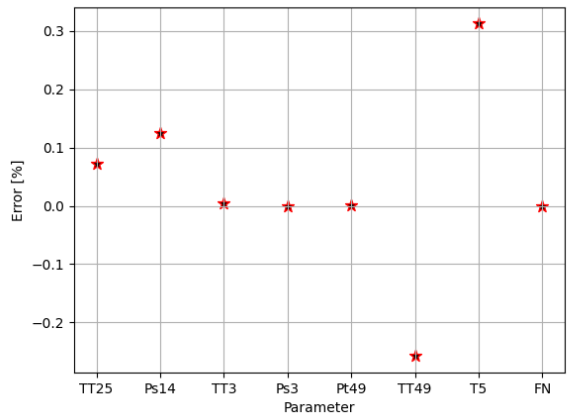

Figure 9.8: Errors between the test cell measurements and simulated results for the CF6-80C2 engine

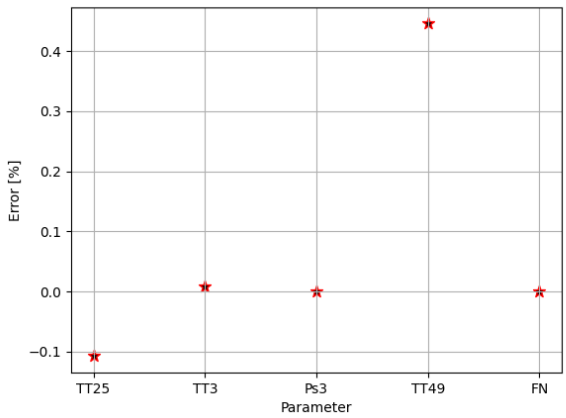

Figure 9.9: Errors between the test cell measurements and simulated results for the GEnx-1B engine

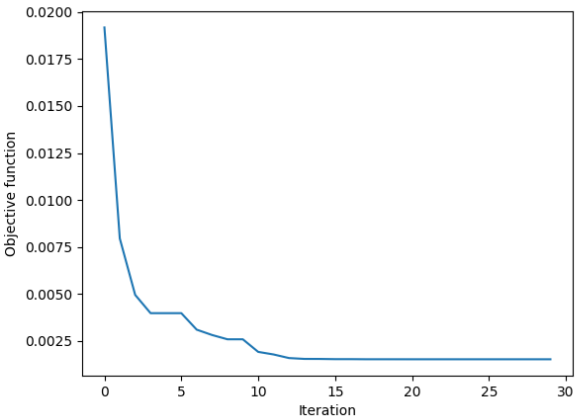

Figure 9.10: Convergence pot GA for the CF6-80C2 engine

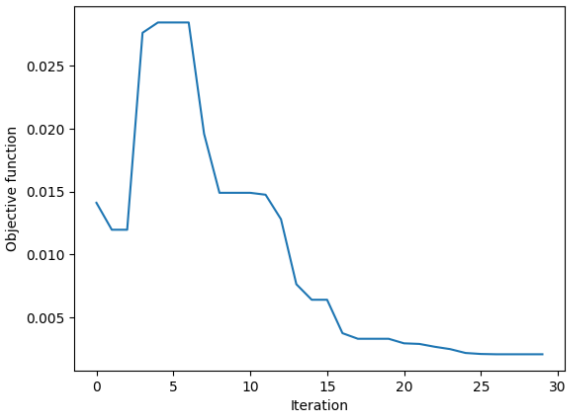

Figure 9.11: Convergence pot GA for the GEnx-1B engine

GEnx-1B model, the reference thrust is not identical (there is difference of 1 %). For both test cases differences can be noticed. This can be due to the different ratings for the CF6-80C2. For the GEnx-1B the differences can be due to engine-to-engine manufacturing deviations and/or health differences. Additionally, since the design problem was underdetermined multiple solutions were possible for the design problem. An example of this is the high turbine efficiencies ($>$ 92 %) of the GEnx, which were required due to the low nozzle velocity coefficients ($<$ 0.92). The latter has been tackled in this work by introducing constraints for the design point model, which was not done during the previous projects.

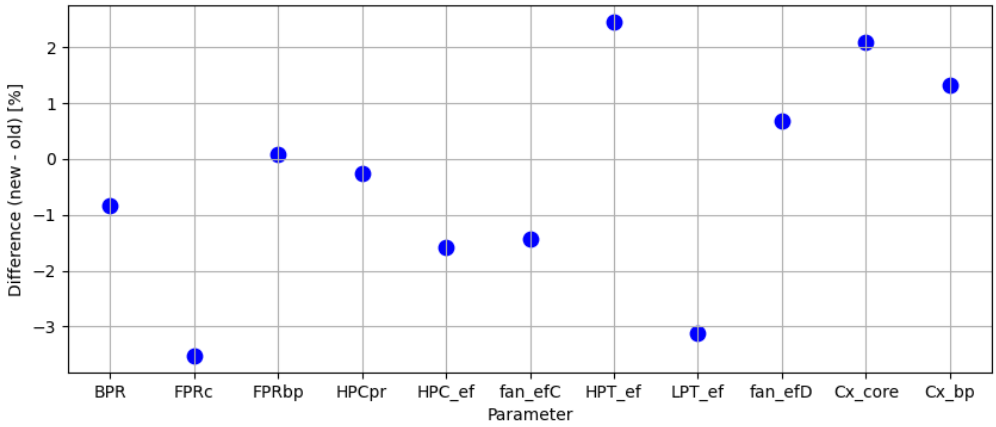

Figure 9.12: Design parameters comparison between the new and old engine model for the CF6-80C2 engine

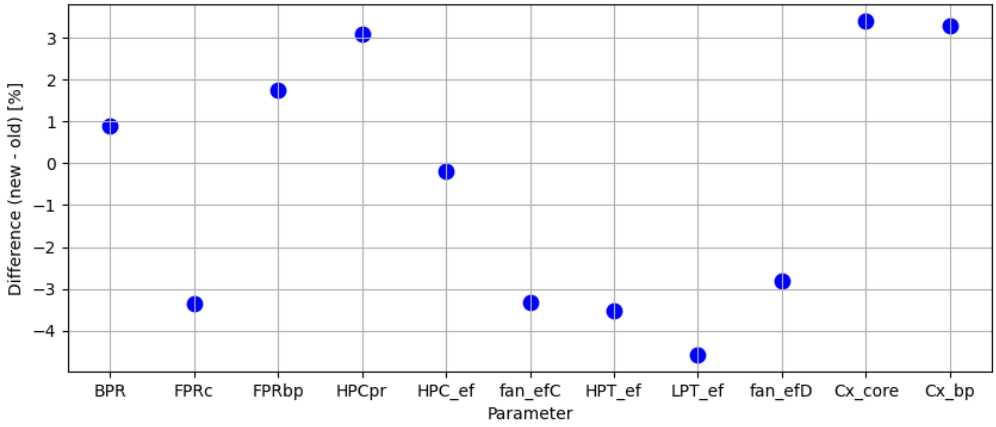

Figure 9.13: Design parameters comparison between the new and old engine model for the GEnx-1B engine

9.2.3. Comparing the design point efficiencies

In this section the turbomachinery efficiencies for both test cases are compared. The compressor efficiencies where constrained by using the relations of Walsh *et al.* [33], depicted in Figure 9.14, and 9.15. The obtained results are also depicted in this figure. Furthermore, the differences between the optimised results and reference data can be found in Table 9.2.

It can be observed that the GEnx HPC loading is slightly lower than the one for the CF6. This can be explained by looking at the definition of the loading coefficient. The GEnx has a higher N2 speed (by more than 1500 rpm, see Table 7.2), which results in a higher tangential velocity. Although the GEnx HPC delivers higher pressure rise, the enthalpy increment is not much higher than the value of the CF6 engine. Moreover, the CF6 HPC has four more stages compared to the GEnx, and leads to a lower enthalpy rise per stage. Since the velocity is squared, the net effect of the higher tangential velocity

and higher enthalpy rise is a lower GEnx HPC loading. The HPC efficiency is higher for the GEnx due to this lower loading and a higher technological level.
It can be noticed as well that the GEnx fan core has a higher loading coefficient. This can be the consequence of the lower N1 spool speed for the GEnx, which leads to a higher loading. Since this graph is only for compressors—and not a single stage fan combined with a booster—the obtained efficiency is higher than the reference curve. The CF6 engine has a higher N1 (almost by 1000 rpm), and has no difficulties meeting the fan core efficiency constraint.
For the fan bypass loading, again the GEnx has a higher value due to the lower N1 speed. The efficiencies for both engines are higher than the reference data. These are both off from these data by approximately 1 % as can also be seen in Table 9.2. The GEnx fan bypass efficiency does not demonstrate a lot of improvements relative to the CF6. This can be caused by the larger fan diameter of the GEnx.
A Smith chart, also from Walsh *et al.* [33], was used to aid the optimiser with selecting the turbine efficiencies and is depicted in Figure 9.16. The outcome for both engines is also included in this figure. Notably, the loading for the LPT of both engines are approximately the same. The GEnx LPT has two more stages compared to the CF6, which lowers the average stage enthalpy change even though the total enthalpy rise is larger. The flow coefficient is lower for the GEnx. This can be attributed to the lower axial velocity for the latter, due to the larger cross-sectional areas of the gas path. The effect of the lower N1 for the GEnx is small, since the LPT has a larger average diameter.
The loading of the GEnx HPT is a bit lower than the CF6, which is again due to the higher N2 speed. Similarly to the LPT flow coefficient, the HPT flow coefficient is lower as well for the GEnx compared to the CF6. This originates form the higher GEnx N2 speed.
From Table 9.2 it can be observed that the GEnx efficiencies are higher than the Smith chart data. This is also the case for the CF6 LPT efficiency. The CF6 HPT efficiency, on the contrary, is a bit lower. This again demonstrates a higher technological level for the GEnx.

Table 9.2: Turbomachinery efficiency differences between simulated and reference values

Parameter	**GEnx-1B**	**CF6-80C2**
Absolute differences (Simulated - Reference) in %		
Fan core polytropic efficiency	4.5	0.4
Fan bypass polytropic efficiency	1.3	1
HPC polytropic efficiency	0.7	-0.5
HPT isentropic efficiency	0.3	-0.7
LPT isentropic efficiency	1.6	0.8

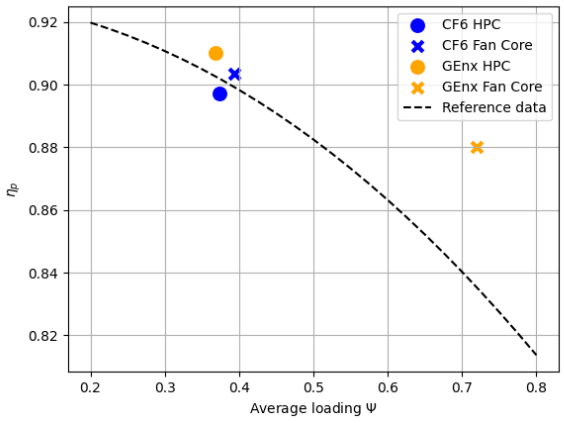

Figure 9.14: Compressor efficiencies outcome

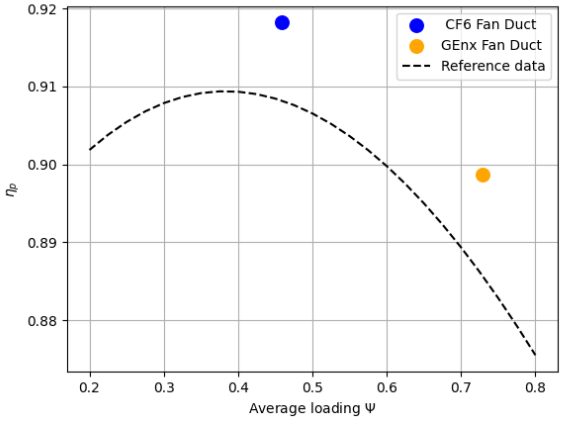

Figure 9.15: Fan bypass efficiency outcome

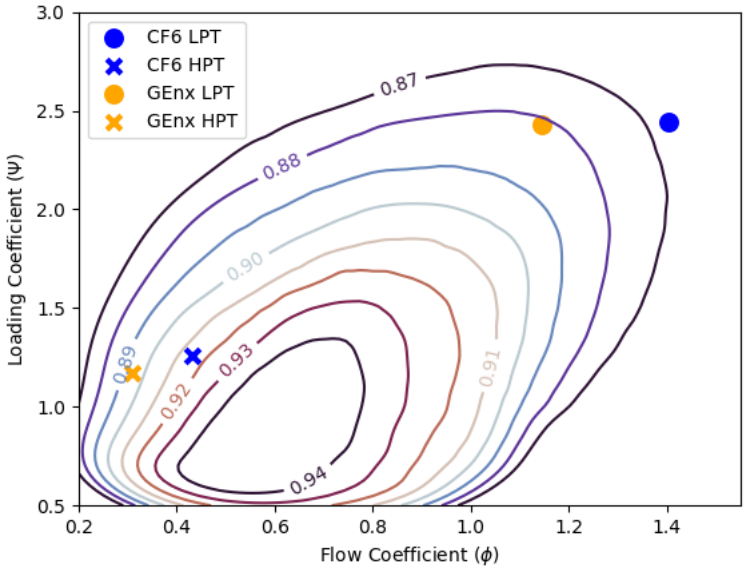

Figure 9.16: Turbine efficiencies on the smith chart

9.2.4. Comparison with trends

In Chapter 3 some general gas turbine and turbomachinery component trends were presented. The overall performance trends illustrate an increase in OPR, BPR, TIT. This has been confirmed by comparing the CF6 with the GEnx engine model. The attained turbomachinery efficiencies were compared with the trends presented by Head *et al.* [24]. The outcome of the latter study showed an increase in polytropic efficiencies with certification year for all the turbomachines. They also displayed a plateau starting from a certification year of around 2005, which indicates that the turbomachinery technological improvements for the current aero engine configurations are reaching a limit. In the results presented before, the increasing efficiency trend was not observed for all the turbomachinery components. There was a dependency on the stage loading. This parameter was not included during the analyses of Head *et al.* [24]. The offset from the reference relations (see Table 9.2) for the component efficiencies of the GEnx, however, is higher than the deviations of the CF6. This illustrates the improved performance for GEnx turbomachinery components.

9.3. Off design modelling results

Using the design point results and off-design data described in Section 9.2 and Section 7.4, respectively, the off-design modelling can be commenced. The procedure for this has already been described in Section 8.2. This section presents the outcome for both, the CF6 and the GEnx turbofan engines. For the sake of brevity the GEnx results will be described more elaborately compared to the CF6 engine. First the selected maps and GA results are presented, respectively. This is followed by the component characteristic maps description. These are obtained after multiple optimisation attempts using different component maps and bounds.

9.3.1. Selected maps

The selected maps for the off-design models of both engines are presented in Table 9.3. For the GEnx engine the same turbine maps are used as the ones for the CF6. The maps are selected either from the GSP, or from the Smooth C and Smooth T map collection. These were obtained after several endeavours, with the aim to obtain realistic optimised maps and operating lines. It was slightly more challenging to find suitable component maps for the CF6 engine, especially the fan core. This is expected to be due to the small operating range of CF6 Off-design operating points, as can be seen in Figure 7.4. This gives the optimiser more freedom and can result in unrealistic component maps and operating lines. There were also some difficulties to get the fan core operating line right, for the GEnx.

The cause for this can be the modelling decision to merge the fan core and booster. By doing this, one tries to capture the physics of two different machines in a single map, which can be challenging. A subsonic booster map was selected for the fan core of both engines. As mentioned in Section 5.2.1, the operating regime of high bypass turbofan engines low pressure modules is subsonic. Moreover, a map of a fan is also not representative for a multistage compressor module.
The selection was done based on the information provided in Section 8.2. Notably, it was not possible to find component maps where all the design parameters were similar. The selected maps were the most suitable ones and gave the best results.

Table 9.3: Selected component maps for the CF6 and GEnx engine

Component	Map	Stages	Design mass flow (Corrected)	Design Pressure
CF6-80C2				
Fan core	Cranfield three Stage Axial Compressor [69]	3	10.6	2.4
Fan bypass	NASA Quiet Engine Program fan bypass map [70]	1	436	1.52
HPC	GE -CF6-6 / LM2500 Compressor [71]	16	65	15
HPT	GSP Big Fan HPT map	-	-	-
LPT	GSP Big Fan LPT map	-	-	-
GEnx-1B				
Fan core	Three Stage Axial Compressor [72]	3	13.4	2.03
Fan bypass	NASA Energy Efficient Engine fan bypass map [73]	1	1100	1.55
HPC	MAN GT6 Industrial gas turbine compressor [74]	11	30	15.5

9.3.2. Algorithm Results

Firstly, the algorithm results are presented and discussed. The convergence graph for the GEnx and CF6 engine is given in Figure 9.18 and 9.17, respectively. The final attained objective (RMS error) is $6.6 \cdot 10^{-3}$ for the GEnx and $4.9 \cdot 10^{-3}$ for the CF6. It is evident from these figures that the optimiser has converged. Moreover, it can be noted that the CF6 model took more iterations to converge. A plausible explanation for this can be the tighter bounds that were used to prevent the optimiser from producing unrealistic maps, caused by the smaller operating range for this engine as mentioned before.
The mean error for all the off-design target parameters, computed along the available operating data range of the GEnx and CF6, is given in Figure 9.20 and 9.19, before and after adaption. The non-averaged errors can be seen in figure Figure E.2 and E.1. These are all sufficiently small and deemed acceptable. Some errors are reduced substantially, while others are only reduced slightly or even increased. The latter being the T_{t3} measurement for the GEnx. One possible explanation for this can be the magnitude of the offset before the optimisation. This is already low, hence the optimiser focussed on the other parameters due to their larger impact on the objective. This can also be the reason that some parameters only decreased marginally. Moreover, at the cost of reducing the errors of some parameters others can increase, whilst still resulting in a lower overall RMS error (objective). From Figure 9.4 it can be observed that the T_{t3} and P_{s3} measurement are both effected by the fan core and HPC pressure ratio. Thus it is possible that the P_{s3} error is reduced considerably at the cost of a slight increase in T_{t3} error.
It can be noted that the largest error is found for the N2 and is approximately 1.1 %. Multiple factors can contribute to this offset. The location of the reference point on the performance map is one of them. Its location affects the relation between the different component performance parameters, as told in Section 8.2, thus to achieve a certain pressure ratio the spool speed will be different. This relation is also affected by the choice of component map, consequently impacting the high pressure spool speed. Thus this error can be further reduced by repositioning the reference point or choosing a different component map. Other factors affecting the N2 speed are the VSV and VBV settings. Otten [17] also proved that modelling the VSV effects reduced the N2 offset. However, since the N2 is of secondary

importance from a thermodynamic perspective [32] it was decided not to continue with improving the model.

In addition to the T_{t3}, the T_{t49} (EGT) error of the CF6 has also increased. The same reasoning as for the GEnx parameter error increase can also be applied here. From the results of the sensitivity analyses presented in Section 9.1 it can be observed that multiple parameters influence the EGT. The fan core pressure ratio and efficiency are amongst these. These also affect the P_{t25} and T_{t25}, and hence their error, which is substantially reduced. Thus it is possible that these errors are reduced at the cost of an T_{t49} error increment. The explanation for the T_{t3} error increase is exactly the same as for the GEnx. The largest error can again be found for the N2 parameter and equates 1.1 %. As explained before for the GEnx this can be attributed to the choice of reference point location or component map. This model is not further improved for the same reason as the one of the GEnx.

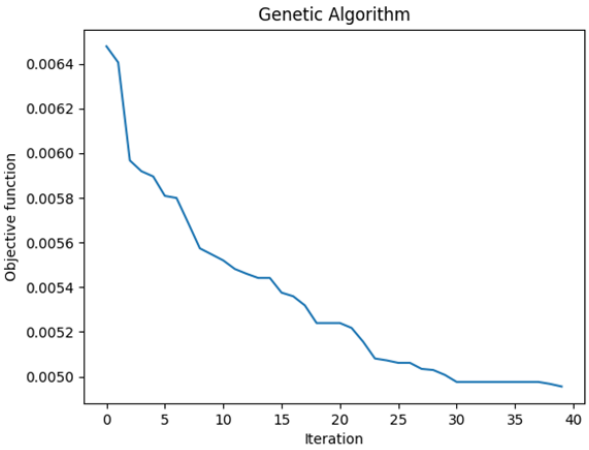

Figure 9.17: CF6 Off-design convergence graph for 20 iterations and 7 individuals

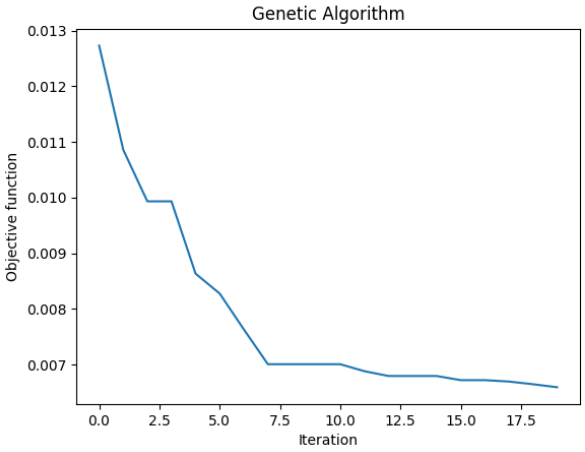

Figure 9.18: GEnx Off-design convergence graph for 20 iterations and 7 individuals

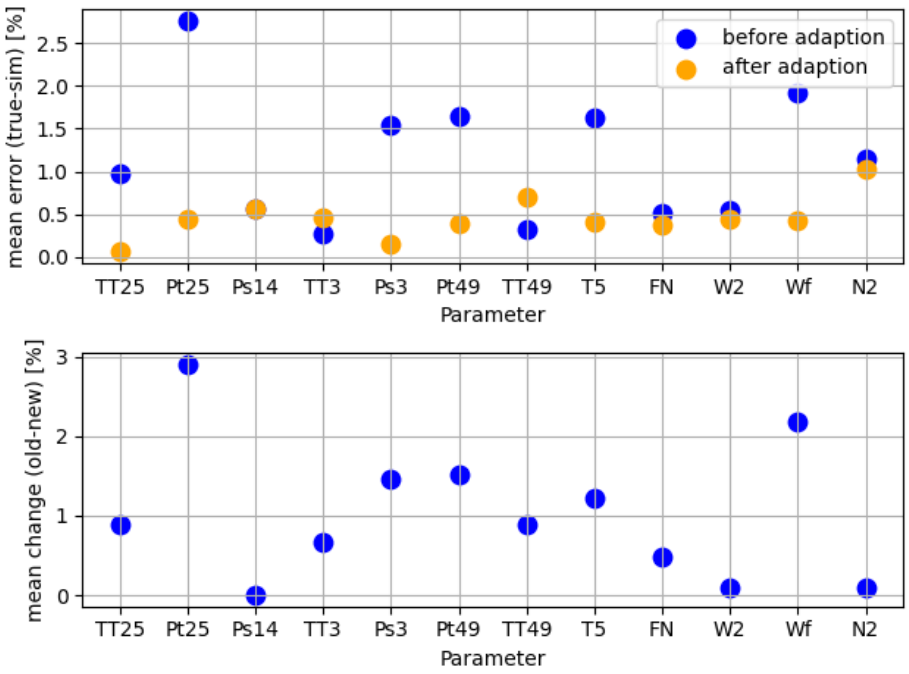

Figure 9.19: Mean error for the CF6 target parameters

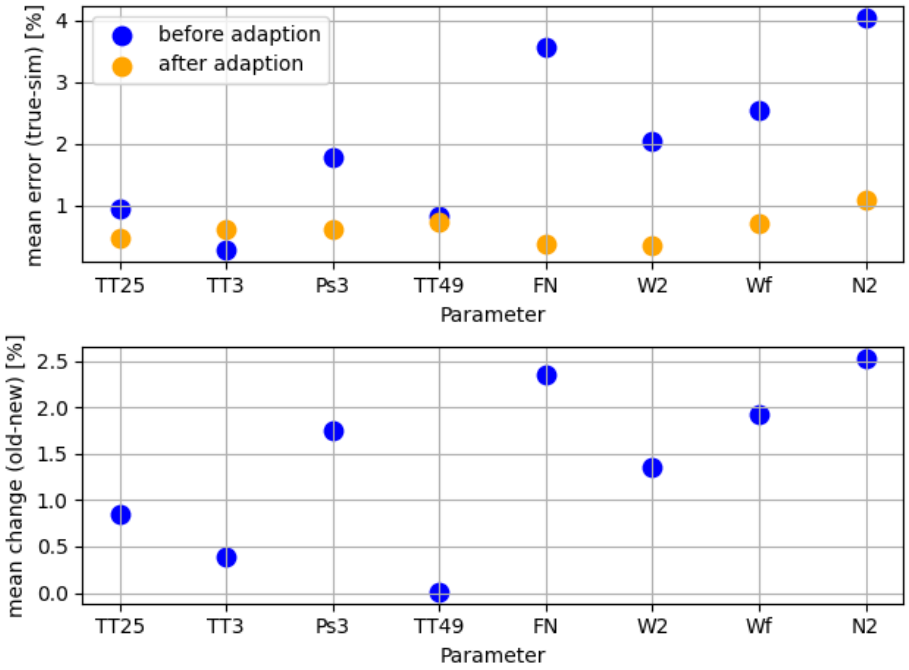

Figure 9.20: Mean error for the GEnx target parameters

9.3.3. Compressor maps

The obtained compressor maps for the GEnx can be seen below. Firstly, the fan core map is illustrated in Figure 9.21. The grey map is the starting map and the black map is the optimised one. It can be observed that in the low speed region the pressure ratio (PR) has increased, while the mass flow and efficiency have been decreased. Close to the design point the changes are minimal. This is due to the nature of the quadratic scaling functions, defined by Equation 5.3. The changes in the region higher than design point are the opposite also due the way the scaling function is defined. The modified map has a lower PR for the same corrected mass flow and N1c. A possible cause for this can be the presence of inlet guide vanes (IGVs) for the reference component. The GEnx booster is not equipped with any IGVs. Additionally, the reference compressor also has a smaller cross-section. This can cause a higher density increment, and consequently a higher pressure ratio. The higher diameter for the GEnx results in larger tip speeds, hence the relatively lower efficiency.

In Figure 9.22 the fan bypass map can be seen. The pressure ratio and mass flow are only slightly modified, with the most notable difference found in the low speed region. The efficiencies, on the other hand, have been lowered moderately. Again the map has been modified the least around the design point. The efficiency drop can again be the cause of the high fan tip speeds, due to the large fan diameter of the GEnx engine. Moreover, the efficiency drop in the low speed region for the reference map is negligibly small, which is not in accordance with the expected trend.

Finally, the HPC map is depicted in Figure 9.23. In the low speed region the pressure ratio and mass flow have reduced, while the efficiency has increased. In the high speed area a small increment in mass flow and pressure ratio can be noted, with the opposite change visible for the efficiency. In the region below the design point the modified map has a higher PR for the same corrected spool speed and mass flow. An explanation for this can be the higher tip speeds for the reference component, which also justifies the lower efficiency. Higher PRs mean higher adverse pressure gradient, hence lower surge PRs.

The results for the CF6 engine can be found in Appendix E. No odd changes are made to the maps. It can be noticed that the efficiency peak of the starting fan core map is located in the low speed region, which is typically not the case for a compressor map. The design point of a compressor is generally located in the high speed region and also has the highest efficiency. The modified map, however, is different and more in line with the expectations. Now the efficiency peak is located close to the high speed region. For the fan core of the CF6 the modified map has a higher pressure ratio for the same corrected mass flow and N1c in the region below the DP. The reference engine has a higher tip speed, which can possibly result in a lower surge line.
The modified fan bypass map, on the other hand, has a lower PR for the same N1c and mass flow. The change, however, is small and can be due to geometry differences. Moreover, the reference map has a lower efficiency, which can be due to the high design Mach number of 0.82.
For the HPC the optimisation resulted in a higher mass flow and pressure ratio for the same N1c. The efficiency has been lowered. The latter can be caused by the higher tip speeds of the CF6-80C2 engine. The other changes can be due to the same reason. Additionally, the higher design reference PR, lower reference mass flow, and variable geometry can also be possible sources for the differences.

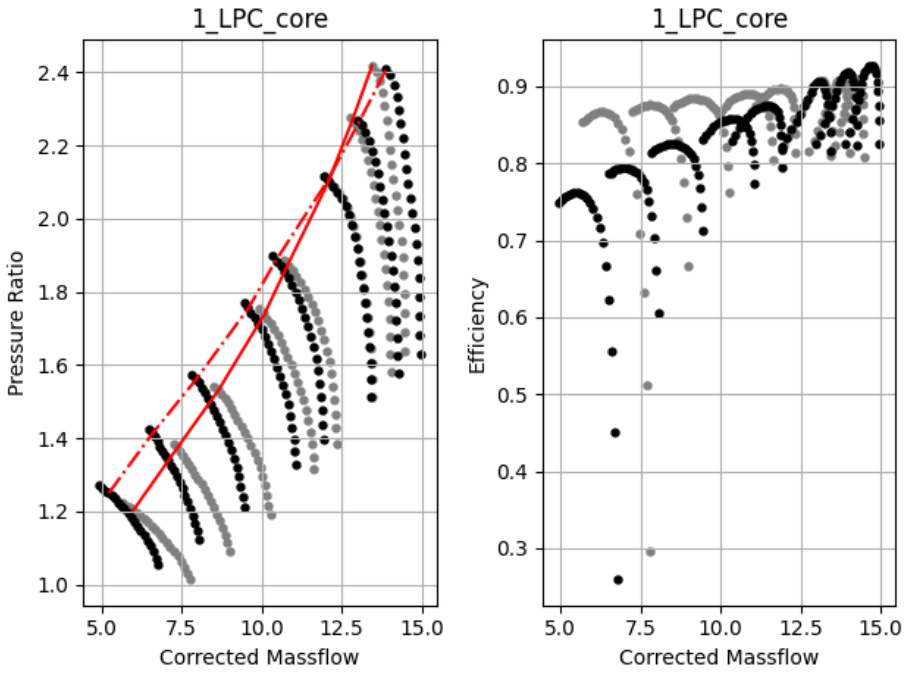

Figure 9.21: Fan core map before (grey) and after (black) adaption

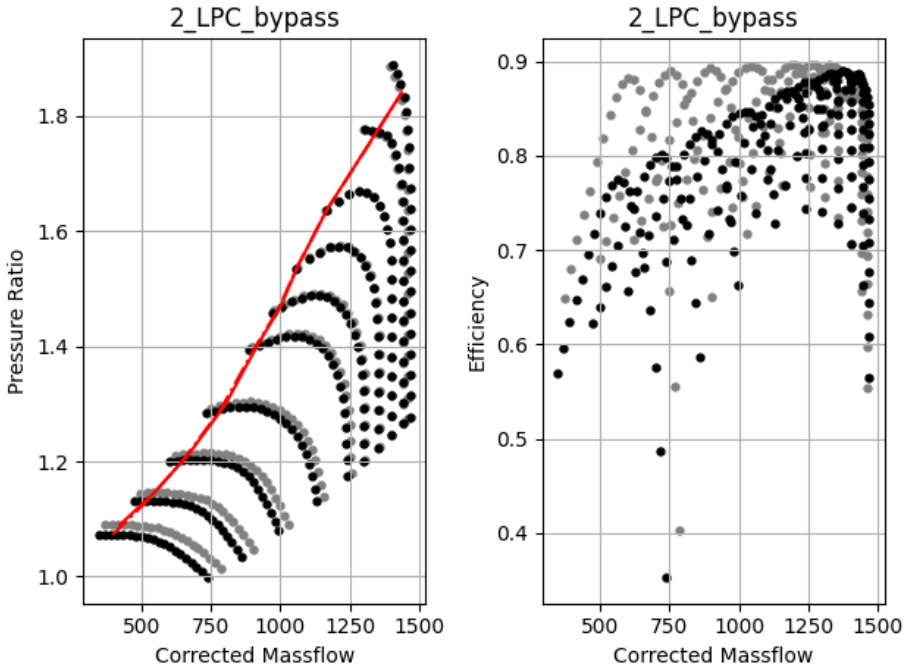

Figure 9.22: Fan bypass map before (grey) and after (black) adaption

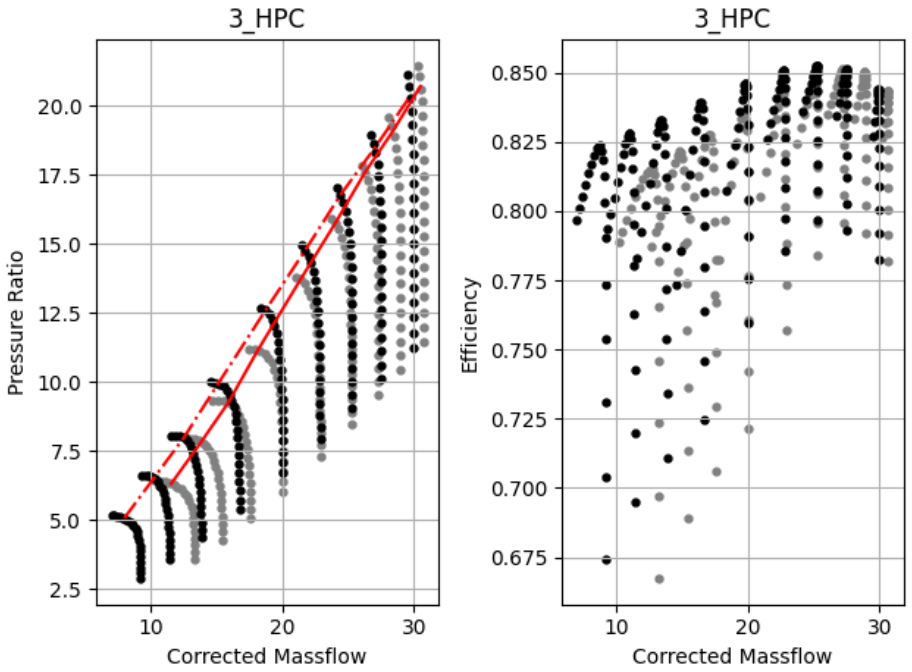

Figure 9.23: HPC map before (grey) and after (black) adaption

9.3.4. Turbine maps

The turbine map for for the HPT and LPT are illustrated in Figure 9.24 and 9.25, respectively. Again the black map indicates the optimisation outcome. The mass flow and pressure ratio for both components remain unmodified as expected. The efficiency has changed in a similar manner for both turbines. An increase can be observed in the low speed (upper) region and a decrease is visible in the high speed (lower) region. For the CF6 maps the changes are similar to the ones of the GEnx engine. The HPT

efficiency has been lowered moderately. The LPT efficiency on the other hand has been modified substantially. As the speed decreases a larger drop in efficiency is visible. Since limited information about the reference map machine is available, it is difficult to come up with a concrete reasoning. The results, however, indicate that larger losses occur for lower corrected spool speeds. This can be due to larger tip speeds, and/or sub-optimal tip clearances. Differences in geometry also play an important role.

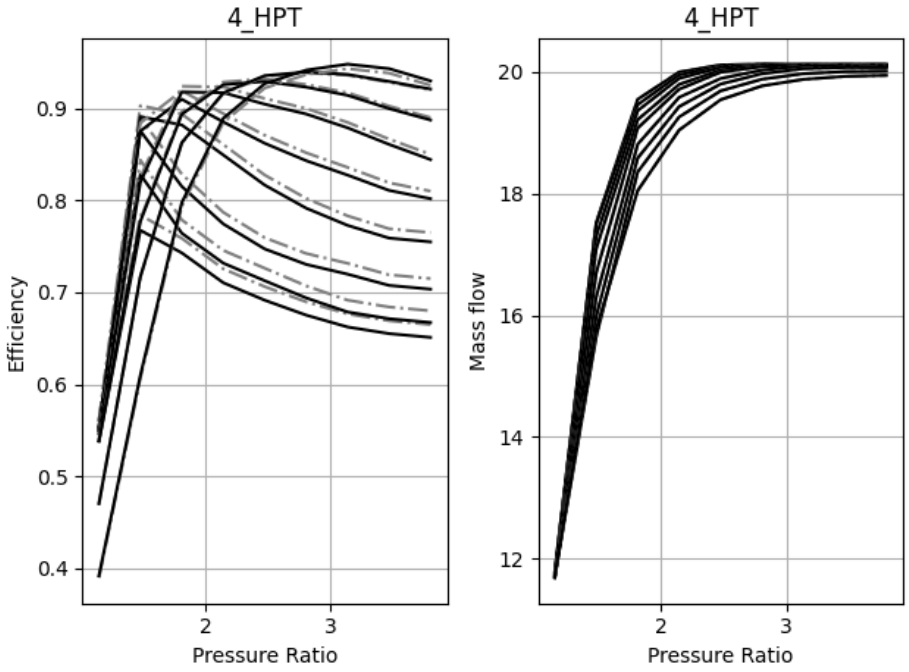

Figure 9.24: HPT map before (grey) and after (black) adaption

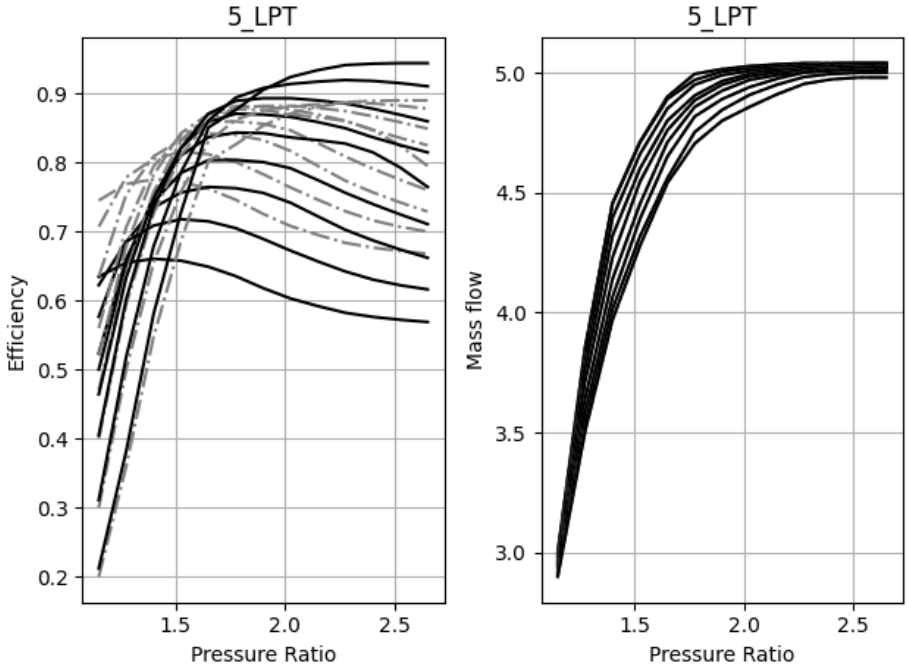

Figure 9.25: LPT map before (grey) and after (black) adaption

9.3.5. Operating lines

The operating line of a turbomachine is dependent on multiple factors. Two of the important ones are the choice of characteristic map and reference point location, as mentioned before. During the off-design modelling process it was required to change the component maps and the reference point location multiple times in order to obtain feasible results. This includes non-drastic changes in pressure ratio, efficiency and mass flow. In Figure 9.26 one of the intermediate results is given. The operating line is clearly not smooth and also diverging from the surge line. It is expected that the compressor operating line maintains the reference point (DP) surge margin at lower spool speeds as well, or gets closer to it. The latter since the compressor stages are struggling to deal with the high adverse pressure gradients and initiate stall. The pressure ratio where surge occurs reduces with mass flow. This is due to the decrement in axial velocity at a constant spool speed, which in turn causes the incidence angle to increase. At incidence angles higher than the optimum angle, flow separation and stalling can occur [4]. Variable geometry and/or bleed is used to remedy this. In Figure 9.27 the improved operating line can be seen which is attained by repositioning the reference point. The surge margin in this case (sea level) is around 10 %, which is slightly on the lower side. For higher altitudes it is expected that the surge margin will increase, due to the lower bypass nozzle pressure ratio [32].
Furthermore, operating lines that run into the surge line were also encountered. This is not realistic and is always avoided for the physical engine (using secondary performance devices) in order to prevent damaging the engine. Repositioning the reference point did not solve this problem, thus it was decided to use a different component map.
For the HPT it was observed that the operating line excursion was relatively small. The pressure ratio and mass flow were almost constant. This behaviour can be explained by looking at Figure 6.6. It can be observed that the operating point of the HPT is almost fixed if the LPT inlet is choked. This is also inline with the literature [7, 32].

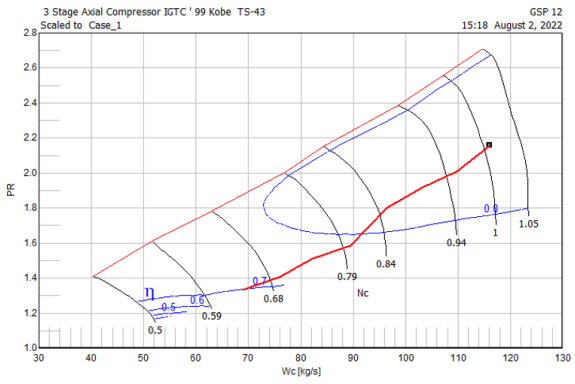

Figure 9.26: GEnx fan core map with un-smooth operating line

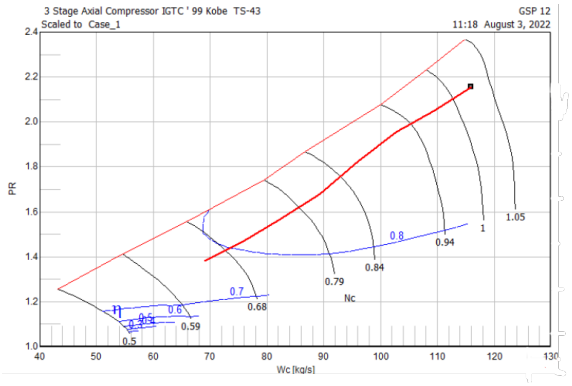

Figure 9.27: GEnx fan core map with smooth operating line

9.3.6. Checking for physical correctness

In Section 5.2.1 multiple relations were defined, that could be analysed in order to check the underlying physics of component characteristics. For the compressor modules of both, the GEnx and CF6 engine, these were in line with the literature. It was observed that for the lower speed range the contours deviated from the general trend, this was also expected due to the increased sensitivity as told before in Section 5.2.1.
The loss correlations for the turbines are also in agreement with the literature. A bucket was clearly noticeable for all of the loss characteristics. Additionally, it was also noticed that the low speed contours deviated from the general trend, as expected. The efficiency to turbine velocity ratio correlations were inspected as well. This can be seen in Figure 9.28 for the LPT of the GEnx map. The parabolic variation of the efficiency can clearly be observed, however, there is a dependency on the velocity ratio. As mentioned in Section 5.2.1, the peak efficiency is only dependent on the turbine stator exit angle. The latter holds for an ideal single stage turbine. This is not the case for the actual engine and can be the cause for this discrepancy. Another reason for this deviation can be due to the map file format differences between Smooth T and GSP. The Smooth T manual advises to uses a high resolution in the low speed region, which is not the case for the GSP maps. The largest disparity is also found in

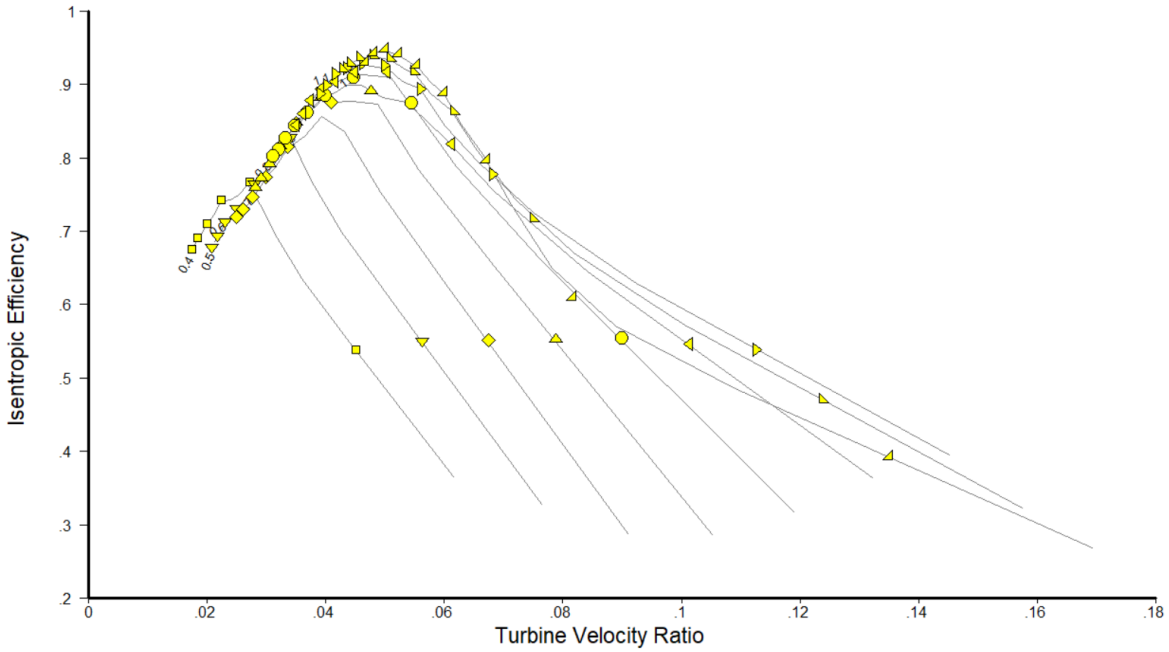

Figure 9.28: Turbine efficiency as a function of the Turbine velocity ratio for the GEnx LPT

the same region. Similar results were attained for the HPT and CF6 turbine maps.

9.3.7. Comparison with old maps

As already known, modelling projects have been conducted in the past for the GEnx and CF6 engine. In this section the differences between the old and new component maps are briefly discussed.

First the CF6 model will be addressed, which was the best model available at the disposal of KLM ES. Firstly, a transonic map was selected for the fan core. This is not the right choice for un-geared high bypass ratio turbofan engines that have relatively low N1 spool speeds. Furthermore, the fan bypass and HPC map do not have smooth efficiency contours. For the turbines, the relations described in Section 5.2.1 do not agree with the expectations, especially the first and second turbine loss characteristics as there was no bucket observable.

The GEnx maps are described subsequently. Again a transonic map was selected for the fan core. The operating regime of the map and the actual module do not match, thus the underlying physics will differ as well. For the fan bypass maps the efficiency contours are not smooth. The latter can lead to jumps in component and overall performance parameters. The turbine loss characteristics defined in Section 5.2.1 were also plotted, and none of these were in line with the literature.

10

GEnx model validation

With the modelling process now finished, it can be investigated how the model performs on data that it has never seen before. The latter being on-wing data, recorded at higher Mach numbers and altitudes. In this chapter it is first analysed how a single model can be generalised to other engines from the same pool. The method described in Chapter 8 can be applied to a specific engine of a certain type. Creating a virtual twin for each engine is, however, not always possible. A prevalent practice is to use a single model for all the engines of the same type. The latter is done due to the scarce data availability. This method, however, does not account for engine-to-engine differences. Subsequently, the validity of the obtained models is proven using CEOD. A discussion for the discrepancies is presented as well.

10.1. Intra vs Inter engine approach

Two approaches can be distinguished when modelling a pool of engines, e.g., the GEnx-1B or the CF6-80C2. These are the inter-, and intra- engine approach [75]. For the inter-engine approach a single generic model is used for representing the entire pool of engines. This model is created using one specific engine data that is representative for the entire class. In the intra-engine approach an engine specific model is used independent of other engines of that pool. While the former (inter-engine) approach is most commonly used, it is not the most accurate. Using an inter-engine approach is favourable since it remedies creating a model for every engine from the pool, which is challenging due to the limited amount of data available.

To illustrate the difference between these two methods, from a health monitoring perspective, Figure 10.1 will be used. In this figure two performance parameters, x_1 and x_2 are plotted against each other. Region A represents normal behaviour from an entire pool of engines. Region B and C indicate the normal and abnormal (deteriorated) performance of a single engine, respectively. If an average performing engine from the class is selected for the inter-engine approach, it is highly probable that the performance degradation of the single engine in this example will not be identified. This highlights the importance of the intra-engine method. Using this method, engine-to-engine differences are eliminated, and deterioration is exposed. The same was also concluded in other studies [8, 13, 29].

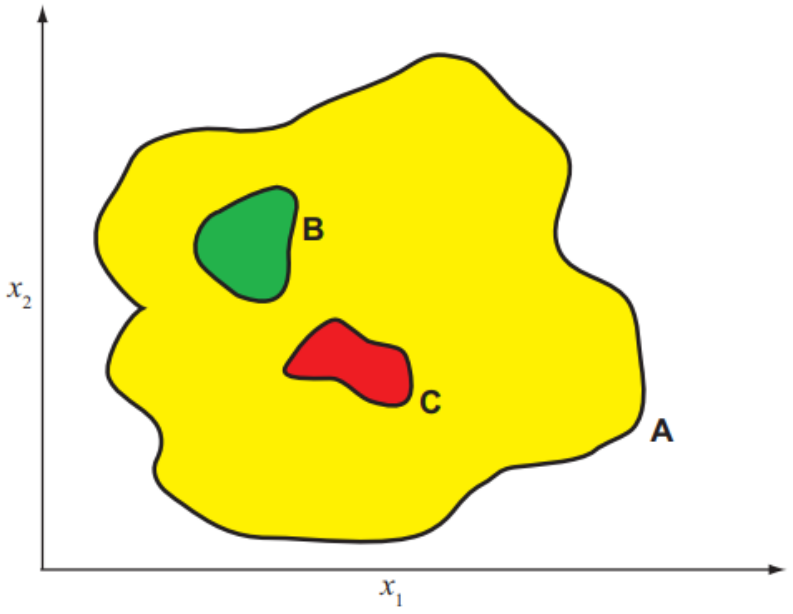

Figure 10.1: Engine behaviour space for an entire class of engines (A) and a single engine (B and C)

10.2. Extending the developed model to other engines

As told above using a single model for the entire engine class is less accurate. However, generally there is not sufficient data to develop a complete model for every engine, especially for off-design modelling. This is also the case for this project. In Chapter 4 it was concluded that the CEOD and test cell performance logs were the most promising data sources. The drawbacks were also mentioned. The test cell performance logs only include a small operating range and the CEOD is lacking some important parameters, e.g., the thrust. The test cell data includes back-to-back testing and calibration reports as told before. These include a larger operating range data, but are only for one specific engine. Consequently, it was decided to only calibrate the design point model and use this outcome as input for the component maps, generated before, during off-design modelling process. To prove the validity of the generated model CEOD will be employed.

The engine used for creating a new DP model is also an GEnx-1B 74/75P2 engine with the Engine Serial Number (ESN) 956xxx. This is the same engine used by some of the previous works[8, 10, 17] concerning the GEnx-1B turbofan engine at KLM ES. The data used is after an engine overhaul that was required due to a Redline Exeedance Event. This in turn was caused by a HPT stage 1 blade mid-chord burndown. Thus the engine can be considered of acceptable health.

The calibration was done using the design point model reported in Section 9.2 as a starting point. Again an optimisation was done using GA, with a similar set-up as described in Chapter 8. The design variables attained before are now used as an initial guess for the GA.

The convergence graph and the optimisation results are given in Figure 10.2 and Figure 10.3, respectively. It is clear that the optimiser has converged, and the errors are sufficiently small. The overall RMS error achieved was $1.11 \cdot 10^{-3}$. The obtained design variables only deviated slightly from the un-calibrated model as can be seen in Table 10.1. An attempt was made to exclude the constraints from the problem, but the results overstepped the constraint bounds considerably. Furthermore, it was observed that the results were obtained at a significantly lower runtime (factor 2), relative to the first DP problem. Since the optimised parameters from Section 9.2 are now used as the starting point, the optimal region is found much faster by GA. This also prevents GA from generating unfeasible parameter vectors, which causes convergence issues in GSP.

The attained design point data will be used as the scaling reference point for the performance characteristics presented in Section 9.3.

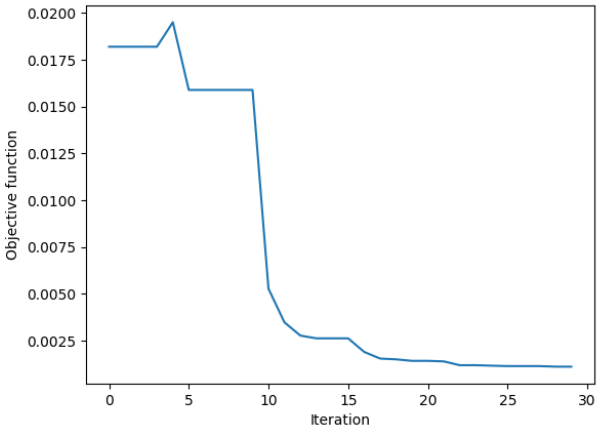

Figure 10.2: Convergence graph GA for calibration process

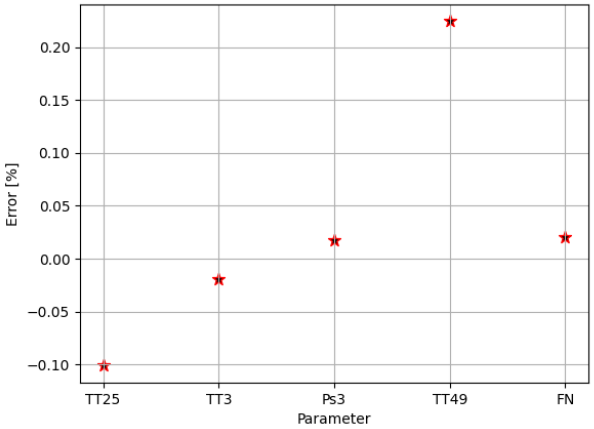

Figure 10.3: Errors between the test cell measurements and simulated results for calibration process

Table 10.1: Change in performance parameters due to the model calibration

Parameter	Change [%]
Overall performance parameters	
Bypass ratio	0
Overall pressure ratio	-0.24
Turbomachinery pressure ratios	
Fan Bypass pressure ratio	-0.91
Fan core + booster pressure ratio	1.67
HPC pressure ratio	-2.09
Turbomachinery efficiencies	
Fan bypass	0.96
Fan core	0.82
HPC	0.6
HPT	-0.3
LPT	1.16
Nozzle coefficients	
Cx Core Nozzle	0.74
Cx bypass Nozzle	-1.64

10.3. Model Validation using CEOD

Firstly, in this section the approach for the CEOD validation is described. This mainly consists of the data selection and pre-processing. This is followed by the attained results from CEOD analyses, including a discussion.

10.3.1. Data preparation

The selected CEOD is from the same engine as was used in the previous section, namely ESN 956xxx. The data used was collected within a few months of the test cell record date. This minimises health deviations potentially caused by operating cycle differences of the engine. Ten flights were selected for the CEOD analyses in order to capture as many flight conditions as possible. Three flight phases were selected for the analyses, namely the take-off, the climb and the cruise phase.

For the data filtering, insights from the study of Rootliep [8] were used. These are summarised below:

- Select the relevant flight phase. These are the take-off, climb and cruise phase in this case.
- From the selection only the steady state points should be chosen. The latter is done by limiting the core speed rate of change between -0.2 and 0.2 %N2/sec.
- Additionally, it should be ensured that points in the cruise phase where the aircraft is climbing to higher altitudes are not selected.
- Remove operating points for which there are outliers in the secondary performance parameters given in Table D.1. By doing so the relations between the primary performance parameters and gas path measurements will be more distinctive. For the filtering limits, the results of Rootliep [8] are used. In the aforementioned study the Interquartile Range (IQR) is employed for outlier filtering.

For each of the three flight phases, the filtering was done separately. Due to the large difference in operating conditions, the performance parameters also differ. Consequently, filtering all the flight phases at once will remove important operating points. Filtering the data will allow to find steady state ”normal” operating points and makes validation of the GSP model straightforward. Finally, it should be noted that the validity of the corrected and calculated parameters is dubious. It is not justified how these are attained.

10.3.2. CEOD analyses results

In the following sections the CEOD results can be found. First the un-calibrated model outcome is presented, and this is followed by the calibrated model results.

Results un-calibrated model

The deviations of the un-calibrated model output from CEOD can be found in Figure 10.4. It can be noticed that the results close to the design conditions (Take-off) are acceptable. The RMS error here is 1.28. At the climb and cruise phase the errors are relatively higher. This is mostly noticeable in the fuel flow and EGT (T_{t49}). From Figure 10.5 it can be observed that the mean absolute error (MAE) is overall lower than one percent, with the largest values found for the fuel flow and EGT at cruise conditions. Note that there are more data used for the cruise phase and these contain more scatter in secondary performance parameters. This is also the reason for the higher MAE at cruise conditions.

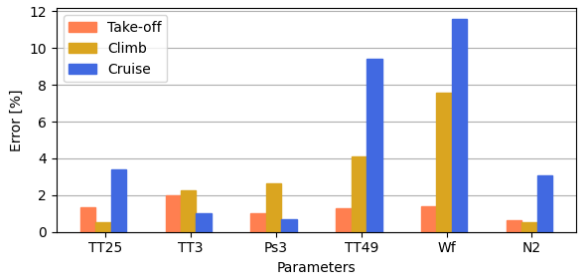

Figure 10.4: Un-calibrated model deviation for the take-off, climb and cruise phase between simulated output and CEOD

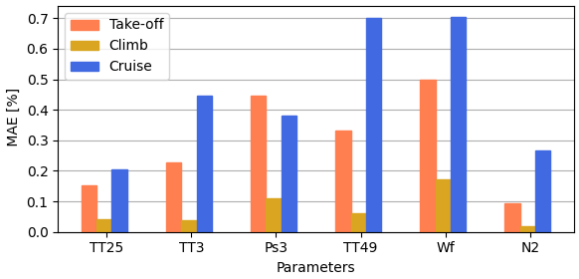

Figure 10.5: Un-calibrated model mean average error (MAE) for the take-off, climb and cruise phase errors between simulated output and CEOD

Results calibrated model

In the following figures the results of the calibrated model are presented. While the deviations at the climb and cruise phase clearly have been reduced, the changes at the take-off phase are minimal. Here the RMS error is almost equal to the un-calibrated model value (<0.01 difference). Thus the calibration did not have a large impact at the take-off phase. This was also expected, since the deferences in the design parameters between the calibrated and un-calibrated model are small. Moreover, this indicates that the un-calibrated model has not been overfitted. The deviations along the corrected speed are also depicted. A clear trend for all the parameters is visible for the climb and cruise phase in Figure 10.9 and 10.10 respectively. Some more scatter can be observed for the cruise phase around the higher N1c. These are points where the aircraft is climbing to higher altitudes during cruise, and have not been filtered out. For the take-off deviations, a trend is less evident. This will be described at the end of this chapter.

Furthermore, from the turbine operating lines at cruise conditions it was noticed that the exhaust nozzles were choked. At the take-off phase the LPT was choked, which was also observed for the test cell operating points.

Although the model has improved by calibrating it, the deviations are still large, in particularly for the fuel flow and EGT, at the climb and cruise phase. Possible causes for these deviations will be addressed in the discussion section.

The mean average error, given in Figure 10.7 has been reduced a bit relative to the un-calibrated model. Again the largest values can be found for the fuel flow and EGT at cruise. These, however, are sufficiently low.

The mean efficiencies for all the turbomachinery at the analysed flight phases can be found in Figure 10.11. These are affected by the operating conditions, and consequently depend on the position of the operating point on each component performance map. These will be elaborated upon in the next section.

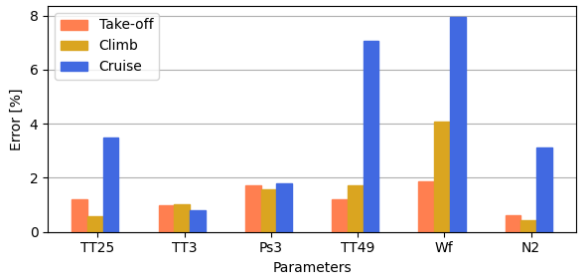

Figure 10.6: Calibrated model mean deviation for the take-off, climb and cruise phase between model output and CEOD

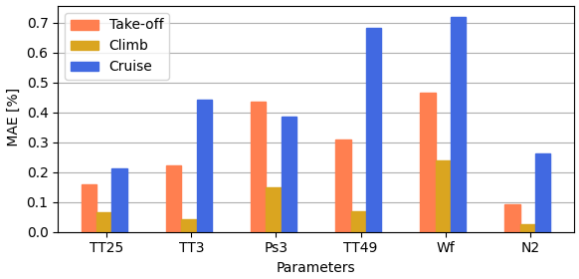

Figure 10.7: Calibrated model mean average error (MAE) for the take-off, climb and cruise phase errors between simulated output and CEOD

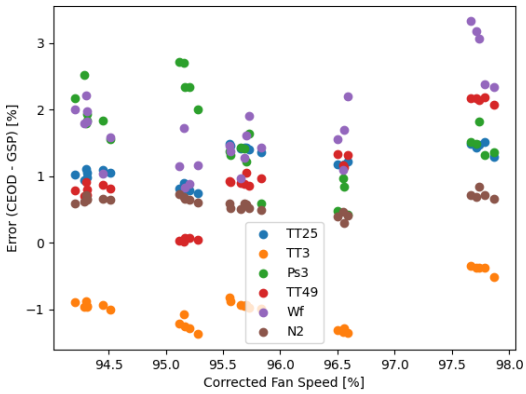

Figure 10.8: Calibrated model Take-off phase deviation from CEOD

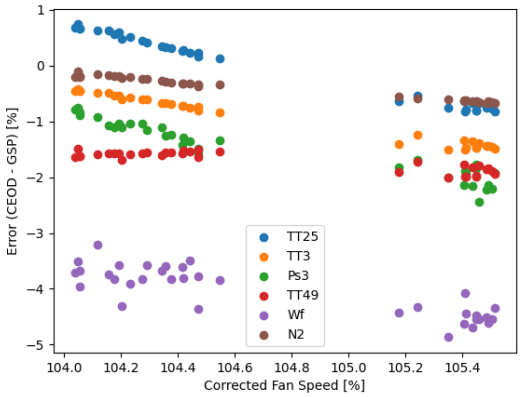

Figure 10.9: Calibrated model Climb phase deviation from CEOD

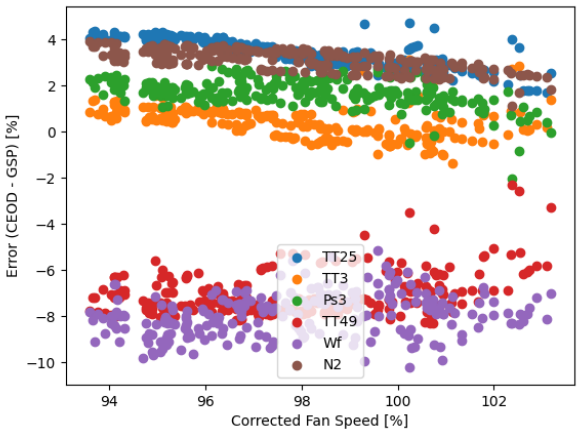

Figure 10.10: Calibrated model Cruise phase deviation from CEOD

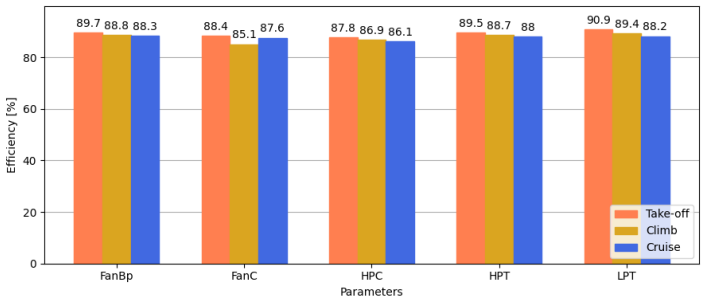

Figure 10.11: Calibrated model mean efficiencies for take-off, climb and cruise

10.4. Discussion

In this section the most important findings and results from the sections above are discussed. The possible causes for the model deviations are addressed as well.

Calibration effects

From the results presented above it is clear that the model has been improved by calibrating it, even though very little for the take-off condition. The design point model is created at sea level static conditions. This point is used to scale the performance characteristics. The closer an operating point gets to the map reference point, the closer the performance parameters are to the design point values. This is the case for all the individual component scaling reference points. Thus component matching is influenced by the reference point. From Table 10.1 is it evident that the changes are minimal. Hence it follows that at the actual take-off operating conditions (non-static)—which is close to the reference point— the differences will be small as well. At points located away from the reference point the differences are more pronounced, which is observable in the climb and cruise deviations. At these points component matching is uncoupled from the DP. Consequently, the improvement due to the calibration is more noticeable. Thus the operating condition changes due to engine-to-engine differences has been accounted for by the calibration. A good example for this is the pressure ratio of the compressors. These differ at the design point, however, they lead to a similar OPR as can be seen in Table 10.1. At off-design conditions the OPR can be different due to the deviation in individual compressor pressure ratios. The latter was also observed in the results.

Moreover, reference point scaling effects has a dependency with the direction. For example, the ellipse like efficiency contours will have different scaling effects along the major and minor axis. This can also be seen in Figure 10.12. For the fan core and LPT, the changes in efficiency are not constant for all the flight phases. It should be noted that the calibration outcome can not entirely be attributed to this offset.

Another cause for the performance deviations with respect to on-wing data for operating points close to the DP is related to the objective for the off-design modelling process. The objective used is the RMS error. As can be noticed from Figure E.2, the deviations are the largest in the low speed range, hence the optimiser mainly focusses on reducing these. Changes close to the DP are small. This is also due to the scaling method used. The scaling polynomial of second order is equal to one at the DP. For operating points in the vicinity of the DP, the changes will be insignificant as a result.

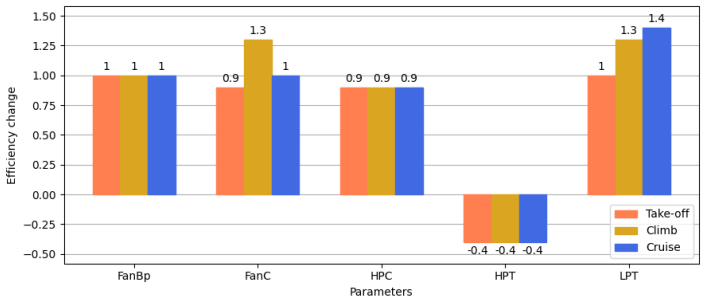

Figure 10.12: Efficiency change by calibrating the model at take-off, climb and cruise

Trends in deviations

Next the trends in the deviation figures along the N1c are discussed. For the take-off results, depicted in Figure 10.8, a small amount of spread is visible (although its minimal). This can also be concluded from the Figure 10.7. A jump can be seen in this figure, just below 98 % N1c. Looking back at the CEOD it was observed that a similar pattern was visible in the computed core mass flow parameter. Thus it can be possible that some flight conditions are not captured by the GSP model. This can for example be caused by losses at the inlet (due to complex inlet flow phenomena) in particularly for the take-off roll phase where high pitch angles are experienced. Moreover, the flight Mach number was used to compute the ambient static conditions from the fan inlet total properties. This can introduce some uncertainties as well, since the local Mach number is different.
In the climb and cruise phase results, trends are clearly visible. Since these are a longer phase a better selection of operating points could be done, that illustrate a clear trend. The operating conditions are also similar. The change along the N1c can be attributed tot the secondary performance parameters (SPPs). These affect the flow capacity and efficiency of the respective module, and consequently the gas path measurements. For cruise a similar trend was observed for the VSV and HPT ACC. For climb, however, no matching behaviour could be found with the SPPs. Another source for this trend can be the component performance parameters stemming from the characteristic maps. They can deviate slightly from the actual (true) values.

Magnitude of deviations

The magnitude of the deviations at climb and cruise are still relatively high after the calibration. In particularly the EGT and fuel flow (Wf) stand out. The possible causes for these deviations are threefold. The first one is associated with the definition of the corrected speed used in GSP. In GSP the relative corrected speed can be used as an input. The latter is defined by Equation 10.1. Here *ds* stands for design, and *std* stands for standard day. Thus the N1c relative is 100 % at the design point. On the performance maps this relative corrected speed is used to determine the operating speed of the module. If the reference point on the component map is placed at 100 % N1c, the outcome will be in line with the expectations. However, if this is not true, the results will differ. During the modelling process the reference points are not placed on same N1c on the map, thus each component will move to a different N1c at off-design even if they are attached to the same shaft. This introduces some uncertainty at all of the three flight phases. Still, this is not the main source of the deviations.
Moreover, the secondary parameters are a source of uncertainties as well. This, however, can be eliminated using the findings of the work done by Otten [17]. In the aforementioned study corrections were applied for the ACCs of the turbines and the VSVs. Correspondingly, the errors for N2, W_f , P_{s3}, T_{t3} and T_{t49} were significantly reduced.

$$N_{corr,rel} = \frac{N/\sqrt{\frac{R \cdot T}{R_{std} \cdot T_{std}}}}{\left(N/\sqrt{\frac{R \cdot T}{R_{std} \cdot T_{std}}}\right)_{ds}} \tag{10.1}$$

$$W\frac{\sqrt{\theta}}{\delta} \propto W\frac{\sqrt{T}}{P} = \frac{AM_{ax}\sqrt{\gamma/R}}{\left(1 + \frac{\gamma-1}{2}M_{ax}^2\right)^{\frac{\gamma+1}{2(\gamma-1)}}} \tag{10.2}$$

Component efficiencies

In Figure 10.11 the component efficiencies are presented for the take-off, climb and cruise phase. It can be observed that the results are contradicting the expectations. Generally it is expected that the component efficiencies are the highest at cruise, due to the duration of this phase, and consequently the amount of fuel consumed. For the starting component maps this was ensured, however, it no longer holds for the adapted maps. This deviation was also recognised in the old model results by Otten [17]. Accounting for the secondary performance parameters (SPP) resolved this disagreement. Reflecting back at the function of SPP, they are incorporated in order to improve the efficiency of a certain module at off-design conditions. The design point of the model is set to take-off. Thus, it is expected that the efficiencies of the modules will be lower at other (off-design) operating conditions when SPPs are not accounted for. As the SPPs settings are increased, the component efficiencies increase. The latter does not hold for the low pressure system, since no SPPs devices are present. Additionally, there is no upstream influence from the other components. This is also expected to be the case for the new GEnx-1B model. It should be mentioned that the SSPs are not the sole contributor to the efficiency discrepancies, as will become evident in the subsequent sections.

Velocity coefficient effects

The results of the current model were also compared with the old model developed by Van Moorselaar [10]. The mean offset from CEOD, and the MAE are depicted in Figure 10.13 and 10.14 respectively. It can be observed that the highest errors are for the cruise and take-off conditions. Once more the discrepancies for the fuel flow and the EGT are the largest. In the old model too low values were used for the velocity coefficient (around 0.91). Additionally, Otten [17] concluded that the velocity coefficient implementation in GSP has not been done correctly at choked conditions (e.g., cruise). For this reason the velocity coefficient was not used during the modelling process.

For flight conditions the Mach number varies from around 0.25 at take-off to 0.85 at cruise. This highly affects the nozzle calculations. Since the velocity coefficient is set to one, there are no losses introduced, thereby limiting the maximum mass flow trough the nozzle and upstream components for choked conditions. The corrected compressor mass flow can be expressed as a function of the Mach number and is given by Equation 10.2[32]. Using the bypass nozzle Mach number at take-off and cruise conditions as input, a change in mass flow of 3.8 % occurs according to this equation. The GSP model, on the contrary, only shows a change of around 1 % for the fan bypass. The pressure ratio of the fan bypass is too high as a result and demands more power, which explains the high fuel flow and EGT deviations. The latter was also mentioned by Otten [17]. Otten improved the model at cruise conditions by adding flow capacity and efficiency changes to the low pressure system. Upon doing the same for the cruise conditions, the deviations were also reduced as is evident from Figure 10.15.

Moreover, it can be observed that old model outperforms the model developed during this project at take-off. The reason for this can also be related to the velocity coefficient. This was confirmed by running the developed model with a bypass velocity coefficient of 0.98. The output is depicted in Figure 10.16. The take-off results have clearly been improved, at the cost of some of the climb and cruise deviations. This can be due to the wrong implementation of the velocity coefficient at choking conditions of the nozzle.

The effect of the velocity coefficients on the trends were analysed as well. For the climb phase a large correlation between the velocity coefficient and the trends was recognised. Using a value of 0.98 for the velocity coefficient reduced the dependency on N1c. The latter was also observed for cruise conditions, however, to a lesser degree. Note that the velocity coefficient affects the operating line, and consequently the efficiencies. Hence, the trends observable in Figure 10.11 will be affected as well.

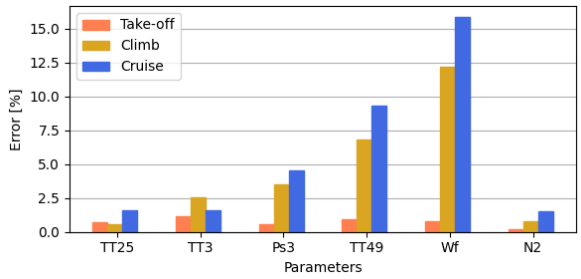

Figure 10.13: Old model mean deviation between simulated output and CEOD measurements

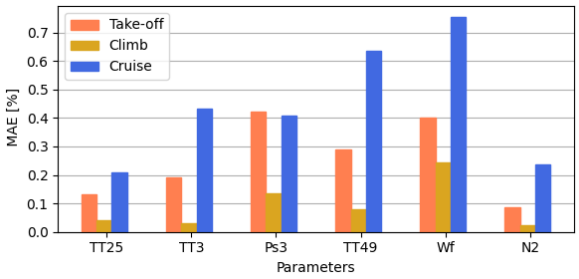

Figure 10.14: Old model mean average error (MAE) for the take-off, climb and cruise phase errors between simulated output and CEOD

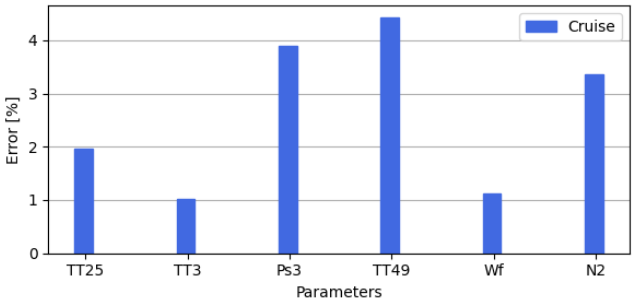

Figure 10.15: Improved model mean deviation between model output and CEOD for cruise conditions

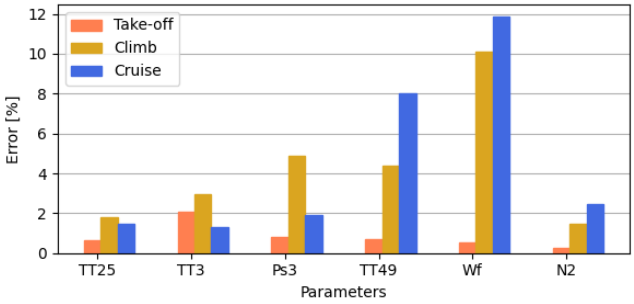

Figure 10.16: Calibrated model Cruise phase deviation from CEOD with C_v = 0.98

Reynolds number effects

Reflecting back at the effect of the velocity coefficient, another phenomenon causing similar effects (flow capacity changes) can be Reynolds number (Re) effects. The latter represents the ratio between inertial and viscous forces, and can be used to describe the boundary layer behaviour on a surface. With increasing Reynolds number the boundary layer becomes thinner, more energetic, turbulent and hydrodynamically rough. There is a certain Re above which losses remain constant. Below this critical Re the viscous losses are increasing and can have effects of secondary order on the engine performance. These become significant if laminar separation is initiated. Due to the high pressure gradients laminar flow does not contain an adequate amount of energy to remain attached, and profile losses occur. Turbulent flow, however, delays separation and can withstand higher pressure gradients.
These Re effects are present on the compressors, and mainly the LPT. It affects the efficiencies and flow capacities. Moreover, the Re effects are more dominant at higher altitudes—i.e during cruise for commercial turbofans— where the density is lower, and consequently the Re as well.
For performance calculations and modelling it is more beneficial to use the Reynolds Number Index (RNI). The RNI is the ratio of the actual Reynolds number and the sea level static Reynolds number at

the same Mach number. Using this definition and some simplifications one ends up with Equation 10.3. When modelling, the RNI corrections can be implemented through coefficients for the efficiency. The corrections for the mass flow are half of the efficiency corrections [32]. The factors can be specified in the component performance map text files. Two factors can be defined, one factor for low RNI and a second factor for high RNI. The corrections are linearly interpolated in between these values. The Re effects were analysed by iteratively changing the aforementioned factors for each module. The best attained results are depicted in Figure 10.17. These were attained for higher correction factors relative to the standard map values, thus higher efficiencies and mass flows at low RNI. By comparing these results with Figure 10.6 it can be observed that the model has been improved significantly for operating conditions with low RNI values. The largest improvements can be found for the EGT and fuel flow for the cruise and climb phase. This can be due to the higher efficiencies, and mass flows for the same iso speed line. The latter leads to lower power requirements from the compressors, and consequently a lower fuel consumption. The T_{t3} and P_{s3}, on the contrary, have slightly been increased. The mean efficiencies, attained after adapting the Reynolds corrections, are depicted in Figure 10.18. It can be observed that these have been increased for the cruise conditions, which is more inline with the expectations.
The best combination of the correction factors can be determined by setting up an minimisation problem, with the goal to reduce the differences between CEOD and model output.

$$RNI = \frac{P}{P_{ref}} \sqrt{\frac{R_{ref} T_{ref}}{RT}} \frac{\mu_{ref}}{\mu} \tag{10.3}$$

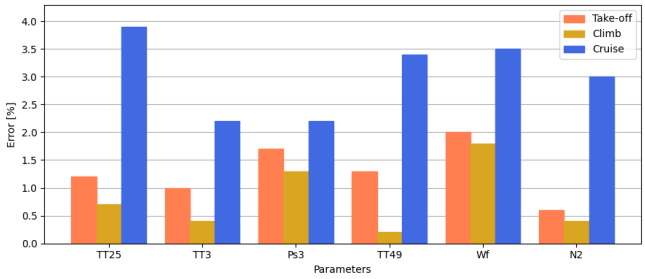

Figure 10.17: Calibrated model mean deviation for the take-off, climb and cruise phase between model output and CEOD with Re corrections

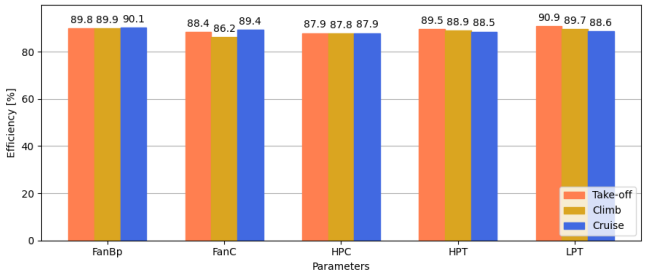

Figure 10.18: Calibrated model mean efficiencies for take-off, climb and cruise with Re corrections

11

Systematic modelling Approach

In this chapter the main steps and key modelling decisions are addressed. This is done for the design and off-design modelling approach. Furthermore, the important findings from the CEOD analyses are presented as well.

11.1. Systematic Approach On-Design Modelling

This section describes the steps for developing a design point model of a turbofan engine. These summarise the procedure used for the GEnx and CF6 design point models, which are used as test cases in this study.

1-Data collection: First of all, the available data sources need to be listed. Multiple sources accessible within an MRO environment have already been mentioned in Chapter 4. From these, the most elaborate and reliable source needs to be selected. It is convenient to select a source with data for a range of operating points, in case off-design modelling needs to be conducted as well. By selecting the same source, engine-to-engine differences will be eliminated, hence increasing the model accuracy. The data in performance sheets and correlation reports should be scrutinised meticulously, as it was noticed that some parameters can be indicated falsely. The units should also be checked, and whether parameters are corrected or not. From the collected data, the design operating point modelling inputs can be selected. Note that different operating points can be selected as the design point, as told in Section 5.1. The top of climb is the most commonly used operating point in literature, however, the data available for this operating point is usually not sufficient to create an accurate model.
Technical drawings of the engines are also available in an MRO environment as told before. The gas path areas or the diameter of the turbomachines can be extracted from these in order to improve the accuracy of the model or compute parameters such as the loading and flow coefficient (defined in Section 6.2). The location for the area measurements needs to be selected based on the sensor positions. These can differ depending on the engine type as mentioned before in Section 7.1. For the Loading and flow coefficient, the average diameter of the turbomachine should be utilised. Note that only using the inlet and outlet stations will not be representative for the module, in particularly if its gas path area changes considerably.

2-Optimisation Set-up: The optimisation set-up can be created once all the required data has been gathered. This includes specifying the design vector, constraints, objective, bounds, and optimiser settings. The choice for design parameters differs from case to case, depending on what is known and what is not. The constraints used in this project have been elaborated upon in Section 8.1. These are intended to bridge the gap caused by the fewer sensors and OEM proprietary data. In this work the root mean square error (RMSE) has been used as the objective. The latter is described by Equation 8.1, and also allows to specify weights for the different target parameters. These parameters are the gas path sensor measurements. Moreover, the design parameter bounds are also highly problem dependent. These can be set using general knowledge regarding the engine. The same holds for the constraint bounds as well. The default optimiser settings can be used as staring values.

3-Creating the GSP model: The GSP model needs to be assembled next. This will consist of the different modules of a turbofan engine. The modules typically used are: the inlet, fan, booster, HPC, combustor, the HPT, LPT and exhaust nozzles. As mentioned before, it is a common practice to merge the fan core and booster in case the measurements between these two components are absent.
Subsequently, all the input parameters can be set in the various modules. These are: the ambient conditions, mass flow, areas for each module (or Mach number), mechanical efficiency, design spool speeds, fuel flow, burner pressure loss, and combustion efficiency. Check if the polytropic or isentropic efficiency is required as an output for the turbomachine modules. For some of the constraints, the polytropic efficiency is required, and for others the isentropic efficiency. This can be selected in GSP. Add an API block to the model, and select the input and output parameters in accordance with the ones defined in the GA set-up. The inputs are usually the design variables, and the outputs are the target parameters or the ones that are required to evaluate the constraints.

4-Design point model optimisation: With the set-up now complete one can commence with generating the model. Small modifications can be required to the initial set-up in order to obtain an acceptable model. These can be, but are not limited to, the areas to match static sensor measurements, design vector bounds, constraint bounds, or optimiser settings. If the optimiser struggles to find an acceptable solution within the bounds or runs into them, they need to be relaxed. On the contrary, if unrealistic solutions are attained, some bounds need to be tightened. A sensitivity analysis can aid with understanding the design choices made by the optimiser.

11.2. Systematic Approach Off-Design Modelling

With the design point one can commence the off-design modelling. The design point will be used as a reference scaling point for the turbomachinery characteristic maps. The steps below follow from the off-design modelling process for the two test cases.

1-Data collection: Ideally, the same reference engine should be used, as the one for design point modelling. If possible, the measurements should also be taken during the same overhaul/ flight. This assures the same component health condition. If points lie closely, one should be removed from the data set, since there will be no additional benefits. The design point, or points close to it, should also be excluded from the analyses. Since this will be used as the scaling point, the error will be minimal, consequently reducing the RMS error.

2-Reference map selection: The procedure for selecting the starting map has already been described in Section 8.2. Suitable reference maps can be selected by choosing the characteristics of a machine with a similar design, and ideally a similar technological level. The underlying physics of these maps should also be correct, as explained in Section 5.2.1.

3-Optimisation Set-up: The steps for the off-design optimisation set-up are similar to the design point problem set-up. In this case the design variables are the parameters of the scaling functions given by Equation 5.3 for each compressor module. The mass flow and pressure ratio are not scaled for the turbines, since the high-pressure region is only of interest. Unrealistic characteristics should be avoided by meticulously selecting the bounds. Large gradients in the scaling curves should be avoided as well. Furthermore, the default optimiser settings can be used as reference values. Again the RMSE can be used for the objective function. Contrary to the design point, the target parameters are sensor data for multiple off-design operating points. Moreover, no constraints were used for the off-design problem. An applicable constraint could be to limit the beta (β) values between zero and one. By doing so the optimiser will exclude solutions where the choke or surge line is breached, and/or the surge margin is low.

4-Creating the GSP model:
The off-design GSP model uses the design point model as a basis. Only now, the model case is changed from design to steady state. Once the latter is done, the maps need to be selected. Next, the design point location on each performance map needs to be specified. The latter can be done by

changing the design point β value and the non dimensional design spool speed. The guidelines for this have been elaborated upon in Section 8.2.
Finally, in the API block the inputs and outputs should be set identical to the ones expected by the optimiser. The inputs are the control variables, and the outputs are the target parameters. These are defined in Table 7.3 for the assessed test cases.

5-Developing the off-design model: The set-up has now been completed and the optimisation can be instantiated. As for the design point modelling procedure, again some small modifications maybe be required to the initial set-up in order to obtain acceptable turbomachinery characteristics. The design vector bounds can be modified in case the output maps are unrealistic. The latter was found to be the case for the CF6 model. From Figure 7.4 it can be observed that the span of available operating points is relatively small. Hence, only a particular region (high speed) of the maps is being focussed upon during the modelling procedure. The low speed area in this case has no anchor point and consequently gives the optimiser more freedom, which requires the bounds to be addapted meticulously. The optimiser settings can also be addapted if needed. The reference scaling point should be moved if the surge margin (SM) is not sufficient, or the operating lines are not smooth. If no acceptable results can be attained, it is possible that the reference maps are not suitable, and should be changed.

11.3. Extending to other engines

In Section 10.2 the importance of an engine specific model has been described. For the CEOD validation in Section 10.3 a different engine has been used due to the lack of CEOD availability for the correlation test engine. A design point calibration was done using test cell data to account for engine-to-engine differences. The component performance maps were kept un-modified. From the CEOD analyses it was observed that the improvements at take-off were small. At climb and cruise, however, significant improvements were noticeable as a result of the calibration. Thus the importance of creating an engine specific model has been successfully illustrated. One can, however, still argue if it is worth it to calibrate the model for adaptive modelling purposes.

11.4. Validation outcome

The CEOD validation outcome indicated that although the test cell match was good (average error of 0.7 %), improvements at higher Mach numbers and altitudes were still possible. An average error of around 1.3 % was attained at take-off. Whilst for the climb and cruise phase, the errors were around 1.7 and 4.1 % respectively. The developed model has deficiencies at these conditions, because sea level static data have been used for developing the model. At high Mach numbers losses occur in the nozzle, which were not accounted for. The velocity coefficient was not used, due to some difficulties encountered with this parameter during projects in the past at KLM ES [17]. The affect of the velocity coefficient was analysed in this work, and its implementation improved the model at take-off. At cruise the deviations were increased. Thus, the deviations at cruise are stemming from a different source.
At higher altitudes the Reynolds number effects become significant, mainly due to the lower density. During the modelling process, the standard corrections as a function of the Reynolds number index (RNI), were used. No difficulties were encountered since test cell data was utilised for modelling. Upon modifying the correction factors by trial and error it has been observed that the model significantly improved at climb and cruise conditions. It is recommended to use CEOD during the modelling process in order to determine the velocity coefficients and Re correction factors. This can be done after the maps have been tuned (scaled) with test cell data.

11.5. Schematic Overview of the modelling approach

In Figure 11.1 the above described approach is presented schematically.

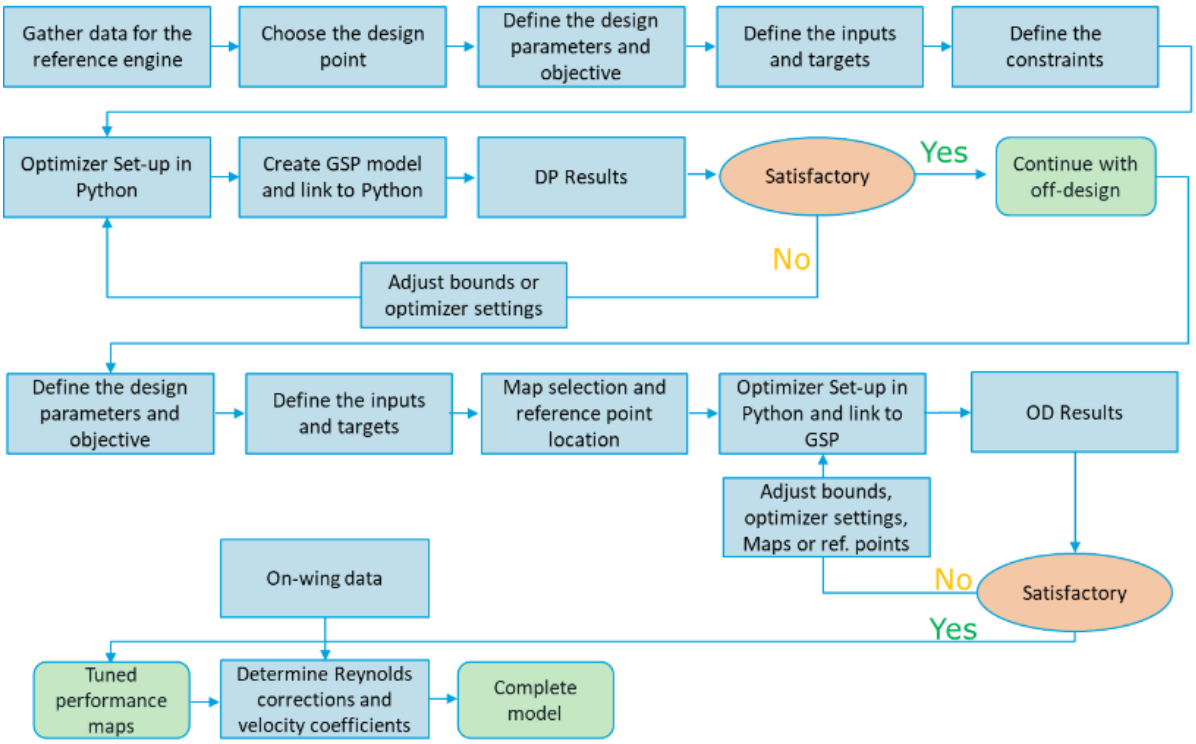

Figure 11.1: Schematic overview of the systematic modelling approach

12

Conclusion and Recommendations

By analysing the outcome of this project some key conclusions can be drawn. These are presented in this chapter. Furthermore, the main research question and sub-questions are answered as well. Finally, this chapter and thesis is closed with recommendations for future work. These include possible methods to improve the modelling approach, or better modelling alternatives that could have been chosen.

12.1. Conclusion

The focus of this study was to develop a systematic modelling approach for *modern* turbofan engines. Emphasis is placed on modern turbofans, since these have fewer sensors installed along the gas path. Moreover, a lot of data is also proprietary to the manufacturer. This increases the difficulty of modelling an inherently complex system. As done generally, the modelling task was split-up into design and off-design modelling. At the design point the key dimensions of the engine are determined. A critical operating condition is generally chosen for this point. For developing the modelling approach the take-off conditions were selected. This is the only critical operating point for which sufficient data were available for modelling purposes. Subsequently, off-design modelling was conducted. This uses the design point as input, and involves tuning/generating component performance maps. A scaling procedure using second order polynomial scaling functions was selected. Baseline maps from open literature were selected for this approach. The data used during the model development phase is test cell data, which is for sea level static conditions. The latter contains more measurements compared to on-wing data. The design and off-design modelling were set-up as optimisation problems with the aim to minimise the difference between measured and simulated data. For this an evolutionary algorithm, called Genetic algorithms, was utilised. During the design point modelling, physical relations were used as constraints to compensate for missing data and sensors. Models for the CF6-80C2 and GEnx-1B engine were developed in parallel in order to verify the systematic modelling approach. The GEnx-1B model was then validated using Continuous Engine Operating Data (CEOD). For the validation, data was filtered from ten flights by selecting steady state points and removing outliers. Below the main conclusions, drawn from the modelling approach and results, are presented:

- **Optimiser selection:** Various optimisation methods are available in the open literature. From the conducted literature study Bayesian optimisation and Genetic algorithms were found to be the most suitable methods. From these methods Genetic algorithms (GA) was selected. This method outperformed Bayesian optimisation for the test cases, in particularly for constrained problems. Lower objectives (factor 4) were attained in a similar time frame using Genetic algorithms.

- **Design point modelling:** In order to bridge the gap caused by the reduced amount of data, constraints for the efficiencies of the different turbomachinery components, and the optimum fan pressure ratio were incorporated. These were not implemented as hard constraints, and were intended to guide the optimiser towards feasible and physical solutions. For the GEnx-1B engine the efficiency constraints had to be relaxed more compared to the CF6-80C2 engine. This confirms the higher turbomachinery technological level for the GEnx. For both engines the attained

RMS error was lower than $1 \cdot 10^{-2}$, thus GA proved to be successful as well for the actual problem and dealt effectively with all the constraints. It is concluded that the used set-up was able to produce feasible and physical solutions, whilst effectively dealing with the reduced amount of data.

- **Off-design modelling:** It was possible to match the test cell data with a sufficiently low overall RMS error (<$1 \cdot 10^{-2}$), whilst attaining maps in line with the literature. The second order polynomial scaling approach is an effective method, however, a small operating data range can lead to unfeasible results, since there is no anchor present in the low operating speed region. The operating line is highly dependent on the location of the reference scaling point and it needs to be placed meticulously. It was observed that realistic and smooth operating lines on the baseline maps, do not always lead to equivalent results for the adapted maps. Moreover, the underlying physics of the maps were also checked for the baseline and optimised maps. It has been concluded that the underlying physics of the component maps are not impaired if second order scaling polynomials are used.

- **Engine specific model:** The developed model for the GEnx has been calibrated at the design point for a different engine. This engine also has CEOD available. For take-off conditions it was observed that the calibration had insignificant effect on the performance deviations with CEOD. For the climb and cruise phase larger improvements were noticeable. Altogether, the importance of creating an engine specific model, instead of a single baseline model for all the pool engines, was demonstrated. It is, however, questionable if developing an engine specific model still has advantages for adaptive modelling.

- **Validation results:** The error between simulated and measured data showed little scatter, and the overall deviations were acceptable. For the calibrated model, an average error of around 1.3 % was attained at take-off. For climb and cruise phases the errors were around 1.7 and 4.1 % respectively. At these two phases the largest deviations were found for the fuel flow and exhaust gas temperature (EGT). It was concluded that this offset was caused by incorrect Reynolds number corrections. The take-off phase deviations were relatively the lowest, however, still a factor 2 higher than the test cell errors. It was concluded that these were caused by the nozzle velocity coefficients, which were not included in the modelling set-up. Altogether the model can be improved substantially by implementing the velocity losses in the nozzles and the Reynolds effects. This indicates the need for utilising on-wing data during the modelling process.

- **Main conclusion:** From this research it can be concluded that general relations can be used to bridge the gap caused by the reduced amount of data. This provides a consistent approach to deal with missing sensors and data, unlike previous modelling projects at KLM ES. Moreover, using an automated machine learning procedure for modelling, is more efficient and effective than a manual process. To make the modelling approach complete, on-wing data should be utilised to account for effects caused by higher Mach numbers and altitudes.

12.2. Recommendations

Although the results are promising, the modelling approach can still be improved. Improvements can be made especially for high Mach numbers and altitudes. This section addresses some recommendations for future work at KLM Engine Services.

- In this study it was assumed that test cell data recorded at sea level static conditions will be sufficient for developing an accurate engine model. This was found to be an invalid assumption. At higher Mach number and altitudes the models were lacking accuracy. This was mainly caused by the omission of the velocity coefficient and not incorporating the Reynolds number effects. Hence, it is recommended to include the velocity coefficient and the Reynolds number effects. This can be done using CEOD and a minimisation problem set-up. Note that the velocity coefficient at the design point and off-design conditions will not be the same.

- For the model generation, the secondary performance parameters effects were also not incorporated. These were assumed to be at their nominal settings during the take-off (sea level static), which is the design point in this case. For off-design conditions these vary, however, their behaviour is assumed to be captured by the performance maps. These settings are also reliant on ambient conditions. A study regarding these has been conducted in the past at KLM Engine Services [17]. It can be analysed how the approach during the aforementioned paper can be used to improve the modelling approach/results.

- The reference engines used during this project are not new. Additionally, their health is not clearly described. From the EGT margin it was concluded that the engines are healthy. The same is also true for the CEOD validation reference engine. It is recommended to repeat the modelling process and/or validation if data from an engine, that better represents the new state, are available. This way deterioration does not influence the modelling results.

- The model of the GEnx has been validated using CEOD. For the CF6 engine only snapshots were available. These were taken at some point during the take-off, and cruise phase. Information on the secondary performance parameters was not available, which made it difficult to pre -process the data. This can be investigated further, and possibly used to check if the same conclusions can be drawn from the on-wing data analyses of the CF6.

- When creating an engine specific model (intra-engine approach), only the design point model was calibrated. It was assumed that the behaviour at off-design (determined from the maps) will not differ due to engine-to-engine differences. This can be verified by tuning the maps for another engine, if sufficient data is available in the future.

- The station 3 measurements for the GEnx engine are recorded in the flow channel going around the combustor, instead of the HPC outlet. During this study it has been assumed that the effects of this position offset are negligible. However, a more in depth analyses should be conducted to validate this.

- The standard fuel properties in GSP were used during this project. It should be verified how good these agree with the actual fuel used during the flights.

References

[1] M. MRAZOVA, "Future directions of fuel efficiency in aviation industry," *INCAS BULLETIN*, vol. 5, no. 4, pp. 71–86, Dec. 2013, ISSN: 20668201. DOI: 10.13111/2066-8201.2013.5.4.8.

[2] F. Yin and A. Gangoli Rao, "Performance Analysis of an Aero Engine with Interstage Turbine Burner," in *Aeronautical Journal*, vol. 121, Cambridge University Press, Nov. 2017, pp. 1605–1626. DOI: 10.1017/aer.2017.93.

[3] F. Sher *et al.*, *Unprecedented Impacts of Aviation Emissions on Global Environmental and Climate Change Scenario*, 2021. DOI: 10.1007/s40726-021-00206-3.

[4] S. Farokhi, *Aircraft Propulsion*.

[5] P. Galison and A. Roland, Eds., *Atmospheric Flight in the Twentieth Century* (Archimedes). Dordrecht: Springer Netherlands, 2000, vol. 3, ISBN: 978-0-7923-6742-0. DOI: 10.1007/978-94-011-4379-0. [Online]. Available: http://link.springer.com/10.1007/978-94-011-4379-0.

[6] E. A. S. A. (EASA), "Type-certificate data sheet for trent xwb series engines," Rolls-Royce Deutschland Ltd & Co KG, 2019.

[7] H. I. H. Saravanamuttoo, H. Cohen, H. Rogers, P. V. Straznicky, and A. C. Nix, *Gas Turbine Theory*, 7th ed. Pearson education Limited, vol. 2017, ISBN: 9781292093093.

[8] T. O. Rootliep, "Turbofan Condition Monitoring using Evolutionary Algorithm based Gas Path Analysis at KLM Engine Services," Delft University of Technology, Delft, The Netherlands, Tech. Rep., 2020.

[9] D. den Haan, "GSP Gas Path Analysis on CF6-80 Engines at KLM Engine Services," Delft University of Technology, Delft, The Netherlands, Tech. Rep., 2010.

[10] M. P. R. Van Moorselaar, "Gas Path Analysis on the GEnx-1B at KLM Engine Services," Delft University of Technology, Delft, The Netherlands, Tech. Rep., 2018.

[11] W. Visser, "Generic Analysis Methods Generic Analysis Methods Generic Analysis Methods Generic Analysis Methods," Ph.D. dissertation, Delft University of Technology, Delft, The Netherlands, 2015.

[12] GSP Development Team, "GSP 11 User Manual," Tech. Rep., 2014. [Online]. Available: www.gspteam.com.

[13] M. L. Verbist, "Gas Path Analysis for Enhanced Aero-Engine Condition Monitoring and Maintenance," Ph.D. dissertation, Delft University of Technology, Delft, The Netherlands, 2017, ISBN: 9789462995369.

[14] B. Lambiris, K. Mathioudakis, A. Stamatis, and K. Papailiou, "Adaptive Modeling of Jet Engine Performance with Application to Condition Monitoring," *Journal of Propulsion and Power*, vol. 10, no. 6, pp. 890–896, 1994, ISSN: 07484658. DOI: 10.2514/3.23828.

[15] S. Garg and D. L. Simon, "Challenges in Aircraft Engine Control and Gas Path Health Management," NASA Glenn Research Center, Lewis Field, Tech. Rep.

[16] J. Kraft, V. Sethi, and R. Singh, "Optimization of Aero Gas Turbine Maintenance Using Advanced Simulation and Diagnostic Methods," *Journal of Engineering for Gas Turbines and Power*, vol. 136, no. 11, 2014, ISSN: 15288919. DOI: 10.1115/1.4027356.

[17] M. Otten, "Development of a GEnx-1B model using on-wing data," Delft University of Technology, Delft, The Netherlands, Tech. Rep., 2021.

[18] P. Beishuizen, "Improving compressor maps of the GE CF6-80C2 engine," Delft University of Technology, Delft, The Netherlands, Tech. Rep., 2012.

[19] S. E. Bouazzaoui, "Modeling of a GSP Diagnostic Tool for the CFM56-7B engines," Delft University of Technology, Delft, The Netherlands, Tech. Rep., 2008.

[20] B Röell, “Test-cell & On-wing Turbofan Performance Comparison at KLM Engine Services,” Delft University of Technology, Delft, The Netherlands, Tech. Rep., 2019.

[21] F. Yin, *AE4238 Lecture-5 Engine Design Trends*, Delft, Netherlands.

[22] K. G. Kyprianidis, “Future Aero Engine Designs: An Evolving Vision,” *Advances in Gas Turbine Technology*, Nov. 2011. DOI: 10.5772/19689.

[23] A. H. Epstein, “Aeropropulsion for commercial aviation in the twenty-first century and research directions needed,” *AIAA Journal*, vol. 52, no. 5, pp. 901–911, 2014, ISSN: 00011452. DOI: 10.2514/1.J052713.

[24] A. J. Head, A. Rao, and F. Yin, “Performance Trends of High-Bypass Civil Turbofans,” Delft University of Technology, Delft, The Netherlands, Tech. Rep., 2015.

[25] W. Camilleri *et al.*, “Concept description and assessment of the main features of a geared intercooled reversed flow core engine,” *Proceedings of the Institution of Mechanical Engineers, Part G: Journal of Aerospace Engineering*, vol. 229, no. 9, pp. 1631–1639, Jul. 2015, ISSN: 20413025. DOI: 10.1177/0954410014557369.

[26] V. Michelassi and J. Ling, “Challenges and opportunities for artificial intelligence and high-fidelity simulations in turbomachinery applications: A perspective,” *Journal of the Global Power and Propulsion Society*, vol. 2021, no. Special Issue, 2021, ISSN: 25153080. DOI: 10.33737/jgpps/135173.

[27] A Bachan, “Impacts of OEMs in the maintenance supply chain,” Tech. Rep.

[28] M. Pelt *et al.*, “Data Mining In MRO,” Aviation Academy Research Programme - Faculty of Technology, Amsterdam University of Applied Sciences, Tech. Rep., 2019. [Online]. Available: www.amsterdamuas.com/car-technology/shared-content/projects/projects-general/data-mining-in-mro.html.

[29] J. Kurzke, “How To Create a Performance Model Of a Gas Turbine From A Limited Amount Of Information,” in *ASME Turbo Expo 2005: Power for Land, Sea and Air*, Nevada, USA, 2005.

[30] M. L. Verbist, W. P. Visser, and J. P. Van Buijtenen, “Experience with gas path analysis for On-wing turbofan condition monitoring,” *Journal of Engineering for Gas Turbines and Power*, vol. 136, no. 1, 2014, ISSN: 07424795. DOI: 10.1115/1.4025347.

[31] S van Vuuren, “Humidity effects on turbofan performance,” Delft University of Technology, 2019.

[32] J. Kurzke and I. Halliwell, *Propulsion and Power*. Springer International Publishing.

[33] P. P. Walsh and P Fletcher, *Gas Turbine Performance*, Second Edition. Blackwell Science Ltd, 2004.

[34] J. W. Chapman, T. M. Lavelle, and J. S. Litt, “Practical Techniques for Modeling Gas Turbine Engine Performance,” *NASA/TM—2016-219147*, 2016.

[35] J. Schutte, J. Sands, J. Tai, and D. Mavris, “Cycle Design Exploration Using Multi-Design Point Approach,” in *Proceedings of the ASME Turbo Expo 2012*, Copenhagen, Denmark, 2012.

[36] C. Soares, *Gas Turbines : a Handbook of Air, Land and Sea Applications.* Second Edition. Butterworth-Heinemann, an imprint of Elsevier, 2015, p. 1021, ISBN: 9780124104617.

[37] J. D. Stevenson, “Simulating Indirect Thrust Measurement Methods as Used on Modern High-Bypass Turbofans,” Ph.D. dissertation, Carleton University, Ontario, Canada, 1990.

[38] R. Avellan, “On the Design of Energy Efficient Aero Engines Some Recent Innovations,” Chalmers University of Technology, 2011, ISBN: 9789173855648.

[39] R. Krishnaraj and G. J. J. Wessley, “Performance analysis of a micro turbofan engine using matlab and gspintended for the propulsion of male uavs,” *International Journal of Pure and Applied Mathematics*, vol. 118, pp. 157–163, 20 2018.

[40] O. Sjögren, C. Xisto, and T. Grönstedt, “Estimation of Design Parameters and Performance for A State-Of-The-Art Turbofan,” in *Proceedings of the ASME Turbo Expo 2021*, 2021.

[41] Y. G. Li, P Pilidis, and M. A. Newby, “An Adaption Approach for Gas Turbine Design-Point Performance Simulation,” Tech. Rep., 2005.

[42] Y. G. Li and P. Pilidis, "GA-based design-point performance adaptation and its comparison with ICM-based approach," *Applied Energy*, vol. 87, no. 1, pp. 340–348, 2010, ISSN: 03062619. DOI: 10.1016/j.apenergy.2009.05.034.

[43] J. Kurzke, "Correlations hidden in compressor maps," 2011. [Online]. Available: www.gasturb.de.

[44] J. Kurzke, *Smooth c 8.2*, 2009. [Online]. Available: https://www.gasturb.de/software/smooth-c-t.html.

[45] J. Kurzke, *Smooth t 8.1*, 2008. [Online]. Available: https://www.gasturb.de/software/smooth-c-t.html.

[46] A. J. Glassman, "Turbine design and application," NASA SP-290, 1972.

[47] M. Sielemann, C. Coïc, M. Hübel, X. Zhao, and K. Kyprianidis, "Introduction to Multi-Point Design Strategies for Aero Engines," Tech. Rep., 2020.

[48] J. P. Jasa, J. S. Gray, J. A. Seidel, C. A. Mader, and J. R. R. A. Martins, "Multipoint Variable Cycle Engine Design Using Gradient-based Optimization," Tech. Rep.

[49] B. Yan, M. Hu, K. Feng, and Z. Jiang, "Enhanced component analytical solution for performance adaptation and diagnostics of gas turbines," *Energies*, vol. 14, 14 Jul. 2021, ISSN: 19961073. DOI: 10.3390/en14144356.

[50] Y. G. Li, M. F. Ghafir, L. Wang, R. Singh, K. Huang, and X. Feng, "Nonlinear multiple points gas turbine off-design performance adaptation using a genetic algorithm," *Journal of Engineering for Gas Turbines and Power*, vol. 133, 7 2011, ISSN: 07424795. DOI: 10.1115/1.4002620.

[51] S. S. Ramdin, "Systematic approach for modelling modern turbofan engines a literature study," Delft University of Technology, 2022.

[52] P. I. Frazier, "A tutorial on bayesian optimization," 2018.

[53] S. F. Smith, "A simple correlation of turbine efficiency," *The Journal of the Royal Aeronautical Society*, vol. 69, pp. 467–470, 655 Jul. 1965, ISSN: 0368-3931. DOI: 10.1017/s0001924000059108.

[54] R. I. Lewis, *Turbomachinery Performance Analysis*. Elsevier Science & Technology Books, 1996, ISBN: 0340631910.

[55] S. L. Dixon and C. A. Hall, *Fluid Mechanics andThermodynamics ofTurbomachinery*, 7th ed. Elsevier Inc, 2014, ISBN: 9780124159549.

[56] A. Guha, "Optimisation of aero gas turbine engines," *Aeronautical Journal*, vol. 105, no. 1049, pp. 345–357, 2001, ISSN: 00019240. DOI: 10.1017/s0001924000012264.

[57] D. Alexandre Rodrigues Martins, "Off-design performance prediction of the cfm56-3 aircraft engine," Technical University of Lisbon, 2015.

[58] H. Mustapha, M. Zelesky, N. Baines, and D. Japikse, *Axial and Radial Turbines*. Concepts NREC., 2003, ISBN: 9780933283183. [Online]. Available: https://books.google.nl/books?id=0_X3zQEACAAJ.

[59] J. Kurzke, "About simplifications in gas turbine performance calculations," Tech. Rep., 2007. [Online]. Available: www.gasturb.de.

[60] R. Storn, "On the usage of differential evolution for function optimization," *Proceedings of North American Fuzzy Information Processing*, pp. 519–523, 1996.

[61] "Recent advances in differential evolution: A survey and experimental analysis," *Artificial Intelligence Review*, vol. 33, pp. 61–106, 1-2 Feb. 2010, ISSN: 02692821. DOI: 10.1007/s10462-009-9137-2.

[62] D. Zaharie, "A comparative analysis of crossover variants in differential evolution," *Proceedings of the International Multiconference on Computer Science and Information Technology*, pp. 171–181, 2007, ISSN: 1896-7094.

[63] R. Storn and K. Price, "Differential evolution-a simple and efficient heuristic for global optimization over continuous spaces," 1997, pp. 341–359.

[64] P. Virtanen *et al.*, “SciPy 1.0: Fundamental Algorithms for Scientific Computing in Python,” *Nature Methods*, vol. 17, pp. 261–272, 2020. DOI: 10.1038/s41592-019-0686-2.

[65] J. Snoek, H. Larochelle, and R. P. Adams, *Practical bayesian optimization of machine learning algorithms*, 2012. DOI: 10.48550/ARXIV.1206.2944. [Online]. Available: https://arxiv.org/abs/1206.2944.

[66] U. Kumar, S. Soman, and Jayadeva, “Benchmarking nlopt and state-of-art algorithms for continuous global optimization via hybrid iaco,” Department of Electrical Engineering, Indian Institute of Technology, Mar. 2015. DOI: 10.1016/j.swevo.2015.10.005. [Online]. Available: http://arxiv.org/abs/1503.03175.

[67] J. Gonzalez, Z. Dai, P. Hennig, and N. Lawrence, “Batch bayesian optimization via local penalization,” in *Proceedings of the 19th International Conference on Artificial Intelligence and Statistics*, A. Gretton and C. C. Robert, Eds., ser. Proceedings of Machine Learning Research, vol. 51, Cadiz, Spain: PMLR, 2016, pp. 648–657. [Online]. Available: https://proceedings.mlr.press/v51/gonzalez16a.html.

[68] T. G. authors, *Gpyopt: A bayesian optimization framework in python*, http://github.com/SheffieldML/GPyOpt, 2016.

[69] D Lippett, G Woollatt, P. C. Ivey, P Timmis, and B. A. Charnley, “The design, development and evaluation of 3d aerofoils for high speed axial compressors: Part 1 – test facility, instrumentation and probe traverse mechanism,” 2005. [Online]. Available: http://www.asme.org/about-asme/terms-of-use.

[70] W. G. Cornell, “Experimental quiet engine program summary report,” General Electric Company - NASA, 1975.

[71] J. Klapproth, M. Miller, and D. Parker, “Aerodynamic development and performance of the cf6-6/lm2500 compressor,” General Electric Company, Apr. 1979. DOI: 10.2514/6.1979-7030.

[72] R Niehuis, A Bohne, and A Hoynacki, “Experimental investigation of unsteady flow phenomena in a three-stage axial compressor,” 2003.

[73] E. J. Hall, R. A. Delaney, S. R. Lynn, and J. P. Veres, “Energy efficient engine low pressure subsystem aerodynamic analysis,” NASA, 1998.

[74] A. Wiedermann, D. Frank, U. Orth, and M. Beukenberg, “Computational and experimental analysis of an industrial gas turbine compressor,” Oct. 2011.

[75] D. Clifton, “Condition monitoring of gas-turbine engines,” Department of Engineering Science, University of Oxford, 2006.

Appendices

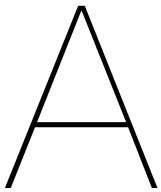

Thesis Assignment

Systematic Method for Engine Performance Modelling at KLM ES

MSc Assignment for Shivan Ramdin (student #4606248), Propulsion & Power (FPP), Aerospace Engineering

Introduction

KLM Engine Services (ES) is part of Air France Industries KLM Engineering & Maintenance Group, overhauling approximately 200 aircraft engines annually. The overhaul shop visit ends with a standardized performance test, to assess compliance to certification rules and customer contracts, before it is released for operation on-wing. At two different locations, the following turbofan engine types are tested:

- CFM56-7B KLM E&M Testcell / Schiphol-Oost
- CF6-80E1 KLM E&M Testcell / Schiphol-Oost
- CF6-80C2 KLM E&M Testcell / Schiphol-Oost
- GEnx-1B Zephyr Testcell / Charles de Gaulle Airport, Paris
- CFMI LEAP-1A & -1B (in gradual introduction)

Over the years KLM ES Engineering has used GSP (Gas turbine Simulation Program) as a supporting tool to analyze and evaluate engine performance data. Gas Path Analysis (GPA) techniques are used to translate engine performance data into component condition information. For optimal performance analysis accuracy, parameter inputs from all gas path sensors at the various engine stations are required. With new engine types such as the GEnx and the LEAP, the OEM does no longer provide the ability to install the additional sensors at the various engine stations, hence data input is limited, resulting in reduced potential to accurately analyze performance. However, the missing information can be compensated for by using accurate and detailed system performance models, which provide relationships between measured and unmeasured parameters. Furthermore, KLM ES has access to test cell and (continuous) in-flight engine performance data.

Key objectives

- To develop a systematic method for next-generation engine performance modelling in GSP.
- Reverse engineer key design parameters and create a design point model for a specific engine case study (GEnx-1B)
- Validate the design point model using literature and available information on existing engine models at KLM ES.
- Identify and document limitations and bottlenecks of performance modelling with the existing (test cell/on-wing) parameter set.
- Assess the potential of using the performance modelling method for engine test cell and on-wing performance analysis and diagnostics.

Assignment

Your work will include the following elements:

1) Introduction to current KLM performance and condition monitoring practice and relation to the maintenance concept.
2) Introduction to GSP (test analysis and gas path analysis models) as applied to KLM engines.
3) A literature study on current trends in gas turbine design and how to validate engine performance models.
4) Assessment of the model quality and uncertainty when modelling with a limited number of known parameters, based on literature of current engine design standards.
5) Development of a GSP design point modelling method that is applicable to the GEnx-1B as well as the LEAP in the future.
6) If time, a preliminary start to component map reverse engineering and off-design modelling.

Report

Results of the work must be reported in English, with a copy of this assignment and an executive summary.

Coaching

The work will be performed in close collaboration with KLM Engine Services (Juan Regueiro, Tim Rootliep)

Date ~~23 July 2021~~ 4 October 2021

Professor,	Delft University supervisor,	Supervisors at KLM
Prof. dr. ir. P. Colonna	Dr. ir. W.P.J. Visser	Juan Regueiro, Tim Rootliep

B

Cycle computation

The thermodynamic relations typically used for design point cycle computations are presented in this section. These computations are done for the stations depicted in Figure 5.2, from the inlet to the outlet of the engine. The main assumptions used for these calculations are that the gas expansion in nozzle is adiabatic and there are no pressure loses across the nozzle. Gas constants C_p for air and gas as well as γ for air and gas all stay constant during the respective processes. Furthermore, the mass flow through the combustion chamber is considered to be equal to the mass flow through the compressor and turbine (no bleed). Additionally, all component efficiencies are assumed to have constant values which are pre-determined and cannot change - in real life cycle calculations it is useful to remember that these values are not set in stone and can slightly vary as they are dependent on many different detailed factors.
The calculations are commenced by first converting ambient static conditions to total properties using Equation B.1 and B.2. Usually the static properties, as observed in the physical world, are used to define the thermodynamic state. For aero engine applications, however, it is very common to use total properties. This alleviates the need to know the exact cross-section areas or velocities. This also convenient for modelling tasks. The relations between the static and total properties are given by Equation B.1 and B.2. For some components like nozzles and mixers, however, the static properties are required [33].

$$T_{tot} = T_s(1 + \frac{\gamma - 1}{2}M^2) = T_s \left(\frac{p_{tot}}{p_s}\right)^{\frac{\gamma-1}{\gamma}} \tag{B.1}$$

$$\frac{p_{tot}}{p_s} = \left(1 + \frac{\gamma - 1}{2}M^2\right)^{\frac{\gamma}{\gamma-1}} \tag{B.2}$$

With the total properties now known, the parameters in front of the fan face (at station 2) are computed. If the inlet is assumed to be adiabatic the total temperature will remain unchanged. The total pressure in the inlet of the engine changes according to the intake pressure ratio. If the inlet isentropic efficiency ($\eta_{is_{inlet}}$) is given instead, Equation B.3 can be used.

$$p_{t,2} = p_{t,1}\left[1 + \eta_{is_{inlet}}\left(\frac{\gamma_a - 1}{2}\right)M_0^2\right]^{\frac{\gamma_a}{\gamma_a - 1}} \tag{B.3}$$

Next, the compression process is initiated. The properties behind the fan (station 24) can be computed first. By using the fan pressure ratio, the pressure behind the fan can be calculated. The total temperature is subsequently retrieved by using Equation B.4. This equation is derived using isentropic process relations between temperature and pressure, and the relation for the isentropic compression efficiency given by Equation B.5.

$$\frac{T_{t,24}}{T_{t,2}} = 1 + \frac{1}{\eta_{is_{fan}}}\left[\left(\frac{p_{t,24}}{p_{t,2}}\right)^{\left(\frac{\gamma_a - 1}{\gamma_a}\right)} - 1\right] \tag{B.4}$$

$$\eta_{is,comp} = \frac{T_{t,b,is} - T_{t,a}}{T_{t,b} - T_{t,a}} \quad \text{(B.5)} \qquad \eta_{ts,\text{exp}} = \frac{T_{t,a} - T_{t,b}}{T_{t,a} - T_{t,b,is}} \quad \text{(B.6)}$$

Turbofan engines have a part of the flow going to the bypass and a part to the core. The core flow can be computed using Equation B.7, and subsequently the bypass mass flow is straightforwardly determined.

$$\dot{m}_{\text{core}} = \frac{\dot{m}_{\text{total}}}{1 + BPR} \quad \text{(B.7)}$$

If the fan core and bypass nozzle section are modelled as one module the properties at station 13 (the bypass duct) will be the same as station 24, else the fan bypass pressure ratio needs to be used for the computations. The properties behind the LPC and HPC are computed using a similar approach, and their respective pressure ratios and efficiencies.
With the properties at station 3 now known, station 4, located at the combustor outlet can be analysed. By considering the combustor pressure losses the pressure can be calculated at this station. Then either the fuel flow, or combustor outlet temperature (T_{04}) is required to complete the calculations at station 4. Equation B.8 describes the relation between the two aforementioned parameters and can be rearranged depending on the to be computed parameter. Here LHV is the lower heating value of the fuel and η_{cc} is the combustion efficiency.

$$\dot{m}_{fuel} = \frac{\dot{m}_3 * C_{P_g} * (T_{t,4} - T_{t,3})}{\eta_{cc} * LHV} \quad \text{(B.8)}$$

The properties following the expansion process by the turbines can be computed next. For the station after the HPT (station 45) Equation B.9 and Equation B.11 can be used. The latter is derived using isentropic process relations between temperature and pressure, and the relation for the isentropic expansion efficiency given by Equation B.6. W_{HPC} is the work that is required to drive the HPC and can be computed using Equation B.10.
For station 5 a similar procedure can be employed. Now, however, the turbine module needs to drive the fan and LPC, hence the work for these two components needs to be provided by the LPC. Note that the fuel flow needs to be added to the core mass flow for computations after the combustor.

$$T_{t,45} = T_{t,4} - \frac{W_{HPC}}{\eta_{mech}\dot{m}_4 C_{p,g}} \quad \text{(B.9)} \qquad W_{module} = \dot{m}_{module} \cdot C_p \cdot \Delta T_{module} \quad \text{(B.10)}$$

$$p_{t,45} = p_{t,4}\left[1 - \frac{1}{\eta_{is,HPT}}\left(1 - \frac{T_{t,45}}{T_{t,4}}\right)^{\frac{\gamma_g}{\gamma_g - 1}}\right] \quad \text{(B.11)}$$

One can proceed now with the exhaust nozzle computations, which are similar for the core and the bypass nozzle. For the sake of brevity only the core calculations are explained.
First it is analysed if the nozzle is choked by checking if the pressure ratio $P_{t,7}/P_a$ is larger than the critical PR given by Equation B.12. Note that $P_{t,7}$ is the same as $P_{t,5}$ if there are no duct losses, and $T_{t,7}$ is equal to $T_{t,5}$ if the duct is adiabatic.

$$\frac{p_{t,7}}{p_{\text{critical}}} = \left[1 - \frac{1}{\eta_{nozzle}}\left(\frac{\gamma_g - 1}{\gamma_g + 1}\right)\right]^{\left(\frac{-\gamma_g}{\gamma_g - 1}\right)} \quad \text{(B.12)}$$

For a choked nozzle the following relations are applicable:

$$T_9 = T_{t,7}\left(\frac{2}{\gamma_g + 1}\right) \qquad p_9 = \frac{p_{t,7}}{PR_{crit}} \quad \text{(B.13)}$$

Using a Mach number of 1, for choked conditions in the nozzle, the jet velocity can be computed as follows: $v_9 = \sqrt{\gamma_g * R * T_a}$. The exhaust area is then computed using Equation B.14.

$$\rho_9 = \frac{p_9}{R * T_9} \qquad A_9 = \frac{\dot{m}_9}{\rho_9 v_9} \quad \text{(B.14)}$$

If the nozzle is not choked, different relations hold. Firstly, the exhaust static pressure is equal to the ambient pressure due to the perfectly expanded nozzle. The exhaust static temperature can subsequently be computed using Equation B.15.

$$T_9 = T_{0,7}\left[1 - \eta_{is,bypass}\left(1 - \left(\frac{p_9}{p_{0,7}}\right)^{\frac{\gamma_g - 1}{\gamma_g}}\right)\right] \tag{B.15}$$

The jet velocity can be computed by using the relation: $V_9 = \sqrt{2 \cdot c_{p,a} \cdot (T_{0,7} - T_9)}$. The exhaust area can then be calculated using the same relations as for a choked nozzle.
With all the properties now known, the thrust can be obtained using Equation B.16, which consists of a momentum and a pressure term. The total thrust can be computed by adding the bypass and the core thrust, both calculation in a similar way. Furthermore, the efficiencies of the gas turbine can be obtained well. These are elaborated upon in Appendix C.

$$F_{\text{core}} = \dot{m}_9 \left(v_9 - v_\infty\right) + A_9 \left(p_9 - p_a\right) \tag{B.16}$$

C

Gas turbine efficiencies

Thermodynamic efficiency
The thermodynamic efficiency is the ratio of gas power generated over the heat added by the combustion process, and is given by Equation C.1. In order to calculate thermodynamic efficiency it is required to obtain gas generator power given by P_{gg} in Equation C.1. This property can be defined as the maximum power theoretically generated by the engine core by expanding gas to ambient conditions, hence the theoretically maximum achieved kinetic energy. To calculate P_{gg} it is first needed to find the total temperature (T_{gg}) of this point. The temperature is found by equating turbine work to the work required to drive both the compressors HPC the fan work contributing to the core flow only. The power required for the fan core can be assumed to be proportional to the mass flow split.

$$\eta_{thdy} = \frac{P_{gg}}{\dot{m} \cdot c_p \Delta T_{cc}} = \frac{P_{gg}}{\dot{m}_3 \cdot c_{p_{gas}} (T_4 - T_3)} \tag{C.1}$$

Jet generation efficiency
This is the ratio of the kinetic energy available at the nozzle exit over the gas power.

$$\eta_{\text{jet gen}} = \frac{\sum \left\{ 1/2 \dot{m} \left(v_j^2 - v_o^2 \right) \right\}}{P_{gg}} \tag{C.2}$$

Propulsive efficiency
The propulsive efficiency is the ratio of the actual thrust produced over the useful kinetic energy at the nozzle exit. Hence, it accounts for losses of kinetic energy

$$\eta_{prop} = \frac{\Sigma \left\{ \dot{m} \left(v_j - v_o \right) \right\} v_o}{\Sigma \left\{ 1/2 \dot{m} \left(v_j^2 - v_o^2 \right) \right\}} \tag{C.3}$$

Thermal efficiency
The thermal efficiency is defined as follows:

$$\eta_{th} = \eta_{cc} \cdot \eta_{thdy} \cdot \eta_{\text{jet gen}} \tag{C.4}$$

ηcc is the combustion efficiency. and accounts for the incomplete combustion process. The following relation can be derived for the thermal efficiency:

$$\eta_{thermal} = \frac{\sum \left\{ 1/2 \dot{m} \left(v_j^2 - v_o^2 \right) \right\}}{\dot{m}_f LHV_f} \tag{C.5}$$

Overall efficiency

Finally, the overall efficiency can be computed, which is a product of the thermal and the propulsive efficiency. The resulting relation can be seen below.

$$\eta_{total} = \frac{\Sigma \left\{ \dot{m} \left(v_j - v_o \right) \right\} v_o}{\dot{m}_f LHV_f} \tag{C.6}$$

Note that the relations above are only valid for an unchoked nozzle. In case of a choked nozzle the expansion to ambient conditions is incomplete, and the thrust will have a pressure term as mentioned before. The equivalent jet velocity needs to be used for the computations then. The latter is computed by assuming that the thrust is only generated due to momentum.

D

Secondary performance parameter included in CEOD

Table D.1: Secondary performance parameters included in CEOD

Parameter	Description	Unit
HPTACCV $_{pos}$	Selected HP Turbine Active Clearance Control Valve Position	[%]
LPTACCV $_{pos}$	Selected LP Turbine Active Clearance Control Valve Position	[%]
CCCV $_{pos}$	Selected Core Compartment Cooling Valve Position	[%]
VBV $_{pos}$	Selected Variable Bleed Valve Position	[%]
TBV$_{pos}$	Selected Transient Bleed Valve Position	[%]
VSV$_{pos}$	Selected Stator Vane Position	[%]
PTO	Total Engine Horsepower Extraction	[hp]
BAI$_{pos}$	Selected BAI(Booster Anti-Ice) Bleed Valve	$[-]$
$\Delta N2$	Core speed rate of change	[% N2/s]
AHPTC	Actual HP Turbine Clearance (calculated)	[in]

E

Off-design results

E.1. Error for the Off-design operating points

In this section the optimisation error for the different off-design operating points is presented. These are depicted in Figure E.2 and E.2, for the GEnx and CF6 model respectively. The dashed lines are the outcome of the optimisation process.

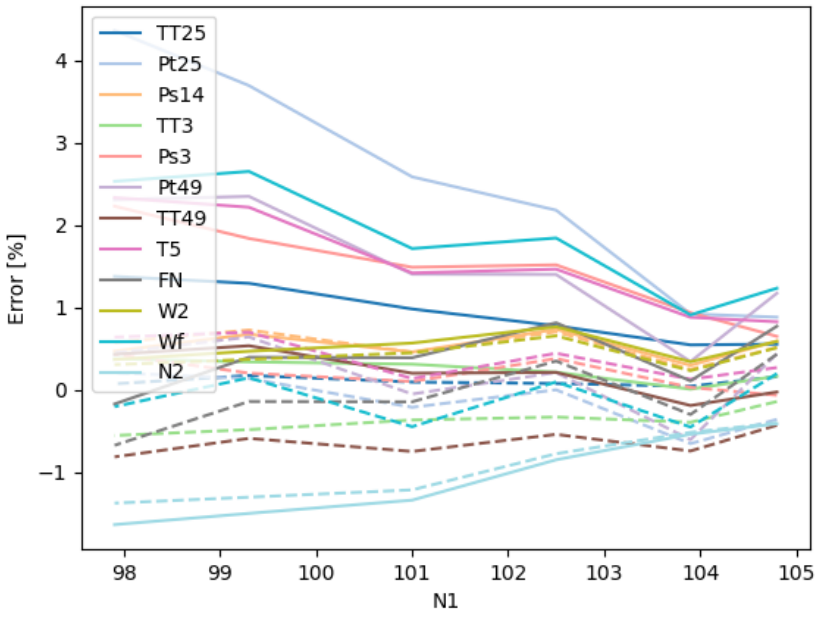

Figure E.1: Errors of the CF6 target parameters for the Off-design operating points

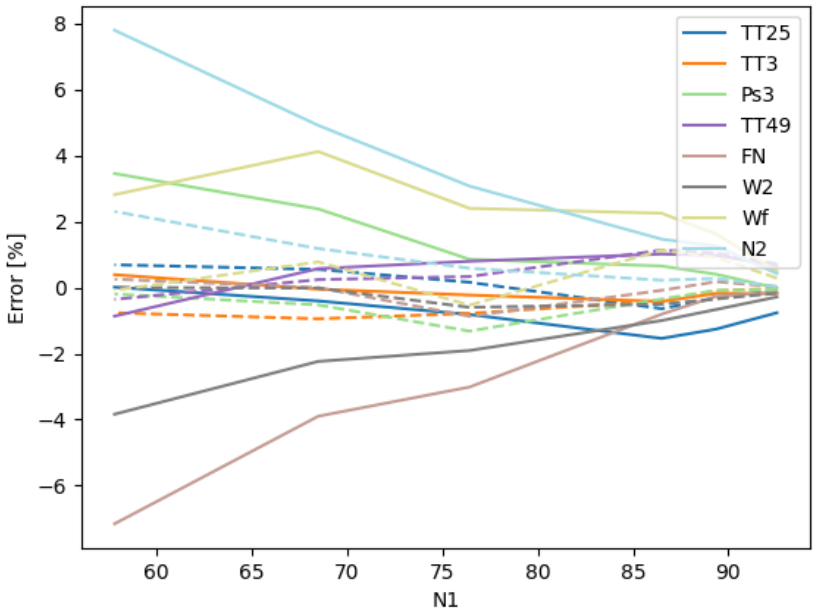

Figure E.2: Errors of the GEnx target parameters for the Off-design operating point

E.2. CF6 component performance characteristics

The component maps of the CF6 engine are given in following figures. Black is used to illustrate the results of the optimisation, whereas grey indicates the starting maps.

Compressor maps CF6

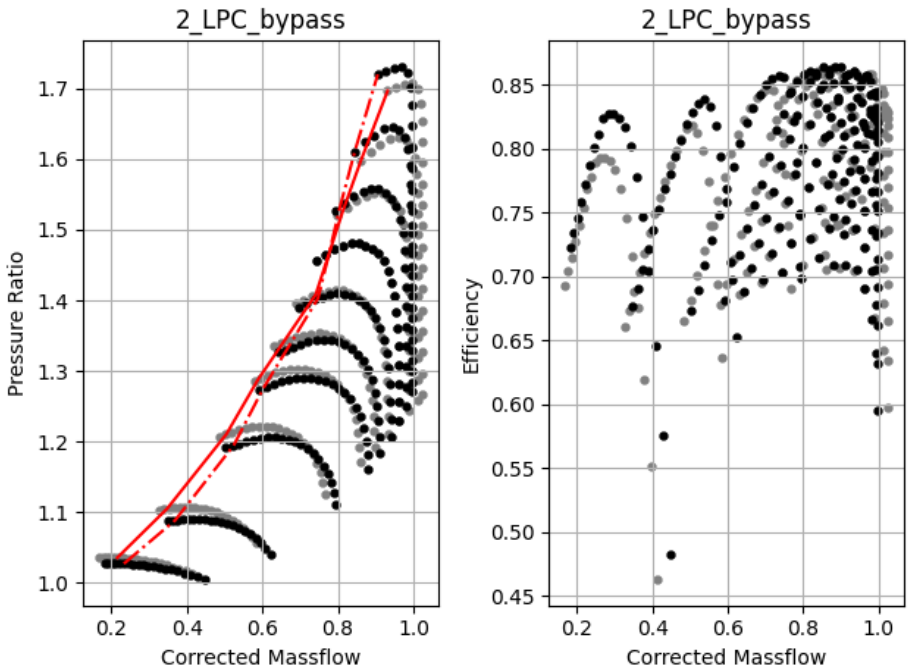

Figure E.3: Fan bypass map before (grey) and after (black) adaption

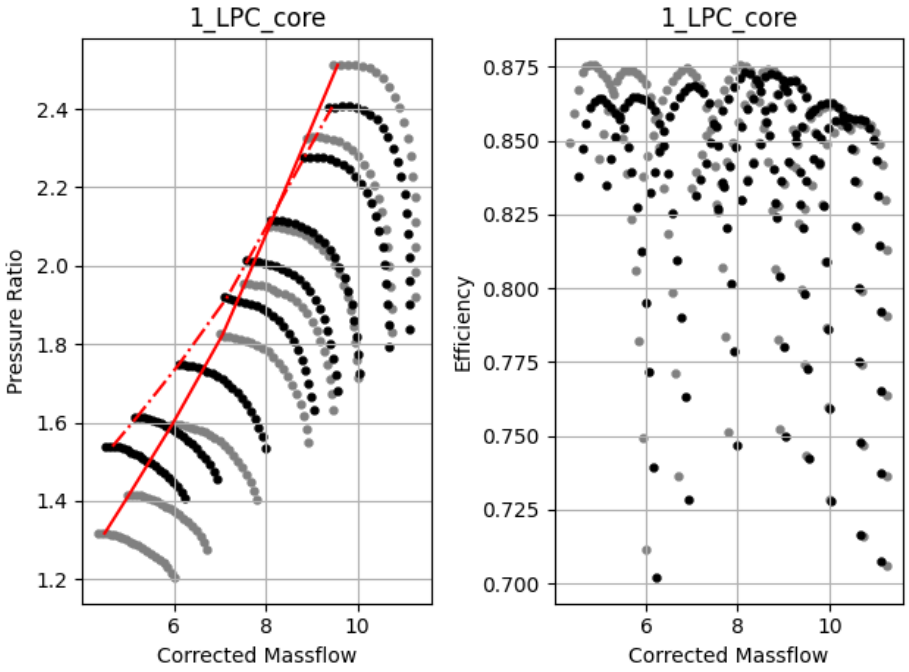

Figure E.4: Fan core map before (grey) and after (black) adaption

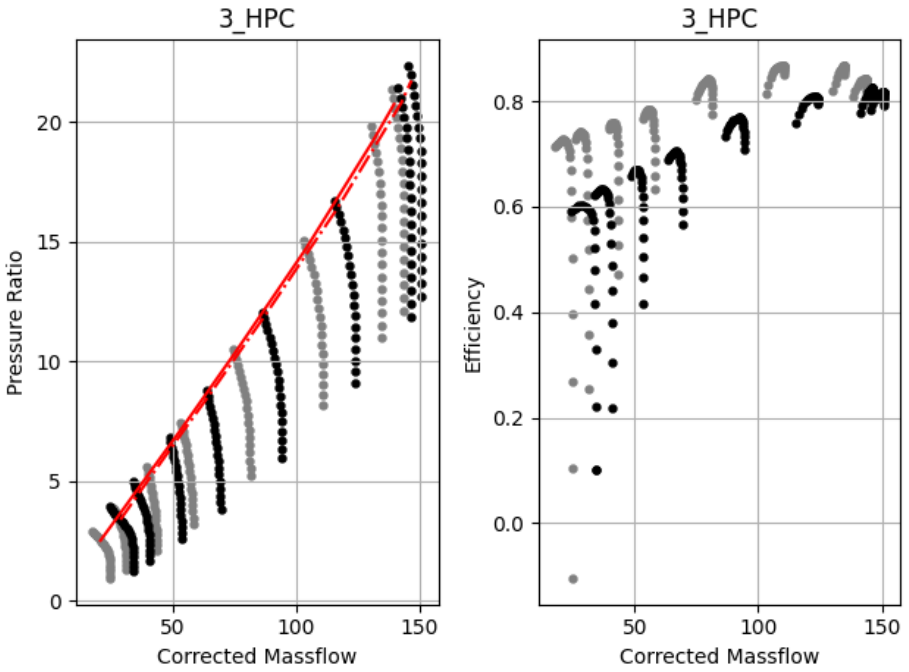

Figure E.5: HPC map before (grey) and after (black) adaption

Turbine maps

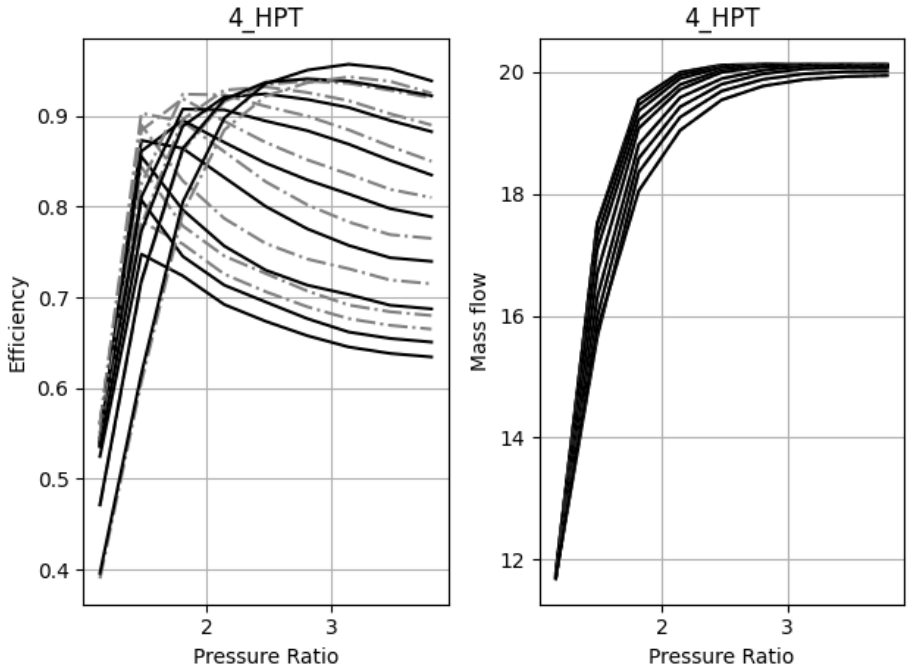

Figure E.6: HPT map before (grey) and after (black) adaption

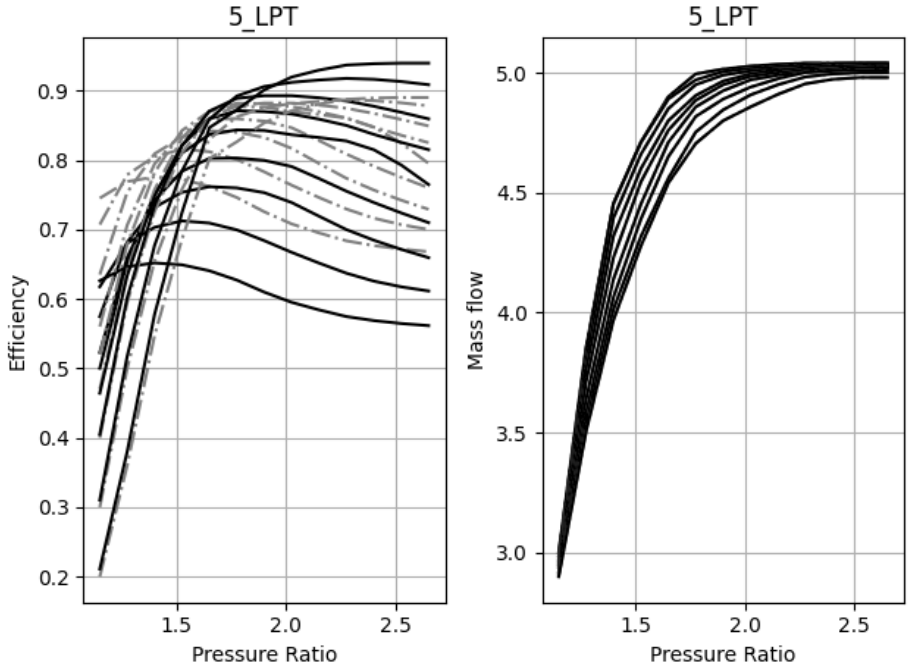

Figure E.7: LPT map before (grey) and after (black) adaption